AN ADAPTIVE DISPERSION FORMULA FOR CHROMATIC ABERRATION CORRECTION AND POLARIZATION ABERRATION ANALYSES IN PLANE SYMMETRIC OPTICAL SYSTEMS

by

Chia-Ling Li

A Dissertation Submitted to the Faculty of the

JAMES C. WYANT COLLEGE OF OPTICAL SCIENCES

In Partial Fulfillment of the Requirements

For the Degree of

DOCTOR OF PHILOSOPHY

In the Graduate College

THE UNIVERSITY OF ARIZONA

2021

THE UNIVERSITY OF ARIZONA
GRADUATE COLLEGE

As members of the Dissertation Committee, we certify that we have read the dissertation prepared by: Chia-Ling Li
titled: An Adaptive Dispersion Formula for Chromatic Aberration Correction and Polarization Aberration Analyses in Plane Symmetric Optical Systems

and recommend that it be accepted as fulfilling the dissertation requirement for the Degree of Doctor of Philosophy.

Jose Sasian
Jose Sasian Date: Aug 13, 2021

James Schwiegerling
James Schwiegerling Date: Aug 13, 2021

Tom D Milster
Tom Milster Date: Aug 13, 2021

Final approval and acceptance of this dissertation is contingent upon the candidate's submission of the final copies of the dissertation to the Graduate College.

I hereby certify that I have read this dissertation prepared under my direction and recommend that it be accepted as fulfilling the dissertation requirement.

Jose Sasian
Jose Sasian Date: Aug 13, 2021
Dissertation Committee
Optical Sciences

ACKNOWLEDGEMENTS

It had been a long journey, and I received a lot of help from a lot of people, especially my advisor, Dr. José Sasián. He offered me research opportunities, provided me with funding, and guided me into the fields of aberration theory and optical design. It was very rewarding and pleasant to be in his research group. I am also grateful for his support, encouragement in life, and his unparalleled patience. Without him, this dissertation would not be completed.

I am also grateful to Dr. Jim Schwiegerling and Dr. Tom D. Milster as my committee members for their invaluable comments and suggestions throughout my doctoral career and for taking the time to help me accomplish this dissertation.

I extend my thanks to all the members of Dr. Sasián's lab, including Mary Liang, Oscar Martinez, Dmitry Reshidko, Masatsugu Nakano, Chih-Yu Huang, Yuhao Wang, Tamer Elazhary, Braulio Albuquerque, Yiqun Ji, Yufeng Yan, Xiaobo Tian, and Hyun Kyoung An. Especially thanks to Dr. Ping Zhou, Dr. Su Peng, Dr. Chang Jin Oh, Dr. Daewook Kim, and Dr. Chunyu Zhao for sharing the experience and knowledge of optical testing.

In addition, I would like to thank my parents, brothers and husband for their endless love and support, allowing me to focus on my studies and pursue my dreams in a different country.

Moreover, I would like to thank the Ministry of Education in Taiwan for providing me with a scholarship GSSA. Last but not least, I would like to thank Synopsis and Zemax for the student licenses of CODE V and OpticStudio, respectively.

Table of Contents

List of Figures

List of Tables

ABSTRACT

This dissertation consists of two parts: an adaptive dispersion formula and polarization aberration functions for general plane symmetric optical systems.

First, an adaptive glass dispersion formula is defined and discussed. The formula exhibits superior convergence with a minimum number of coefficients. Using this formula, the correction of chromatic aberration per spectrum order can be rationalized. Comparisons between the formula and the Sellmeier or Buchdahl formulas for glasses in the Schott catalogue are made. The six-coefficient adaptive formula is found to be the most accurate with an average maximum index of refraction error of 2.91×10^{-6} within the visible band.

Second, a new set of polarization aberration functions for general plane symmetric optical systems is proposed. These new polarization aberration functions are derived based on the paraxial approximation and the second-order approximation. The polarization aberrations of an optical system are the sum of the contributions from each surface. In other words, this new set of polarization aberration functions provides insight of polarization aberration surface by surface. The polarization aberrations of optical systems with tilted or decentered elements, and refractive or reflective elements, are discussed and analyzed. Compared with CODE V real ray tracing simulation, the difference is less than 2.5% for an imaging system with three curved mirrors.

1. Introduction

1.1 Imaging Systems

Imaging and non-imaging are two different types of optic systems. For an imaging system, it forms images of objects using refractive, reflective, or diffractive optical elements. Camera, microscope, and telescope are typical examples of imaging optical systems. The object of an imaging system can be self-luminous, reflective, or scattering. For a non-imaging system, it shapes the light source with designed transfer function to form desired light radiation as the output, for instance, an automobile head light, back light of a flat panel display, and solar energy concentrator.

Aberration is a property in imaging optical systems, and it had been studied over hundreds of years. Ideally, image should be formed as a duplication of the object with desired magnification and location. However, aberrations usually degrade the sharpness of image and distorts the imaging plane. For example, when an object point source emits a spherical wavefront, which passes through an imaging system, due to surface figures of the optical lenses, the output wavefront may be deviated from spherical shape. So, the image of the point source would be blurred and deformed. Aberrations of the imaging system need to be corrected to minimize the image quality degradation.

Aberrations are also known as deviations from Gaussian optics, first order optics, and paraxial optics. These three are the optics of perfect optical system, where spherical surfaces would form ideal images. There are three main types of aberrations: monochromatic aberrations, chromatic aberrations, and polarization aberrations. Examples

of monochromatic aberrations are spherical aberration, coma, astigmatism, and distortion. In terms of chromatic aberrations, longitudinal chromatic aberration and lateral chromatic aberration are two major types. Chromatic aberrations arise from the fact that the refractive index is a function of wavelength. If the light source has a broad spectrum, image quality could be influenced by the chromatics aberrations. For polarization aberration, it can be categorized into physical and geometrical types. Physical type is divided into diattenuation aberration and retardance aberration while geometrical type is the skew aberration. Polarization aberrations represent how the polarization states vary across the pupil.

1.2 Monochromatic Aberrations

Monochromatic aberrations describe wavefront deformation monochromatically or quasimonochromatically [1]. The Snell's Law describes how the light refracts at interfaces. In paraxial approximation, $\sin(\theta)$ in Snell's Law is approximated and represented by θ, which is the first term of its Taylor expansion. After including more terms, for example the second term, the results would be embodied the third-order monochromatic aberrations. These third order aberrations are widely known as Seidel aberrations. In addition to the first two terms of Taylor expansion, there are more higher order terms contributing to more higher order aberrations. Exact ray tracing essentially would be equivalent to summing up all the terms including high order terms.

Spherical aberration, coma, astigmatism, field curvature, and distortion are five primary aberrations of Seidel aberrations developed in 1856 [2]. Spherical aberration is defined as the difference of refraction or reflection among rays that propagate through a

spherical surface at different pupil radii. Coma, which happens in the off-axis field only, comes from the variation in magnification over the pupil. Astigmatism is another type of off-axis aberration in which rays propagate in two perpendicular planes with different power and focal lengths. Field curvature describes a flat object plane that would not perfectly conjugate to a flat image plane. Distortion comes from the variation in magnification over the field, where barrel distortion is a decrease in image magnification with distance from the optical axis, and pincushion distortion is an increase in image magnification with the distance from the optical axis.

On top of third order, for the fifth order monochromatic aberrations, there are 9 primary aberrations developed firstly by K. Schwarzschild in 1905 [2]. Five out of 10 are the improvements upon the primary Seidel aberrations, and 4 out of 10 are new forms of wavefront deviation, such as oblique spherical aberration. All these monochromatic aberrations and corresponding mathematical forms provide important insight into the image quality of an imaging optical system.

1.3 Chromatic Aberrations

If the light source is not monochromatic, the dispersion of the optics material would affect the imaging quality and the corresponding Seidel and higher order aberrations. However, the effects on Seidel and higher order aberrations are not as pronounced as chromatic aberrations, which comes from the fact that rays with different wavelengths would propagate along different paths through the system. Snell's law, thin lens equation, and lens maker equation are all functions of refractive index of materials, which are

wavelength dependent. In general, refractive index of an optical material is larger at shorter wavelength. Abbe number, also known as the V-number, is widely utilized as a metric of material dispersion. High values of Abbe number indicate lower dispersion.

There are two major types of chromatics aberrations, longitudinal chromatic aberration and lateral chromatic aberration. Longitudinal chromatic aberration is also called as axial color or chromatic change of focus. It describes the range of image location of an optical system as spanning a given wavelength range. On the other hand, lateral chromatic aberration is also called as lateral color or chromatic change of magnification. It refers to the wavelength dependent magnification of an optical system. The off-axis object point would be formed at different image heights at different colors. Both longitudinal chromatic aberration and lateral chromatic aberration essentially come from the fact that the focal length of an optical system is a function of wavelength.

A combination of two lenses, one positive and one negative, is one straightforward way to minimize chromatic aberration of an optical system. Theoretically, this lens combination is achromatized at two specific wavelengths, and chromatic aberrations in between these two specific wavelengths decrease. The optimization of image quality and minimization of chromatic aberrations are dependent on both lens surface recipe and Abbe number of optics material. Figure 1.1 shows the Abbe number v.s. refractive index for various glasses [3]. Vertical axis is the refractive index of optical material at 587.6 nm, and horizontal axis is the Abbe number. Flint glass and Crown glass are the two main materials used to correct chromatics aberrations. Flint glass has relatively high refractive index and

low Abbe number (55 or less), while crown glass has low refractive index and high Abbe number (50 or higher). A convex lens of crown glass is usually combined with a concave lens of flint glass to form an achromatic doublet lens.

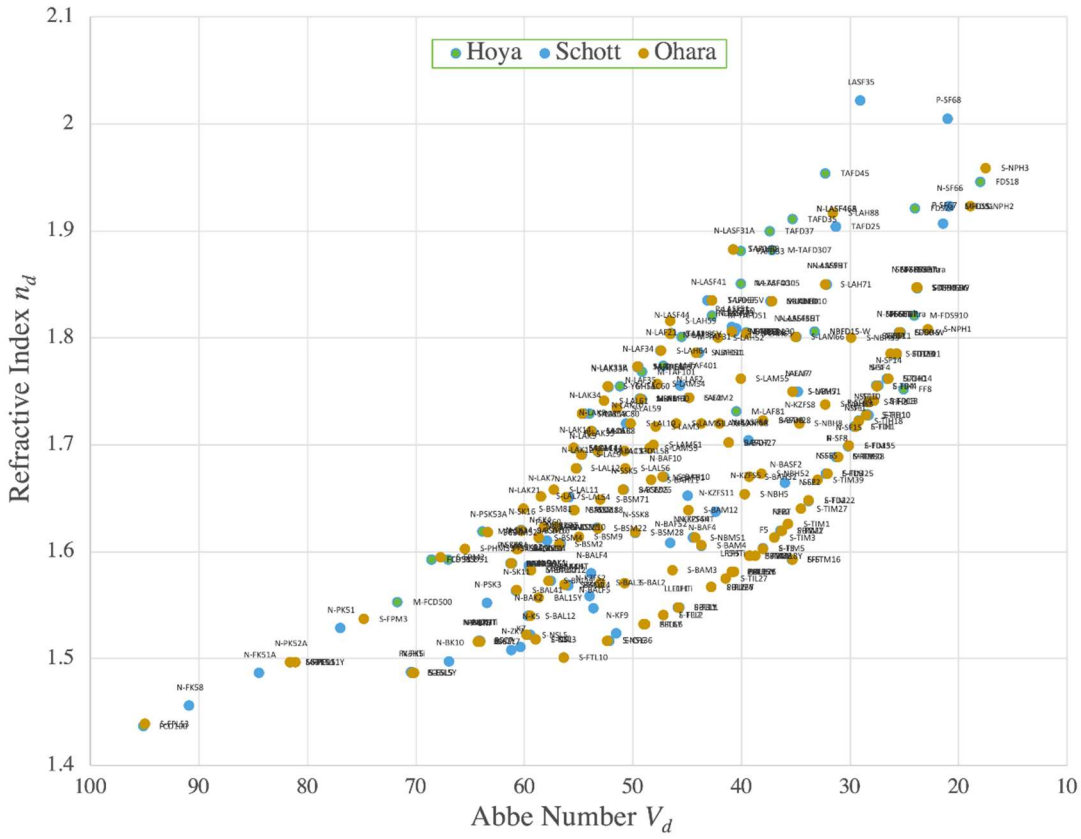

Figure 1.1 Abbe number v.s. refractive index for various glasses [3]

1.4 Polarization Aberrations

Polarization aberrations of an optical system describe how the polarization state of light varies when this polarized light passes through the optical system. For an ideal polarization aberration free optical system, a uniform polarization input optical field should yield a constant polarization output field without polarization change after propagating through the system. An identity Jones matrix can be utilized to describe the polarization

response of such an ideal optical system. Deviations from the identity Jones matrix are so-called polarization aberrations. In conventional optical system without considering polarization aberrations, the amplitude response function or point spread function at the image plane is the Fourier transform of the optical field at the exit pupil. After incorporating polarization aberrations, the Jones matrix is introduced, and the amplitude response function is generalized to the amplitude response matrix, while the exit pupil is also generalized to the exit Jones pupil [4].

Polarization aberrations can be categorized into physical and geometrical types. Physical polarization aberrations come from Fresnel aberrations, thin film coatings, and anisotropic optical materials. Fresnel aberrations refer to the polarization state change due to the Fresnel effects at interfaces between different optical media. These non-uniform polarization variations across the pupil can be further categorized into diattenuation aberration and retardance aberration. Diattenuation aberration is the polarization dependent transmittance and reflectance, while retardance aberration is the polarization dependent optical path difference.

Geometrical polarization aberration can be observed in an optical system after physical polarization aberrations are removed. Geometrical polarization aberration is also called as skew aberration [4]. In an axial symmetric optical system, there is no skew aberration for the meridional rays, but there are skew aberrations for skew rays. Skew aberration is a polarization rotator, which rotates polarization states between entrance pupil and exit pupil based on geometric transformation of an optical system. It rotates linearly

polarized light or the axis of elliptical polarized light. It is independent of the incident polarization state, and the diattenuation and retardance of optical elements.

1.5 Summary of Contents

This work presents two research topics: a new dispersion formula for understanding the correction of axial color and polarization aberration analyses in plane symmetric optical systems. An adaptive dispersion formula that provides less index fitting error on average is presented and studied. Polarization aberrations in plane symmetric optical systems are investigated and a new set of polarization aberration functions is proposed on top of the polarization aberration functions for axial symmetric optical systems.

Chapter 2 presents an adaptive dispersion formula which is essentially a truncated polynomial with one adaptive term is studied. This is an insightful way to understand and carry out the correction of chromatic change of focus aberration. Chapter 3 presents different methodology to describe polarization aberrations. An extended derivation of polarization aberration for plane symmetric optical systems is shown, and practical application examples are demonstrated. Chapter 4 concludes by presenting closing remarks. Appendices A and B are supplemental materials of the adaptive dispersion formula.

2. Adaptive Dispersion Formula for Index Interpolation and Chromatic Aberration Correction

2.1 Introduction

A dispersion formula is utilized to relate the refractive index of optical material to the wavelength of light. Generally speaking, the refractive index of a material will only have a few measurement data at selecting wavelengths. To know the value of refractive index at a particular wavelength, we need to use the dispersion formula to get an interpolated value. Therefore, it is important to have an accurate dispersion formula. There are several dispersion formulas available, and these can be classified into two types. The first type is in the form of an algebraic fraction, and the second type is in a polynomial form. For example, in 1871, Wolfgang Sellmeier developed a formula which belongs to the first type and is [5]

$$n^2(\lambda) = 1 + \frac{B_1\lambda^2}{\lambda^2 - C_1} + \frac{B_2\lambda^2}{\lambda^2 - C_2} + \cdots + \frac{B_i\lambda^2}{\lambda^2 - C_i}, \tag{2.1}$$

where n is the index of refraction at wavelength λ. B_i and C_i are Sellmeier coefficients, which vary from glass to glass. In 1954, Hans Buchdahl introduced a change of coordinate from wavelength space λ to a chromatic coordinate ω and developed a power series of ω called Buchdahl dispersion formula [6-10]

$$n(\omega) = n_0 + \nu_1\omega^1 + \nu_2\omega^2 + \cdots + \nu_j\omega^j, \tag{2.2}$$

where n is the index of refraction at chromatic coordinate ω. Although this model is a polynomial of ω, it is still classified as of the first type model since the relationship between coordinates ω and λ is

$$\omega = \frac{\lambda - \lambda_0}{1 + \alpha(\lambda - \lambda_0)}, \tag{2.3}$$

which is in the form of an algebraic fraction. This relationship for ω provides the functional nonlinearity between n and λ in $n(\lambda)$ space. In Eq. (2.2) and Eq. (2.3), λ_0 is the reference wavelength, and n_0 is the index of refraction at reference wavelength λ_0. v_j and α are the Buchdahl coefficients. The coefficient α plays the role of a convergence coefficient which varies with λ_0 and lies within narrow limits for common glasses. For instance, if 0.574 μm is chosen for λ_0 in the visible band, then the optimal value of α is around 2.5. However, in practice the coefficient α is fixed for all glasses to allow the chromatic coordinates to be useful for correcting chromatic aberration [9].

A Taylor series, which is an example of the second type of dispersion formulas, can be used to describe the dispersive behavior of glass. Such a series is desirable for theoretical studies of chromatic aberration correction. Thus, some efforts have been made to develop such a series in wavelength space. For example, a truncated Taylor series centered at the reference wavelength λ_0 is [10]

$$n = n_0 + a_1(\lambda - \lambda_0)^1 + a_2(\lambda - \lambda_0)^2 + \cdots + a_p(\lambda - \lambda_0)^p, \tag{2.4}$$

where a_p is a Taylor series coefficient. However, a major problem of this polynomial is its weak convergence. A large number of terms are required to achieve a specific accuracy for known index of refraction data. The more terms that are added, the more oscillation (or

ripple) can potentially take place. If so, the interpolated index for a given wavelength can have a large error. Thus dispersion formulas that have a small number of terms and that are precise are desirable. However, as shown below the fitting precision can be improved by using more terms.

In this chapter, an adaptive dispersion formula that provides less index fitting error on average is presented and studied [11]. The coefficients of the formula when multiplied by the sag of a lens provide directly the amount of primary, secondary, tertiary, etc. spectra. This decomposition is an insightful way to understand and carry out the correction of chromatic aberration per spectrum order in a lens system.

2.2 Adaptive Dispersion Formula

In this study, the interest in a dispersion formula of the second type is partly motivated by the interest in rationalizing the correction of chromatic aberration. Thus a normalized chromatic coordinate is defined as

$$\Delta\lambda = \frac{\lambda - \lambda_0}{\Lambda}, \tag{2.5}$$

where Λ is a constant and is the larger value of ($\lambda_{max} - \lambda_0$) or ($\lambda_0 - \lambda_{min}$). Here λ_{max} and λ_{min} are the extreme values of wavelength range of interest. This unitless normalized chromatic coordinate $\Delta\lambda$ has a linear relationship with λ, and its value is limited within ± 1. The central value of $\Delta\lambda$, which depends on the reference wavelength $\lambda_{0,}$ is not necessary zero.

Now an adaptive dispersion formula using the normalized chromatic coordinate is defined as

$$n = n_0 + A_1(\Delta\lambda) + A_2(\Delta\lambda)^2 + \cdots + A_q(\Delta\lambda)^q + \frac{A_{q+1}(\Delta\lambda)^{q+1}}{1 + K(\Delta\lambda)}, \tag{2.6}$$

where q is an even positive integer. A_q and K are coefficients that are determined for each specific glass. n_0 is the index of refraction at the reference wavelength λ_0. Equation (2.6) is a polynomial on $\Delta\lambda$, except for the last term. The last term, being odd on $\Delta\lambda$, is keystone distorted. The formula is adaptive because it selects the best keystone distortion coefficient K for a given glass, and also converges by using a small number of coefficients. In practice, as discussed below, only the A_1, A_2, A_3, A_4, A_5 coefficients are used for the correction of chromatic aberrations.

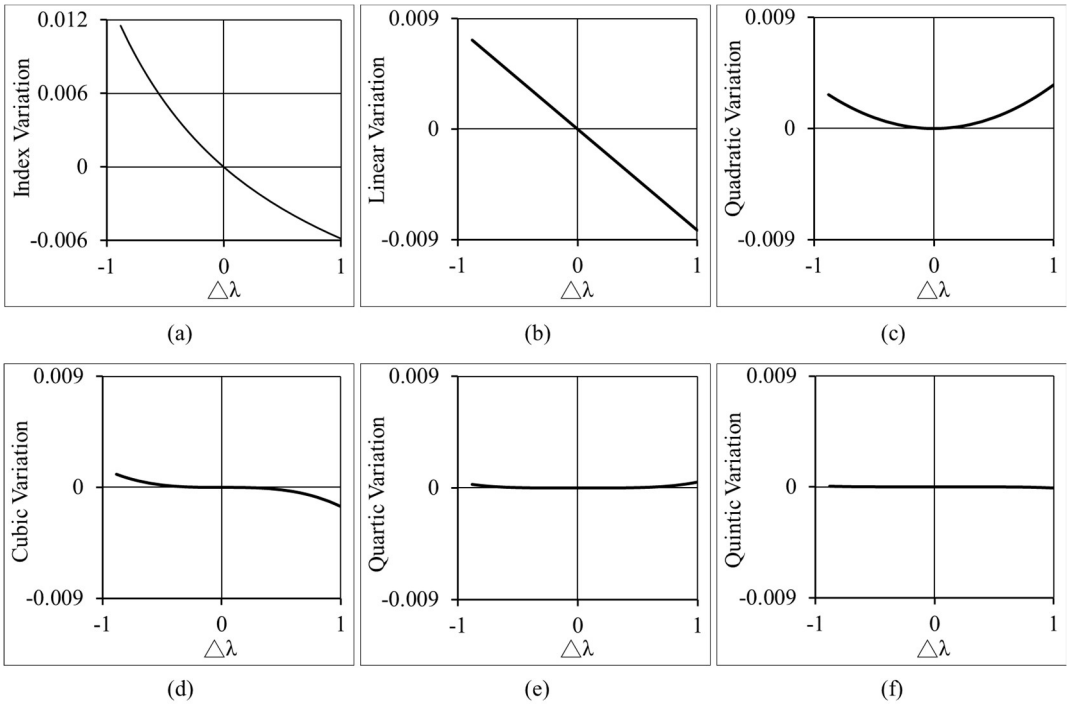

Figure 2.1 Index variation for N-BK7 glass: (a) total variation, (b) linear variation, (c) quadratic variation, (d) cubic variation, (e) quartic variation, and (f) quintic variation.

Figure 2.1 shows graphically how the index of refraction for N-BK7 glass is decomposed with the adaptive dispersion formula. The total index variation is a summation of linear, quadratic, cubic, quartic, and quintic variations, which are drawn at the same scale. The linear term dominates the index variation, and the quadratic term comes second.

2.3 Index Fitting

There are eleven measured indices measured within the visible band for each Schott glass. All the index data can be found in Schott glass catalogue [12]. The eleven values of the measured indices of refraction are assumed to be error free and are used as the target values. One way to fit the dispersion formula to the measured indices of refraction and obtain the dispersion formula coefficients is to apply the least-squares method [13-14]. Here, the refractive index fitting is performed within the commercial lens design software, Zemax OpticStudio, using the built-in orthogonal descent algorithm for optimization. A Zemax macro is written to calculate the RMS differences between the calculated indices and the measured indices, and then return the RMS difference value to the merit function. The dispersion formula coefficients are varied as to minimize the RMS difference and thus the formula coefficients are found.

2.4 Dispersion Formula Fitting Accuracy

First, twenty Schott glasses from each zone in the glass map are selected for studying the accuracy of dispersion formulas. λ_{max} is 0.7065188 μm and λ_{min} is 0.4046561 μm. 0.546074 μm is chosen for λ_0 in both Buchdahl and the adaptive formulas since it can make the formulas converge better. The selected glasses are F2, LF5, LLF1, N-BAF10, N-

BAK4, N-BALF4, N-BASF2, N-BK7, N-FK51A, N-K5, N-KF9, N-KZFS4, N-LAF2, N-LAK9, N-LASF40, N-PK51, N-PSK53A, N-SK16, N-SSK5, and N-SF66. The target fitting indices are the measured indices at wavelengths in the visible range: 0.4046561, 0.4358343, 0.4799914, 0.4861327, 0.546074, 0.5875618, 0.5892938, 0.6328, 0.6438469, 0.6562725, and 0.7065188 μm [12].

A comparison between Sellmeier, Buchdahl, and the adaptive dispersion formulas is presented in Table 2.1. The columns provide the maximum fitting error and RMS fitting error for each dispersion formula. The bottom row of the table provides a summary of the index fitting in average values. Since Schott uses the Sellmeier formula with six coefficients, the six-coefficient adaptive formula and the six-coefficient Buchdahl formula are used for fair comparisons. In order to understand the convergence performances of the adaptive and Buchdahl formulas, the four-coefficient adaptive formula and the four-coefficient Buchdahl formula are also included for comparisons. From the bottom row of the table, the six-coefficient adaptive formula has the smallest fitting errors on average, and the four-coefficient adaptive formula performs similarly in fitting as the Sellmeier formula. The six-coefficient Buchdahl formula (including α as a fitting variable) performs as well as the Sellmeier formula, but the four-coefficient Buchdahl formula has larger fitting errors than the Sellmeier formula. So, the keystone distortion coefficient K does allow the adaptive formula to have smaller fitting errors and less terms. Clearly, the six-coefficient adaptive formula and the four-coefficient adaptive formula provide the best index fitting on average.

Table 2.1 Fitting errors for different dispersion formulas (unit of error: $\times 10^{-6}$)

	Glass	Glascode	Adaptive Formula		Buchdahl		Sellmeier		Adaptive Formula		Buchdahl	
			six coefficients (q=4)		six coefficients (j=5)		six coefficients (i=3)		four coefficients (q=2)		four coefficients (j=3)	
			Max error	RMS error	Max error	RMS error	Max error	RMS error	Max error	RMS error	Max error	RMS error
1	F2	620364.36	3.28	1.66	3.48	1.67	3.67	1.78	3.66	1.78	3.85	1.78
2	LF5	581409.322	3.88	2.27	3.86	2.25	3.90	2.71	3.88	2.28	4.35	2.49
3	LLF1	548458.294	2.10	1.15	5.93	2.88	4.91	2.35	4.24	2.25	6.21	3.31
4	N-BAF10	670471.375	2.22	1.01	3.25	2.15	3.42	2.15	2.27	1.30	6.76	4.13
5	N-BAK4	569560.305	1.52	0.87	1.42	0.86	3.90	2.68	3.30	1.82	7.65	4.93
6	N-BALF4	580539.311	2.43	1.46	3.72	1.57	3.90	2.21	3.12	1.53	8.47	4.57
7	N-BASF2	664360.315	2.61	1.24	2.78	1.29	3.20	1.99	2.96	1.28	2.72	1.62
8	N-BK7	517642.251	1.74	0.91	2.79	1.40	3.64	2.07	3.14	1.81	9.13	6.22
9	N-FK51A	487845.368	2.00	0.98	2.96	1.83	2.95	1.93	2.21	1.63	3.05	1.82
10	N-K5	522595.259	2.98	1.44	3.00	1.41	4.50	2.68	2.80	1.52	9.25	5.90
11	N-KF9	523515.25	3.24	1.89	3.62	2.32	3.69	2.35	3.27	2.34	5.85	3.20
12	N-KZFS4	613445.3	3.21	1.57	3.38	2.08	3.44	2.28	3.19	2.39	6.33	4.28
13	N-LAF2	744449.43	3.48	1.59	5.45	2.13	4.45	2.14	4.18	2.08	8.56	4.63
14	N-LAK9	691547.351	2.18	1.09	2.19	1.08	2.20	1.09	2.27	1.24	8.56	5.41
15	N-LASF40	834373.443	3.38	2.05	5.96	2.59	3.79	2.45	3.67	2.15	7.23	2.61
16	N-PK51	529770.386	3.38	1.92	3.47	1.98	4.25	2.93	3.60	2.10	8.01	4.28
17	N-PSK53A	618634.357	4.38	2.79	5.34	2.84	4.31	2.60	4.29	2.62	6.85	3.27
18	N-SK16	620603.358	2.28	1.14	3.44	1.88	3.68	2.03	2.51	1.98	8.21	5.24
19	N-SSK5	658509.371	3.39	1.78	3.63	1.89	4.90	3.02	4.63	3.14	5.02	3.18
20	N-SF66	923209.4	1.93	1.18	3.01	1.63	4.01	2.60	3.65	1.83	4.12	2.39
Average			2.78	1.50	3.63	1.89	3.83	2.30	3.34	1.95	6.51	3.76

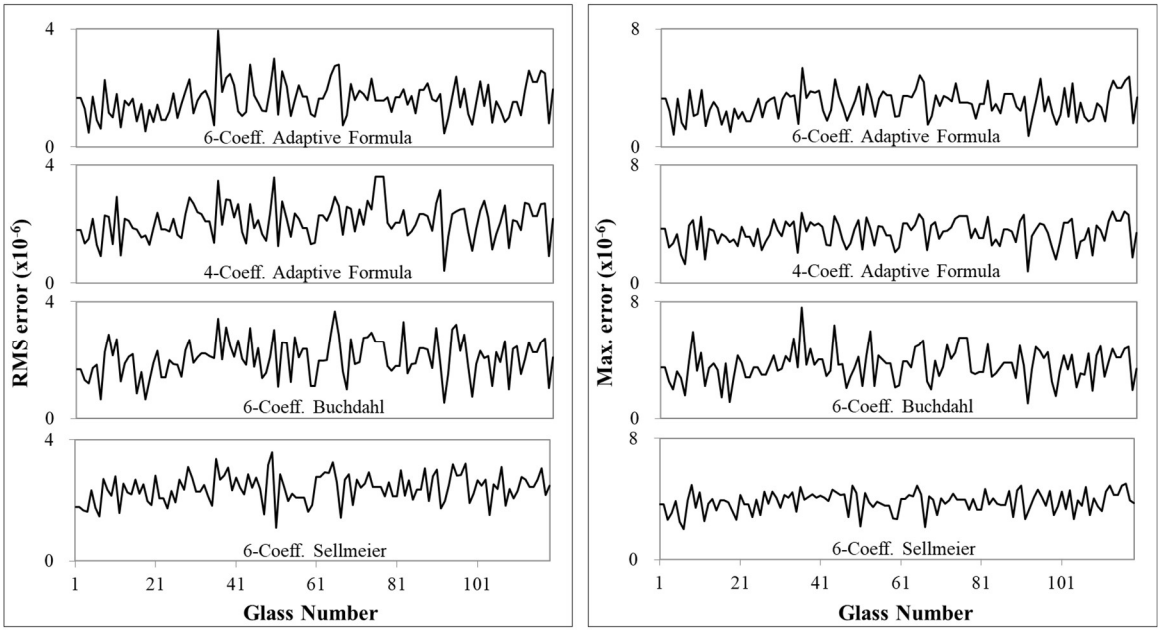

(a) RMS fitting error (b) Maximum fitting error

Figure 2.2 Fitting error graphical analyses

Second, the fitting performances of different dispersion formulas for all 119 glasses in the Schott catalogue [12] are compared. From Figure 2.2 and the table in Appendix A, we find similar results to those in Table 2.1. The six-coefficient adaptive formula is found to be the most accurate, while the four-coefficient adaptive formula is as good as the Sellmeier formula.

Moreover, the six-coefficient Sellmeier formula for N-BK7 glass is fitted with the four and six coefficients adaptive formulas. This is performed by the orthogonal descent algorithm within the lens design software Zemax OpticStudio, and a macro is written to calculate the RMS differences between the indices calculated from Sellmeier and the adaptive formulas. We assume that the 300 indices of refraction calculated from Sellmeier formula in visible band are error free. As shown in Figure 2.3, the maximum fitting errors of the four and six coefficients adaptive formulas are about 5×10^{-7} and 5×10^{-9} respectively. This indicates that the adaptive formulas can substantially mimic the Sellmeier formula. It also shows that including more terms in the adaptive formula can reduce ripple amplitude and improve the fit.

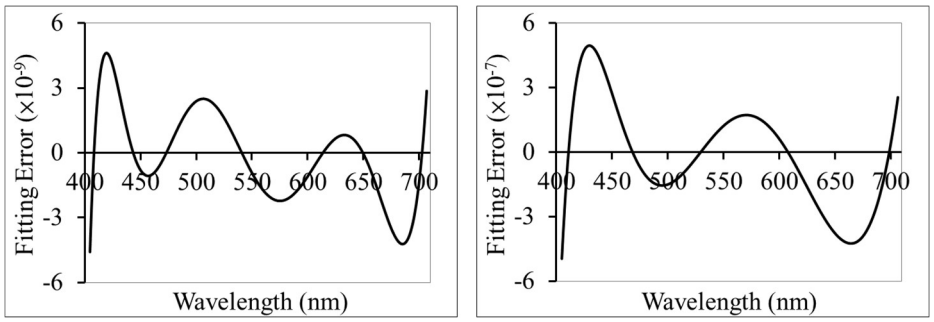

Figure 2.3 Index fitting errors of the adaptive formula for N-BK7 as fitted to the six-coefficient Sellmeier formula: (a) six-coefficient adaptive formula, (b) four-coefficient adaptive formula.

2.5 Correction of Chromatic Change of Focus per Spectrum Order

Another purpose of the adaptive formula is to help us realize the correction of chromatic change of focus per spectrum order. The chromatic change of focus $\partial_\lambda \mathrm{W}_{020}$ aberration (axial color) for a system of N thin lenses in air is given by [15]

$$\begin{aligned}\partial_\lambda \mathrm{W}_{020} &= \sum_{i=1}^{N}\left[\frac{y_i^2}{2}(c_{1i}\text{-}c_{2i})(\mathrm{n}_i\text{ - }\mathrm{n}_{0i})\right] \\ &= \sum_{i=1}^{N}\left[S_i\left(A_{1i}(\Delta\lambda)+A_{2i}(\Delta\lambda)^2+\cdots+A_{qi}(\Delta\lambda)^q+\frac{A_{q+1,i}(\Delta\lambda)^{q+1}}{1+K_i(\Delta\lambda)}\right)\right],\end{aligned} \tag{2.7}$$

where y is the first-order marginal ray height at the thin lens, c_1 and c_2 are the curvatures of the surfaces, and

$$S=\frac{y^2}{2}(c_1-c_2) \tag{2.8}$$

is the thickness variation from the surface sag at height y. Therefore, the chromatic change of focus is proportional to the product of index variation and thickness variation S.

Since the chromatic coordinate $\Delta\lambda$ is dimensionless and normalized to unity, the coefficients A_1, A_2, A_3, A_4, A_5 multiplied by S directly provide the amount of chromatic change of focus as linear, quadratic, cubic, etc. spectra that are contributed by the lens. This aberration is expressed as an optical path difference between the extreme wavelengths 0.4046561 μm and 0.7065188 μm.

For correcting primary, secondary, and tertiary spectra in a system of N thin lenses, for example, we must satisfy

$$\sum_{i=1}^{N} S_i A_{1i} = \sum_{i=1}^{N} S_i A_{2i} = \sum_{i=1}^{N} S_i A_{3i} = 0. \tag{2.9}$$

Clearly, by expressing the index of refraction as a polynomial of the chromatic coordinate $\Delta\lambda$, we can perform the correction of chromatic aberration per order of spectrum. This is an insightful and useful aberration correction decomposition. Appendix B provides the coefficients A_1, A_2, A_3, and K of the four-coefficient adaptive formula for the glasses in Schott catalogue using λ_0 0.546074 μm, λ_{max} 0.7065188 μm, and λ_{min} 0.4046561 μm.

For N-BK7 glass, A_1 is -0.0082 (see the table in Appendix B). Therefore, for a positive lens with a sag of 1 mm at the edge of the aperture, the contribution to primary spectrum as an optical path difference is -0.0082 mm. This can be corrected with a negative lens made out of F2 glass which has a coefficient A_1 -0.0176 and would require a sag value of -0.4688 mm. As another example, the combination of glasses N-FK51A and N-PSK3 can correct for primary and secondary spectra as shown graphically in Figure 2.4. The primary and secondary spectra are almost zero. The residual is dominated by the tertiary spectrum. This correction is done by cancelation of similar spectrum orders contributed by the positive lens N-FK51A with 1 mm sag at the edge of the aperture and the negative lens N-PSK3 with a sag value of -0.6628 mm. From this starting point of thin lenses, a real apochromat with N-FK51A and N-PSK3 thick lenses can be obtained as Figure 2.5(a) and (b). From the chromatic focal shift figure in Figure 2.5(c), the doublet corrects for the primary and secondary spectra.

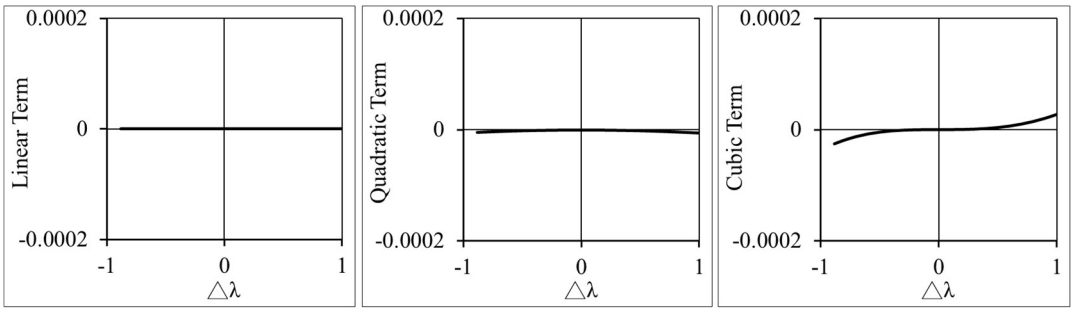

Figure 2.4 Cancelation of primary and secondary spectra in a doublet by using N-FK51A and N-PSK3 glasses: (a) linear term, (b) quadratic term, (c) residual cubic term.

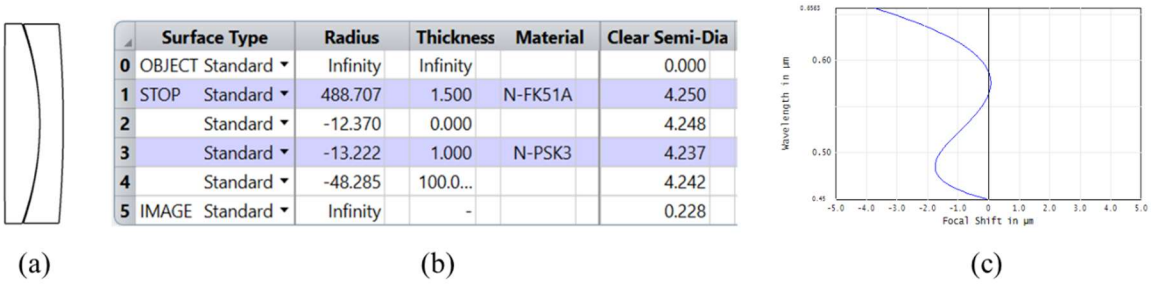

Figure 2.5 Apochromat with N-FK51A and N-PSK3 glasses: (a) layout, (b) lens data, (c) chromatic focal shift

2.6 Conclusions

An adaptive dispersion formula which is essentially a truncated polynomial with one adaptive term is studied. A coefficient *K* in the adaptive term permits the convergence and makes the formula adaptive to each type of glass. Commercial lens design software with built-in orthogonal descent optimization algorithm is used for fitting formula coefficients. An index fitting comparison with 119 glasses in the Schott catalogue and for wavelengths in the visible band is presented. As six coefficients are adopted, the adaptive formula provides an average refractive index error of 2.91×10^{-6}, while Buchdahl formula

and Sellmeier formula have refractive index errors of 3.63×10^{-6} and 3.82×10^{-6} on average respectively. The adaptive formula coefficients when multiplied by the sag of a lens provide directly the amount of chromatic change of focus as primary, secondary, tertiary, etc. spectra. This is an insightful way to understand and carry out the correction of chromatic change of focus aberration. A table of coefficients for Schott glasses and for the four coefficient adaptive formula is also provided.

3. Polarization Aberration Analyses in Plane Symmetric Optical Systems

3.1 Introduction

Light is an electromagnetic wave with polarization properties, and its polarization state may be changed based on the interfaces and properties of the medium it passes through, such as Fresnel effects, thin film coating effects, birefringence of the medium, and birefringence caused by stress. Moreover, the geometry of the lens can also alter coordinate systems and change the polarization state. These could be the origins of polarization aberrations [16].

The first four items are the physical factors, which are related to the refractive indices of material. Refractive index is a complex number (m+ik), where m is the real part of refractive index and k is the extinction coefficient. Dielectric materials have zero or small $|k|$ values, while metals have large $|k|$ values. Figure 3.1 shows the transmittance of the dielectric coating MgF_2 on glass substrate and the reflectance of the metal coating Al on glass substrate with different incident angles of light. Transmittance and reflectance are the ratios of transmitted irradiance and reflected irradiance to incident irradiance, respectively. In the figure, the transmittance, reflectance, and phase all depend on the incident angle and the polarization state of light. The polarization state of light can always be decomposed into two orthogonal eigen states, namely the p and s states. The electric field of p state is oscillating in the plane of incidence, while the electric field of s state is perpendicular to the plane of incidence. The common electric field amplitude of p and s

states is treated as an amplitude aberration contribution (apodization), while the common phase of p and s light is treated as a geometrical wavefront aberration. The difference of transmittance or reflectance between p and s states causes diattenuation, and the difference of phases causes retardance. The reflectance phase difference between p and s states is larger because of a larger magnitude of the extinction coefficient of Al, which is |-6.43| at wavelength 587nm. On the contrary, the transmittance phase difference is small because MgF_2 has zero extinction coefficient. The small phase difference comes from the thin film interference. In general, the larger magnitude of the extinction coefficient, the stronger the light absorption capacity of the material, and the greater the retardance caused.

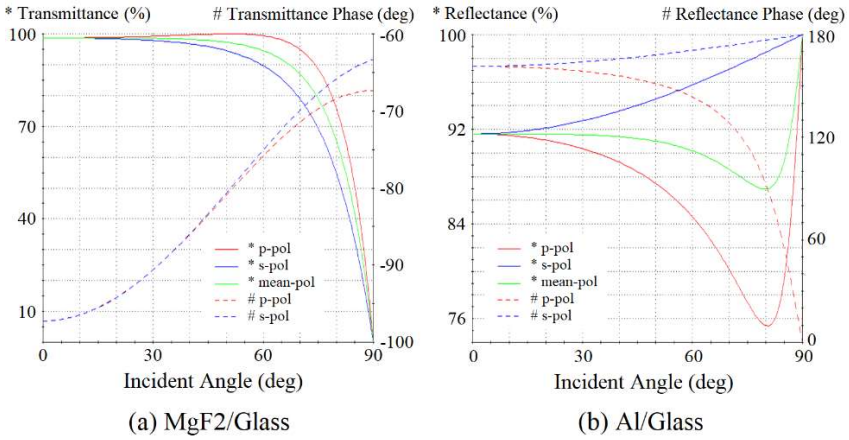

Figure 3.1 Polarization effects from coatings

Birefringence is a unique optical property of material, where the refractive indices can be different along different axes of material. Different indices between axes can change the polarization state and the propagation direction of light. Anisotropic materials, such as crystal and calcite, are intrinsically birefringent [17-18]. Isotropic materials, for example plastics and glasses, are not birefringent, but under thermal strain, mechanical loading, or

mold flow stress, isotropic materials lose their isotropy and become birefringent extrinsically. This effect is called stress induced birefringence [19]. When there are materials with birefringence in an optical system, the polarization effects have to be examined carefully. If the birefringent optical components are not perfectly manufactured or perfectly aligned in the optical system, polarization aberrations will occur and degrade optical system performance, such as MTF.

The geometry of an optical lens can also alter the polarization state of light. Geometrical ray bending, especially for skew rays, will rotate the local x-y coordinates with respect to the global Cartesian coordinates, so that the polarization state at the entrance pupil will be rotated when the ray reaches the exit pupil. This intrinsic geometrical transformation across the pupil is the skew aberration. It occurs even for non-polarizing optical systems. For example, a linear polarized skew ray could be rotated by a few degrees in a high NA system [20-22].

The polarization effects in optical systems have been discussed and analyzed in many literatures [23-30]. Polarization aberrations are the changes in the amplitude, phase, or polarization state associated with light paths between the entrance and the exit pupils of an optical system, which can degrade image quality. Polarization aberrations, whether from physical or geometrical factors, can be calculated and analyzed by several commercially available software, such as CODE V, Zemax, and FRED. The software uses real ray tracing with polarization calculation enabled to get the polarization characteristics of the ray at each interface in the optical system. However, a fundamental understanding and an

analytical form of the polarization aberrations would certainly be a great help to optical design, especially when designing optical systems with high NA values and systems with coatings or mirrors.

Jones vectors and Jones matrices [31-32] have been used in optical systems for polarization ray tracing over the past few decades. The Jones vector describes the electric filed of the light; while the Jones matrix describes polarization effects, such as the Fresnel effects from interfaces, the diattenuation of polarizers, and the retardance of waveplates. Originally, a 2×2 Jones matrix was used to describe the polarization effects in local x-y coordinate system [33-34]. In 1987, Chipman introduced the polarization aberration functions which were calculated by the expanded Jones matrices in terms of Pauli spin matrices [35-38]. The polarization aberration functions were used for isotropic lenses and mirror systems with weak polarization effects in paraxial approximation. Later, Chipman introduced the 3×3 polarization ray tracing matrix [39-40], which utilizes global x-y-z coordinate system to translate polarization effects of polarization sensitive components. This methodology is a new way of doing polarization ray tracing and straightforward. More studies on the three-dimensional polarization ray tracing method were presented and the methods were coded as a CODE V macro and the Polaris-M software [41-44].

Aberration theory provides basic understanding of an optical system, and an effective optimization of an optical system's performance also requires analysis using aberration theory. However, the development of aberration theory is not straightforward, and there is still much to explore. In this chapter, polarization aberration functions for

general plane symmetric optical systems are presented. The background of the new set of polarization aberration functions is reviewed in Section 3.2. An extended derivation of these polarization aberrations is described in Section 3.3. Practical application examples are given in Section 3.4. Finally, conclusions are summarized in Section 3.5.

3.2 Polarization Aberrations in Axial Symmetric Optical Imaging Systems

Recently, Sasián proposed an alternative approach to illustrate the polarization aberrations [45-47]. A set of polarization fields, the $\vec{R}_n$ and $\vec{T}_n$ fields, was also constructed to describe the optical field at the entrance pupil or exit pupil of the optical system as a linear combination of these two basic fields. This whole approach followed the vector expression of Shack's vector wavefront aberration theory, and further extended it to describe the polarization aberrations.

3.2.1 The orthogonal vector fields for describing the polarization fields

In the 1970s, Shack introduced the third-order wavefront aberration theory in vector form for an axial symmetric system at the University of Arizona. In 1988, Sasián adopted the concept of Shack's work and introduced the vector wavefront aberration function for a plane symmetric system, which is written as [48]

$$W\left(\vec{i},\vec{H},\vec{\rho}\right)=\sum_{k,m,n,p,q}^{\infty} W_{\substack{2k+n+p,\\ 2m+n+q,\\ n,p,q}} \left(\vec{H}\cdot\vec{H}\right)^{k}\left(\vec{\rho}\cdot\vec{\rho}\right)^{m}\left(\vec{H}\cdot\vec{\rho}\right)^{n}\left(\vec{i}\cdot\vec{H}\right)^{p}\left(\vec{i}\cdot\vec{\rho}\right)^{q}. \tag{3.1}$$

$\vec{i}$ is the unit vector of the direction of plane of symmetry. It is fixed in orientation, and it defines the coordinate system. $\vec{H}$ and $\vec{\rho}$ are the normalized field and aperture vectors of

the system, respectively. The angles between these three vectors are shown in Figure 3.2. $W_{2k+n+p,2m+n+q,n,p,q}$ is the aberration coefficient with lower indices indicating the powers of H, ρ, $\cos(\theta)$, $\cos(\alpha)$, and $\cos(\beta)$ for a particular aberration term. A set of unit vectors $\vec{j}$, $\vec{h}$, $\vec{k}$, $\vec{r}$, $\vec{t}$ are introduced according to vectors $\vec{i}$, $\vec{H}$, and $\vec{\rho}$. The relationships between these vectors are shown in Figure 3.3. A single ray is defined by a field point at $\vec{H}$ (or $H\vec{h}$) and a pupil point at $\vec{\rho}$ (or $\rho\vec{r}$). Then the vector fields $\vec{R}_n$ are constructed by

$$\vec{R}_n = \vec{\nabla}_\rho W\left(\vec{i}, \vec{H}, \vec{\rho}\right), \tag{3.2}$$

and the vector fields $\vec{T}_n$ are derived by rotating the $\vec{R}_n$ fields by 90 degrees. The $\vec{R}_n$ and $\vec{T}_n$ fields are orthogonal, and the inner products of $\vec{R}_n$ and $\vec{T}_n$ fields are zero, where the subscript n is the field number. This field construction methodology is inspired by the references [49-51]. Figure 3.4 shows the first 18 $\vec{R}_n$ and the first 18 $\vec{T}_n$ fields over the pupil with a specific field vector $\vec{H}$, like the $\vec{R}_2$ field. There are 6 first-order fields and 30 third-order fields. These low order fields are mainly concerned in most of the amplitude polarization aberrations [45-47].

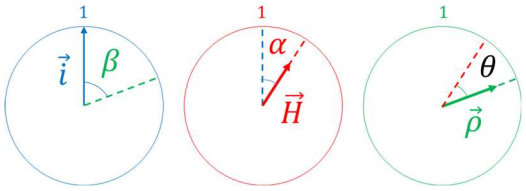

Figure 3.2 Unit vector $\vec{i}$, field vector $\vec{H}$, and aperture vector $\vec{\rho}$

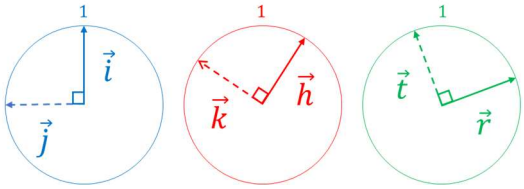

Figure 3.3 Unit vectors $\vec{i}$, $\vec{j}$, $\vec{h}$, $\vec{k}$, $\vec{r}$, and $\vec{t}$. $\vec{i} \perp \vec{j}$, $\vec{h} \perp \vec{k}$, and $\vec{r} \perp \vec{t}$. $\vec{h} \parallel \vec{H}$ and $\vec{r} \parallel \vec{\rho}$

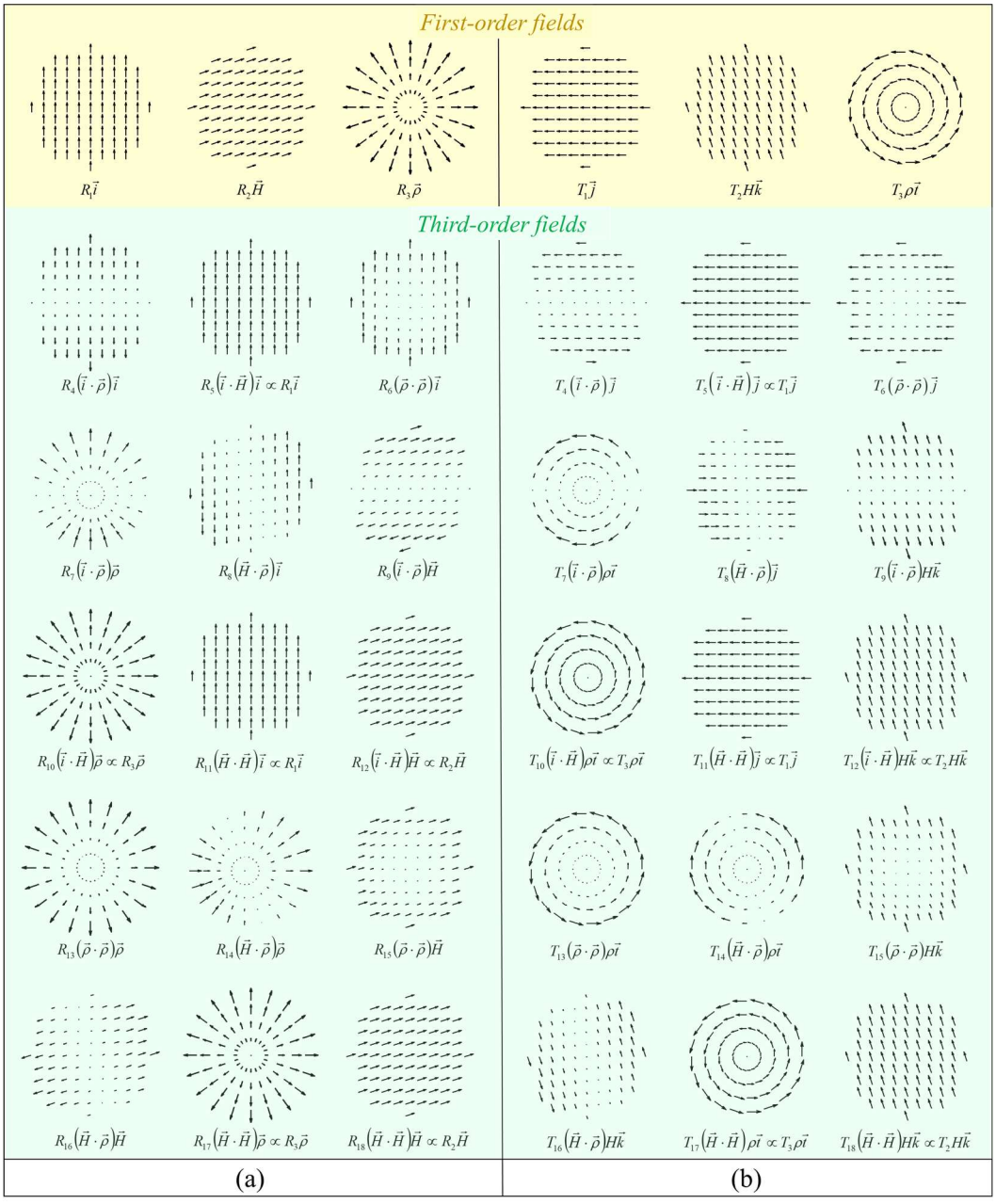

Figure 3.4 Polarization fields up to third order: (a) $\vec{R}_n$ fields and (b) $\vec{T}_n$ fields

3.2.2 Polarization aberration functions for refractive axial symmetric systems

Sasián also introduced the polarization aberration functions of the field and aperture vectors for an axial symmetric optical system under second order approximation [47]. Firstly, the optical field $\vec{E}$ at the entrance pupil of a single spherical optical surface with stop located at the center of curvature, which coincides with the entrance and exit pupil locations, is expressed as

$$\vec{E}\left(\vec{H},\vec{\rho}\right)=\vec{A}\left(\vec{H},\vec{\rho}\right)\exp\left\{i\frac{2\pi}{\lambda}\Phi\left(\vec{H},\vec{\rho}\right)\right\}, \tag{3.3}$$

where $\vec{A}\left(\vec{H},\vec{\rho}\right)$ is the field amplitude describing the polarization state of the optical field. $\vec{A}\left(\vec{H},\vec{\rho}\right)$ is plane symmetric and could be decomposed into a superposition of the $\vec{R}_n$ and $\vec{T}_n$ fields. $\Phi\left(\vec{H},\vec{\rho}\right)$ is the optical phase related to the general wavefront aberrations. The time dependence is neglected here. After refraction from the surface, the on axis optical field $\vec{E}$ is changed to $\vec{E}^*$ based on the Fresnel equations at the exit pupil:

$$\vec{E}^*=\left[t_s\left(\vec{E}\cdot\vec{t}\right)\vec{t}+t_p\left(\vec{E}\cdot\vec{r}\right)\vec{r}\times e^{i\frac{2\pi}{\lambda}\Delta\delta A^2\left(\vec{\rho}\cdot\vec{\rho}\right)}\right]\times e^{i\frac{2\pi}{\lambda}\delta A^2\left(\vec{\rho}\cdot\vec{\rho}\right)}. \tag{3.4}$$

The optical field is simultaneously affected by the diattenuation and retardance at the surface. Here, by using paraxial approximation, the pupils are flat, and the rays are almost parallel to the optical axis. Therefore, the directions of p and s states before and after refraction are $\vec{r}$ and $\vec{t}$, where $\vec{r}$ is the direction of $\vec{\rho}$. Since the surface is a curved surface with curvature *C*, the angle of incidence ϕ across the surface varies linearly with the incident angle *i* of the first-order marginal ray as $\phi\left(\rho\right)=i\rho$. The amplitudes of Fresnel

coefficients, t_s and t_p, of an uncoated surface under second order approximation can be expressed as:

$$t_s = T + TtA^2\left(\vec{\rho}\cdot\vec{\rho}\right), \text{ and} \tag{3.5}$$

$$t_p = T + T\left(t+\Delta t\right)A^2\left(\vec{\rho}\cdot\vec{\rho}\right), \tag{3.6}$$

where $T = \frac{2n}{n+n'}$, $t = \frac{1}{2}\left(\frac{n-n'}{n^2n'}\right)$, $\Delta t = \frac{1}{2}\left(\frac{n-n'}{nn'}\right)^2$, and $A = ni$. T and t are related to apodization, and Δt describes the diattenuation. A is the unitless refraction invariant of the first-order marginal ray. n and n' are the indices of refraction before and after the surface. When the cosine effect of projected area for refraction power is also included, T and t would be modified as $\frac{2\sqrt{nn'}}{n+n'}$ and $-\left(\frac{n-n'}{2nn'}\right)^2$, respectively. The phases of Fresnel coefficients cause the phase of s-polarized light to change by $\frac{2\pi}{\lambda}\delta A^2\left(\vec{\rho}\cdot\vec{\rho}\right)$ and the phase of p-polarized light to change by $\frac{2\pi}{\lambda}(\delta+\Delta\delta)A^2\left(\vec{\rho}\cdot\vec{\rho}\right)$, where δ is the common phase change, and $\Delta\delta$ describes the retardance. δ and $\Delta\delta$ are functions of wavelength, which causes chromatic variations of polarization. δ and $\Delta\delta$ have a unit of length, rather than a unit of angle, because it is more straightforward to describe the properties of δ and $\Delta\delta$ in relation to the wavelength of optical field. Regarding chromatic polarization aberration, it is outside the scope of this dissertation and would not be discussed further. For coated surfaces, the coefficients t_s, t_p, δ, and $\Delta\delta$ can be derived from multilayer coating equations

[52-54] or calculated by fitting the formulas to the data from a thin film design program. Figure 3.5 shows the Fresnel coefficients under second order approximation.

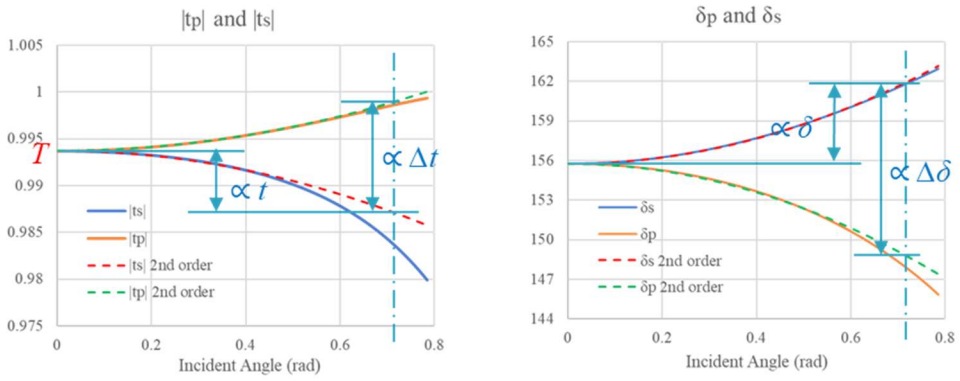

(a) (b)

Figure 3.5 Fresnel coefficients under second order approximation: (a) amplitude and (b) phase

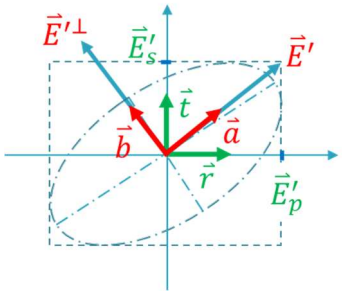

Figure 3.6 The unit vectors $\vec{a}$ and $\vec{b}$

If retardance $\Delta\delta$ is not present, $\vec{E}^*$ becomes $\vec{E}'$, and Eq. (3.4) can be rewritten as

$$\vec{E}' = \left[T\vec{E} + TtA^2 \left(\vec{\rho} \cdot \vec{\rho} \right) \vec{E} + T\Delta tA^2 \left(\vec{E} \cdot \vec{\rho} \right) \vec{\rho} \right] \times e^{i\frac{2\pi}{\lambda}\delta A^2 (\vec{\rho} \cdot \vec{\rho})}. \tag{3.7}$$

The polarization state of $\vec{E}'$ is linear polarized. The directions of the first two items are parallel to $\vec{E}$. However, the presence of the third item, which is the diattenuation term, would alter the polarization state and make $\vec{E}'$ no longer parallel to $\vec{E}$. Thus, a unit vector $\vec{a}$ parallel to $\vec{E}'$, and a unit vector $\vec{b}$ perpendicular to $\vec{E}'$ are defined and shown in Figure

3.6. $\vec{E}'$ could be written as $\left|\vec{E}'\right|\vec{a}$, and $\vec{E}'^{\perp}$ is created as $\left|\vec{E}'\right|\vec{b}$. With this new orthogonal system $\vec{a}$ and $\vec{b}$, the optical field $\vec{E}^{*}$ (as the ellipse in Figure 3.6) can be split into a component $\vec{E}_1^{o}$ parallel to $\vec{a}$ and a component $\vec{E}_1^{e}$ parallel to $\vec{b}$:

$$\begin{aligned}\vec{E}_1^{o} &= \sqrt{\cos^2\left[\frac{\pi}{\lambda}\Delta\delta A^2\left(\vec{\rho}\cdot\vec{\rho}\right)\right]+\sin^2\left[\frac{\pi}{\lambda}\Delta\delta A^2\left(\vec{\rho}\cdot\vec{\rho}\right)\right]\left[\left(\vec{a}\cdot\vec{r}\right)^2-\left(\vec{a}\cdot\vec{t}\right)^2\right]^2}\ \vec{E}' \\ &\quad\times e^{i\frac{\pi}{\lambda}\Delta\delta A^2\left(\vec{\rho}\cdot\vec{\rho}\right)}\times e^{i\tan^{-1}\left\{\tan\left[\frac{\pi}{\lambda}\Delta\delta A^2\left(\vec{\rho}\cdot\vec{\rho}\right)\right]\times\left[\left(\vec{a}\cdot\vec{r}\right)^2-\left(\vec{a}\cdot\vec{t}\right)^2\right]\right\}} \\ &\cong \vec{E}'\cdot e^{i\frac{2\pi}{\lambda}\Delta\delta A^2\left(\vec{a}\cdot\vec{\rho}\right)^2},\end{aligned} \tag{3.8}$$

and

$$\begin{aligned}\vec{E}_1^{e} &= \left[2\left(\vec{a}\cdot\vec{r}\right)\left(\vec{b}\cdot\vec{r}\right)\right]\sin\left[\frac{\pi}{\lambda}\Delta\delta A^2\left(\vec{\rho}\cdot\vec{\rho}\right)\right]\vec{E}'^{\perp}\cdot e^{i\frac{\pi}{\lambda}\Delta\delta A^2\left(\vec{\rho}\cdot\vec{\rho}\right)+i\frac{\pi}{2}} \\ &\cong \left[\frac{2\pi}{\lambda}\Delta\delta A^2\left(\vec{a}\cdot\vec{\rho}\right)\left(\vec{b}\cdot\vec{\rho}\right)\right]\vec{E}'^{\perp}\cdot e^{i\frac{\pi}{\lambda}\Delta\delta A^2\left(\vec{\rho}\cdot\vec{\rho}\right)+i\frac{\pi}{2}}.\end{aligned} \tag{3.9}$$

The approximate values are calculated from the second-order approximation. The superscripts *o* and *e* have nothing to do with the ordinary and extraordinary rays in anisotropic materials. When the optical axis of the uniaxial birefringent component coincides with the symmetry axis of the optical system containing this component, Eq. (3.8) and Eq. (3.9) are like to describe the electric field distribution of light in such a system. In this chapter, *o* is in the direction without retardance, and *e* is perpendicular to *o.* If the sinusoidal functions in Eq. (3.8) and Eq. (3.9) are kept without making too many approximations, the isogyres of birefringent materials are clearly visible after some calculations simulating the cross-polarizer effect [55].

After performing stop shifting, $\vec{E}_1^o$ and $\vec{E}_1^e$ fields for a single surface system with a general stop location are derived. Then Sasián deducted the final orthogonal optical fields, $\vec{E}^o$ and $\vec{E}^e$, and the polarization aberration functions at the exit pupil for an axial symmetric optical system with *q* surfaces. Second order approximation is used to simplify the derivation of formulas [47]. $\vec{E}^o$ and $\vec{E}^e$ are

$$\vec{E}^o\left(\vec{H},\vec{\rho}\right)=\vec{A}'\left(\vec{H},\vec{\rho}\right)\cdot e^{i\frac{2\pi}{\lambda}\left[\Phi\left(\vec{H},\vec{\rho}\right)+\delta\left(\vec{H},\vec{\rho}\right)+\Delta\delta_b\left(\vec{H},\vec{\rho}\right)\right]}, \tag{3.10}$$

and

$$\vec{E}^e\left(\vec{H},\vec{\rho}\right)=\left[\frac{2\pi}{\lambda}\Delta\delta_c\left(\vec{H},\vec{\rho}\right)\right]\vec{A}'^{\perp}\left(\vec{H},\vec{\rho}\right)\cdot e^{i\frac{2\pi}{\lambda}\left[\Phi\left(\vec{H},\vec{\rho}\right)+\delta\left(\vec{H},\vec{\rho}\right)+\frac{1}{2}\Delta\delta_a\left(\vec{H},\vec{\rho}\right)+\frac{\lambda}{4}\right]}, \tag{3.11}$$

where $\vec{A}'\left(\vec{H},\vec{\rho}\right)$ is the field amplitude function at the exit pupil

$$\vec{A}'\left(\vec{H},\vec{\rho}\right)=\left\{\begin{array}{c} P_0\vec{A}+P_1\left(\vec{\rho}\cdot\vec{\rho}\right)\vec{A}+P_2\left(\vec{H}\cdot\vec{\rho}\right)\vec{A}+P_3\left(\vec{H}\cdot\vec{H}\right)\vec{A}+ \\ \Delta P_1\left(\vec{A}\cdot\vec{\rho}\right)\vec{\rho}+\Delta P_2\left[\left(\vec{A}\cdot\vec{H}\right)\vec{\rho}+\left(\vec{A}\cdot\vec{\rho}\right)\vec{H}\right]+\Delta P_3\left(\vec{A}\cdot\vec{H}\right)\vec{H} \end{array}\right\}, \tag{3.12}$$

and $\vec{A}'^{\perp}\left(\vec{H},\vec{\rho}\right)$ is $\left|\vec{A}'\left(\vec{H},\vec{\rho}\right)\right|\vec{b}$. $\vec{A}$ is the field amplitude at the entrance pupil of the optical system with *q* surfaces. P_0, P_1, P_2, and P_3 are the polarization aberration coefficients for constant piston, defocus, tilt, and quadratic piston common apodizations. These are scalar aberrations and are independent of the polarization state of the incoming field $\vec{A}$. On the other hand, ΔP_1, ΔP_2, and ΔP_3 are the polarization aberration coefficients for diattenuations. These terms are vector aberrations and are dependent of the polarization state of the incoming field $\vec{A}$ from Eq. (3.12). They alter the orientation of the incoming field $\vec{A}$. All these polarization aberration coefficients are listed in Table 3.1. $\overline{A}$ in Table 3.1 is the

unitless refraction invariant of the first-order chief ray, and $\overline{i}$ is the paraxial angle (slope) of incidence of chief ray at a given surface. $\overline{u}$ and $\overline{y}$ are the chief ray slope and the chief ray heigh at the surface, respectively. *u* and *y* are the same quantities relative to the marginal ray. *C* is the curvature of the surface.

In Eqs. (3.10) and (3.11), $\delta\left(\vec{H},\vec{\rho}\right)$ represents the phase change common to $\vec{E}^o$ and $\vec{E}^e$ fields, while $\Delta\delta_a\left(\vec{H},\vec{\rho}\right)$ and $\Delta\delta_b\left(\vec{H},\vec{\rho}\right)$ are the retardance functions of $\vec{E}^e$ and $\vec{E}^o$ fields, respectively. $\Delta\delta_c\left(\vec{H},\vec{\rho}\right)$ is also a retardance function. However, the difference is that it does not affect the phase, but the amplitude of the $\vec{E}^e$ field. These four functions at the exit pupil are defined as

$$\delta\left(\vec{H},\vec{\rho}\right)=\delta_1\left(\vec{\rho}\cdot\vec{\rho}\right)+\delta_2\left(\vec{H}\cdot\vec{\rho}\right)+\delta_3\left(\vec{H}\cdot\vec{H}\right), \tag{3.13}$$

$$\Delta\delta_a\left(\vec{H},\vec{\rho}\right)=\Delta\delta_1\left(\vec{\rho}\cdot\vec{\rho}\right)+2\Delta\delta_2\left(\vec{H}\cdot\vec{\rho}\right)+\Delta\delta_3\left(\vec{H}\cdot\vec{H}\right), \tag{3.14}$$

$$\Delta\delta_b\left(\vec{H},\vec{\rho}\right)=\Delta\delta_1\left(\vec{a}\cdot\vec{\rho}\right)^2+2\Delta\delta_2\left(\vec{a}\cdot\vec{H}\right)\left(\vec{a}\cdot\vec{\rho}\right)+\Delta\delta_3\left(\vec{a}\cdot\vec{H}\right)^2, \tag{3.15}$$

and

$$\begin{aligned}\Delta\delta_c\left(\vec{H},\vec{\rho}\right)=\Delta\delta_1\left(\vec{a}\cdot\vec{\rho}\right)\left(\vec{b}\cdot\vec{\rho}\right)+\Delta\delta_2\left(\vec{a}\cdot\vec{\rho}\right)\left(\vec{b}\cdot\vec{H}\right)+\\ \Delta\delta_2\left(\vec{a}\cdot\vec{H}\right)\left(\vec{b}\cdot\vec{\rho}\right)+\Delta\delta_3\left(\vec{a}\cdot\vec{H}\right)\left(\vec{b}\cdot\vec{H}\right).\end{aligned} \tag{3.16}$$

From Eq. (3.13) to Eq. (3.16), it is easy to find that $\delta\left(\vec{H},\vec{\rho}\right)$ and $\Delta\delta_a\left(\vec{H},\vec{\rho}\right)$ have nothing to do with the polarization state of the incoming field $\vec{A}$, while $\Delta\delta_b\left(\vec{H},\vec{\rho}\right)$ and $\Delta\delta_c\left(\vec{H},\vec{\rho}\right)$ are relevant because of the presence of $\vec{a}$ in them. δ_1, δ_2, and δ_3 are the

polarization aberration coefficients for defocus, tilt, and quadratic piston common phase changes, which change the first order properties of the optical system. $\Delta\delta_1$, $\Delta\delta_2$, and $\Delta\delta_3$ are the polarization aberration coefficients for retardance. All these polarization aberration coefficients are listed in Table 3.1, too.

3.2.3 Polarization aberration functions for reflective axial symmetric systems

In all axial symmetric imaging systems, not only lenses but also mirrors are the main components. There are many famous mirror systems, such as Schmidt camera, Gregorian telescope, and Cassegrain telescopes. Therefore, a set of similar polarization aberration functions for mirror systems are necessary.

Following the content in Section 3.2.2, the optical field $\vec{E}$ at the entrance pupil is expressed as Eq. (3.3). After reflection from the surface, the on axis optical field $\vec{E}$ is changed to $\vec{E}^*$ based on the Fresnel equations at the exit pupil:

$$\vec{E}^* = \left[r_s \left(\vec{E} \cdot \vec{t} \right) \vec{t} + r_p \left(\vec{E} \cdot \vec{r} \right) \vec{r} \times e^{i\frac{2\pi}{\lambda}\Delta\delta A^2(\vec{\rho}\cdot\vec{\rho})} \right] \times e^{i\frac{2\pi}{\lambda}\delta A^2(\vec{\rho}\cdot\vec{\rho})}. \tag{3.17}$$

The amplitudes of Fresnel coefficients, r_s and r_p, of an uncoated surface under second order approximation are:

$$r_s = R + RrA^2 \left(\vec{\rho} \cdot \vec{\rho} \right), \text{ and} \tag{3.18}$$

$$r_p = R + R\left(r + \Delta r \right) A^2 \left(\vec{\rho} \cdot \vec{\rho} \right), \tag{3.19}$$

where $R=\frac{n-n'}{n+n'}$, $r=\frac{1}{nn'}$, $\Delta r=-\frac{2}{nn'}$, and $A=ni$. R and r are related to apodization, and Δr describes the diattenuation. For reflection, the reflectance is the sum of r_s^2 and r_p^2. Unlike transmittance, it does not contain the cosine factor. So, there is no need to modify the R and r coefficients when the energy conservation is taken into account. The phases of Fresnel coefficients cause the phase of s-polarized light to change by $\frac{2\pi}{\lambda}\delta A^2\left(\vec{\rho}\cdot\vec{\rho}\right)$ and the phase of p-polarized light to change by $\pi+\frac{2\pi}{\lambda}(\delta+\Delta\delta)A^2\left(\vec{\rho}\cdot\vec{\rho}\right)$, where δ is the common phase change, and $\Delta\delta$ describes the retardance. The π phase shift for the p-polarized light after reflection is added in order to maintain the right-hand rule, which is not an aberration and is neglected in this dissertation.

For an uncoated mirror with refractive index (m+ik), the coefficients R, r, Δr, δ, and $\Delta\delta$ can be further deduced. By replacing n' in Fresnel reflection equation with m+ik, simplifying the real and imaginary parts separately, and calculating the amplitude and phase of this complicated complex number with second order approximation, it is not difficult to get the coefficients: $R=\sqrt{\frac{(n-m)^2+k^2}{(n+m)^2+k^2}}$, $r=\frac{m}{n(m^2+k^2)}$, $\Delta r=-\frac{2m}{n(m^2+k^2)}$, $\delta=-\frac{k}{n(m^2+k^2)}$, and $\Delta\delta=\frac{2k}{n(m^2+k^2)}$. There is a common piston phase $\frac{2kn}{m^2+k^2-n^2}$ for s-polarized light and p-polarized light, and it will be neglected here. For coated surfaces, it is easier to calculate the coefficients by fitting the formulas to the data from a thin film design program.

Since the equations of r_s and r_p are in the same form as the equations of t_s and t_p, the following derivation will be exactly the same as the derivation of the refractive optical system. The final polarization aberration functions of the reflective system are similar to that of the refractive system, as long as T is replaced by R, t is replaced by r, and Δt is replaced by Δr. The coefficients for reflective surfaces are added into Table 3.1, too. When an optical system has both reflective and refractive optics, the polarization aberration coefficients are still calculated as the sum of the contributions from each surface, while T and R are the product of the contributions from each surface. Taking the Cassegrain telescope as an example, Figure 3.7 shows that the basic structure of this telescope is a set of reflectors plus an eyepiece, and this system has four surfaces, two of which are reflective and two of which are refractive. The P_1 coefficient is calculated as

$$R_1 R_2 T_3 T_4 \left(r_1 A_1^2 + r_2 A_2^2 + t_3 A_3^2 + t_4 A_4^2 \right). \tag{3.20}$$

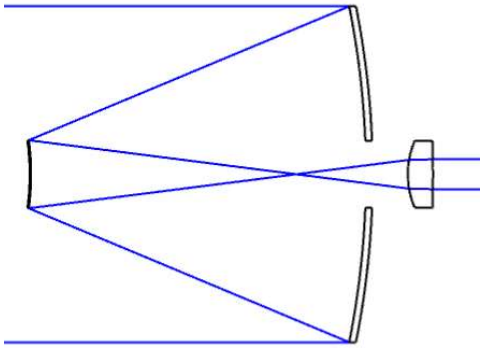

Figure 3.7 Cassegrain telescope with eyepiece

This new approach proposed by Sasián to describe the polarization aberrations is based on the assumptions of paraxial approximation and second order approximation. Also, absorption and dichroism of light are neglected. The advantage under these assumptions is

that the polarization aberrations of the entire system are the sum of the polarization aberrations of the individual surfaces. All the polarization coefficients can be calculated from the first-order ray tracing data and the system structure parameters. These make the polarization coefficients similar to the Seidel coefficients of wavefront aberrations. This method is applicable to axial symmetric optical systems with spherical or slightly aspherical surfaces. The polarization state distribution of the incident optical field over the pupil can be plane symmetric, double plane symmetric or axial symmetric with respect to the optical axis of the system. For most of the optical systems the polarization aberrations are usually much smaller than the general wavefront aberrations. In many cases an approximate low order expansion of polarization aberrations is more useful than the exact value because the low order terms dominate.

Table 3.1 Polarization aberration coefficients for an axial symmetric optical system with q surfaces

$P_0 = T_q$	constant piston apodization	$\delta_1 = \sum_{j=1}^{q}\left(\delta A^2\right)_j$	defocus phase change
$P_1 = T_q\sum_{j=1}^{q}\left(tA^2\right)_j$	defocus apodization	$\delta_2 = 2\sum_{j=1}^{q}\left(\delta A\bar{A}\right)_j$	tilt phase change
$P_2 = 2T_q\sum_{j=1}^{q}\left(tA\bar{A}\right)_j$	tilt apodization	$\delta_3 = \sum_{j=1}^{q}\left(\delta \bar{A}^2\right)_j$	quadratic piston phase change
$P_3 = T_q\sum_{j=1}^{q}\left(t\bar{A}^2\right)_j$	quadratic piston apodization	$\Delta\delta_1 = \sum_{j=1}^{q}\left(\Delta\delta A^2\right)_j$	
$\Delta P_1 = T_q\sum_{j=1}^{q}\left(\Delta tA^2\right)_j$		$\Delta\delta_2 = \sum_{j=1}^{q}\left(\Delta\delta A\bar{A}\right)_j$	
$\Delta P_2 = T_q\sum_{j=1}^{q}\left(\Delta tA\bar{A}\right)_j$		$\Delta\delta_3 = \sum_{j=1}^{q}\left(\Delta\delta \bar{A}^2\right)_j$	
$\Delta P_3 = T_q\sum_{j=1}^{q}\left(\Delta t\bar{A}^2\right)_j$		$T_q = \prod_{j=1}^{q}\left(\frac{2n}{n+n'}\right)_j$	$\left(\text{or } \prod_{j=1}^{q}\left(\frac{2\sqrt{nn'}}{n+n'}\right)_j \text{ power transmission effect included}\right)$
$A_j = \left(ni\right)_j = \left(nu + nyC\right)_j$		$t_j = \frac{1}{2}\left(\frac{n-n'}{n^2n'}\right)_j$	$\left(\text{or } -\left(\frac{n-n'}{2nn'}\right)_j^2 \text{ power transmission effect included}\right)$
$\bar{A}_j = \left(n\bar{i}\right)_j = \left(n\bar{u} + n\bar{y}C\right)_j$		$\Delta t_j = \frac{1}{2}\left(\frac{n-n'}{nn'}\right)_j^2$	
$R_q = \prod_{j=1}^{q}\left(\sqrt{\frac{(n-m)^2+k^2}{(n+m)^2+k^2}}\right)_j$		$\delta_j = \left(-\frac{k}{n\left(m^2+k^2\right)}\right)_j$	
$r_j = \left(\frac{m}{n\left(m^2+k^2\right)}\right)_j$		$\Delta\delta_j = \left(\frac{2k}{n\left(m^2+k^2\right)}\right)_j$	
$\Delta r_j = \left(-\frac{2m}{n\left(m^2+k^2\right)}\right)_j$		*For uncoated mirror surfaces*	

3.3 Polarization Aberrations in Plane Symmetric Optical Imaging Systems

An axial symmetric optical system does not change its characteristics when it is rotated at any angle with respect to the optical axis of the system. It only has an axial symmetric wavefront deformation for an object point on axis. Most of the optical systems are axial symmetric, such as objective lenses, camera lenses, and Maksutov telescope. The surfaces of optical components could be spherical or aspherical. When the degrees of symmetry are reduced, it becomes a double-plane symmetric optical system, which is symmetric about two orthogonal planes, for instance x-z and y-z planes [56-58]. That is to say, the right half of the system characteristics would be the same as the left half, while the upper half of the system characteristics would be the same as the lower half as the optical axis is along the z axis. A famous example of double-plane symmetric system is the anamorphic camera lens. When the degrees of symmetry are further reduced, it becomes a plane symmetric optical system that is symmetric about one plane, for example the y-z plane [59-60]. One half of the system is a mirror image of the other half. Scheimpflug camera is a typical example. On the other hand, a system constructed by an eccentric or off-axis section of an axial symmetric optical system is sometimes treated as a plane symmetric system as well. However, this kind of system has an inherent axis of symmetry that passing through the centers of curvature of all components [61]. Essentially, it is still a type of the axial symmetric system. The aberrations of such system can be calculated from the equivalent axial symmetric system and then choosing the specific portion of the aperture [38, 62].

In general, double-plane symmetry is a special case of plane symmetry, and axial symmetry is a special case of double-plane symmetry. When the symmetry is reduced, more aberration terms will be generated. Figure 3.8 illustrates the symmetry of optical systems and the corresponding examples.

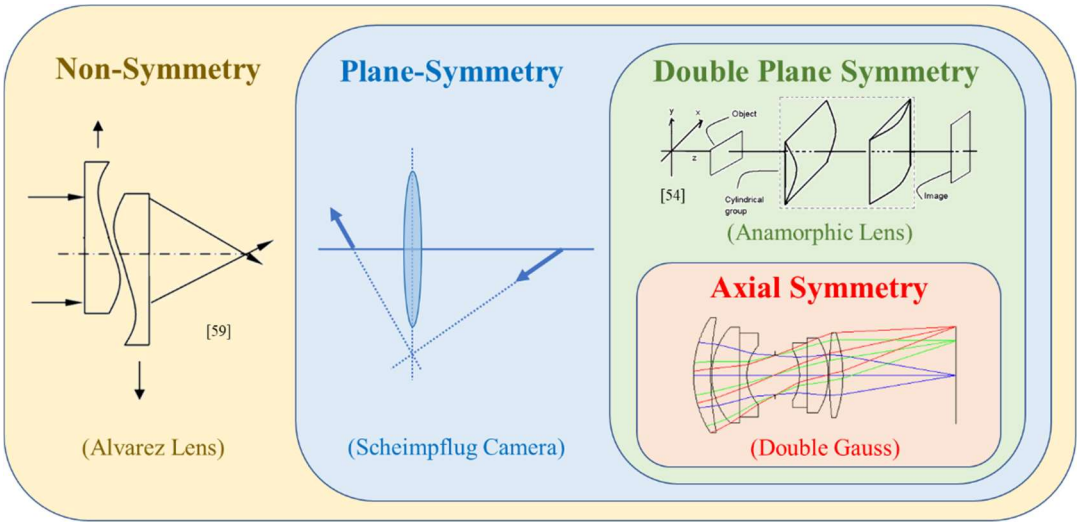

Figure 3.8 The symmetry of an optical system and examples

Recently, more and more optical systems have adopted non-symmetric designs to achieve better image quality and to reduce the number of elements in the system. There are a lot of literature discussing the non-symmetric optical systems, and several aberration functions had been proposed to compare with the traditional axial symmetric aberration functions. An example of the non-symmetric system is the Alvarez lens [63], which is often used to adjust the focal length. A significant step was carried out by Buchroeder in 1976 [64]. He introduced the aberration theory for tilted component optical systems. Each component in the system is axial symmetric and can be tilted in any direction about its nodal point so that a ray is not deviated but slightly shifted after passing through the

component. Later Shack and Thompson [65-70] developed the wavefront aberration function for tilted and decentered optical component systems in vector form as

$$W\left(\vec{H},\vec{\rho}\right)=\sum_{j}\sum_{p,n,m}^{\infty}\left(W_{k,l,m}\right)_{j}\left[\left(\vec{H}-\vec{\sigma}_{j}\right)\cdot\left(\vec{H}-\vec{\sigma}_{j}\right)\right]^{p}\left(\vec{\rho}\cdot\vec{\rho}\right)^{n}\left[\left(\vec{H}-\vec{\sigma}_{j}\right)\cdot\vec{\rho}\right]^{m}, \qquad (3.21)$$

where j specifies the disturbed component, and $\vec{\sigma}_j$ is the normalized field displacement vector from the tilted and decentered component j. This vector wavefront aberration theory, also known as the nodal aberration theory, is applied broadly in optical engineering. The main idea to convert the axial symmetric aberration function into a non-symmetric aberration function is to replace the field vector $\vec{H}$ with the effective field vector $(\vec{H}-\vec{\sigma})$ in the axial symmetric aberration function. When there is only one component tilted and decentered or there are multiple components tilted and decentered in the same direction in an axial symmetric system, the system becomes a plane symmetric system. Figure 3.9 is a schematic diagram illustrating that the center of aberration field changes with the field displacement vector $\vec{\sigma}$ for a plane symmetric system. However, an axial symmetric system could turn into non-symmetric if the components are tilted and decentered in multiple directions. Figure 3.10 shows that different directions of $\vec{\sigma}_j$ may cause no symmetry in the system. Based on the work from Thompson, Moore et al. further extended Sasián's aberration function [71] for plane symmetric systems into an aberration function of non-symmetric systems [72].

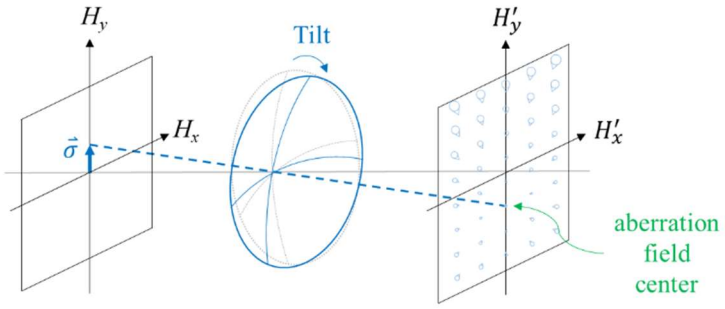

Figure 3.9 Schematic diagram of the field displacement caused by the tilt of a single surface

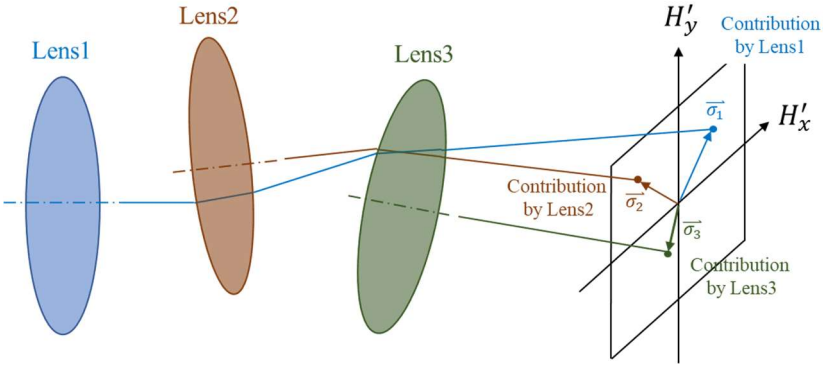

Figure 3.10 Schematic diagram of the field displacements caused by the tilts of multiple lenses

The derivations of wavefront aberration functions for plane symmetric [48] and non-symmetric systems [66] could be applied to the derivation of polarization aberration function for plane symmetric systems. McGuire and Chipman followed the work of Buchroeder and introduced the polarization aberration finctions of tilted and decentered optical systems [38]. In this section, the applicability of the polarization aberration functions in Section 3.2 will be extended to plane symmetric optical systems, using the method of Buchroeder. The optical field is also plane symmetric, and it can be decomposed by the $\vec{R}_n$ and $\vec{T}_n$ fields.

As shown in Figure 3.2, the three vectors $\vec{i}$, $\vec{H}$, and $\vec{\rho}$ are utilized to describe a ray in a plane symmetric optical system. $\vec{i}$ is the unit vector of the direction of plane of symmetry. $\vec{i}$ is a fixed direction in the first and second quadrants, and it is usually defined as the +y direction (0,1). In this case, the plane of symmetry is the y-z plane.

In order to describe the optical system, a reference must be established. All the aberration functions are expanded based on this reference. In an axial symmetric system, the reference is the optical axis. For a plane symmetric optical system, this reference is a selected ray called the optical axis ray (OAR), which proporgates in the plane of symmetry. The three vectors $\vec{i}$, $\vec{H}$, and $\vec{\rho}$ are all perpendicular to the OAR with their feet located on the OAR. When looking towards the OAR, the distribution of these three vectors is shown in Figure 3.11. The OAR would pass through the center of the field of view and the center of the pupils. The aperture stop is assumed to be circular, perpendicular to the OAR, and centered on the OAR. Although the field vector $\vec{H}$ is perpendicular to the OAR, the object plane and the image plane may not be perpendicular to the OAR due to the Scheimpflug principle. The pupils may not be perpendicular to the OAR either as shown in Figure 3.12.

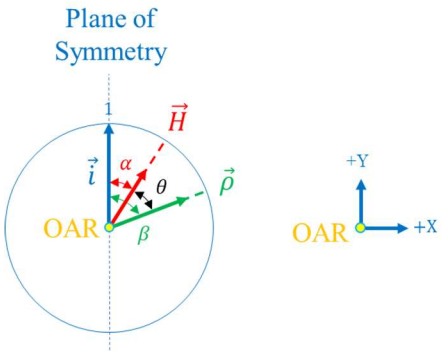

Figure 3.11 Unit vector $\vec{i}$, field vector $\vec{H}$, and aperture vector $\vec{\rho}$ with OAR

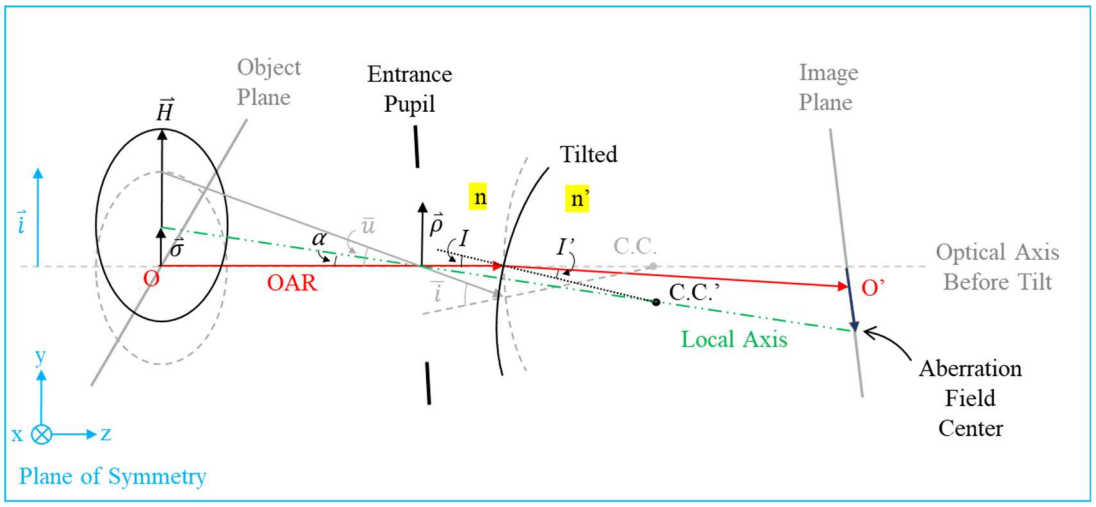

Figure 3.12 Plane symmetric system with one tilted surface

Figure 3.12 shows an axial symmetric system with a spherical surface in gray dash lines. This unperturbed system has an optical axis along the +z axis. The slope of the chief ray is $\bar{u}$, and the incident angle of chief ray at the surface is $\bar{i}$. When the surface is tilted clockwise about the x axis as shown in black solid line, the system becomes plane symmetric with the direction of the plane of symmetry $\vec{i}$ in +y direction. The plane of symmetry, which is also the tangential plane, would be the y-z plane. The sagittal plane would be a set of planes containing the OAR and perpendicular to the tangential plane. The OAR is incident on the surface at an angle of incidence *I* and an angle of refraction *I'*. The tilt of the surface leads to a field displacement $\vec{\sigma}$ in the +y direction, i.e., the $\vec{i}$ direction. The local axis, which is the axis of symmetry, is defined as an axis passing through the top of $\vec{\sigma}$, the center of the pupil, and the center of curvature of the tilted surface. α is the slope of the local axis with respect to the original optical axis. In axial symmetry systems, the OAR and the local axis coincide, where the common axis is the optical axis.

Buchroeder performs aberration expansion based on the local axis so that the effective field vector is $(\vec{H}-\vec{\sigma})$, where $\vec{\sigma}$ is

$$\vec{\sigma}=\left(\frac{\alpha}{\bar{u}}\right)\vec{i}=\left(\frac{I}{\bar{i}}\right)\vec{i}\cong\left(\frac{n\sin I}{n\sin\bar{i}}\right)\vec{i}=\left(\frac{\bar{A}_0}{\bar{A}}\right)\vec{i}. \tag{3.22}$$

In Eq. (3.22), $\vec{\sigma}$ is normalized by $\vec{i}$. $\bar{A}$ is the refraction invariant of chief ray before surface tilt, and $\bar{A}_0$ is defined as $n\sin(I)$. When the aberration expansion is made based on the OAR, the effective field vector would be $(\vec{H}+\vec{\sigma})$. Figure 3.13 shows the effective field vectors for the field vector $\vec{H}$ in general direction.

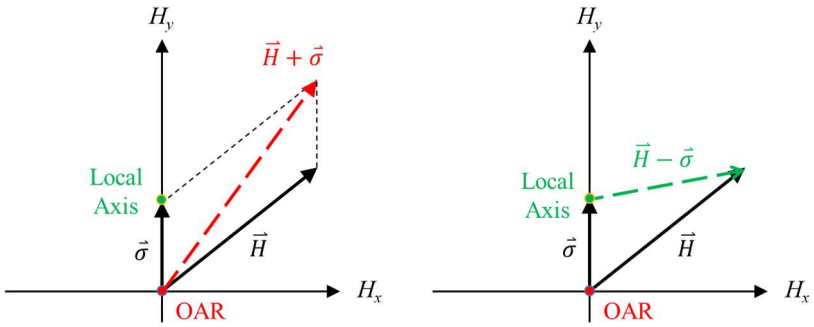

Figure 3.13 The effective field vector based on (a) the OAR and (b) the local axis

In this chapter, the polarization aberrations will be expanded about the OAR [60]. $(\vec{H}+\vec{\sigma})$ will be used to replace $\vec{H}$ in equations from Eq. (3.12) to Eq. (3.16):

$$\begin{aligned}\vec{A}'\left((\vec{H}+\vec{\sigma}),\vec{\rho}\right)=&P_0\vec{A}+P_1\left(\vec{\rho}\cdot\vec{\rho}\right)\vec{A}+P_2\left[(\vec{H}+\vec{\sigma})\cdot\vec{\rho}\right]\vec{A}\\&+P_3\left[(\vec{H}+\vec{\sigma})\cdot(\vec{H}+\vec{\sigma})\right]\vec{A}+\Delta P_1\left(\vec{A}\cdot\vec{\rho}\right)\vec{\rho}\\&+\Delta P_2\left[\left(\vec{A}\cdot(\vec{H}+\vec{\sigma})\right)\vec{\rho}+\left(\vec{A}\cdot\vec{\rho}\right)(\vec{H}+\vec{\sigma})\right]\\&+\Delta P_3\left[\vec{A}\cdot(\vec{H}+\vec{\sigma})\right](\vec{H}+\vec{\sigma}),\end{aligned} \tag{3.23}$$

$$\delta\left((\vec{H}+\vec{\sigma}),\vec{\rho}\right)=\delta_1\left(\vec{\rho}\cdot\vec{\rho}\right)+\delta_2\left((\vec{H}+\vec{\sigma})\cdot\vec{\rho}\right)+\delta_3\left((\vec{H}+\vec{\sigma})\cdot(\vec{H}+\vec{\sigma})\right), \tag{3.24}$$

$$\Delta\delta_a\left((\vec{H}+\vec{\sigma}),\vec{\rho}\right)=\Delta\delta_1\left(\vec{\rho}\cdot\vec{\rho}\right)+2\Delta\delta_2\left((\vec{H}+\vec{\sigma})\cdot\vec{\rho}\right)+\Delta\delta_3\left((\vec{H}+\vec{\sigma})\cdot(\vec{H}+\vec{\sigma})\right), \tag{3.25}$$

$$\Delta\delta_b\left((\vec{H}+\vec{\sigma}),\vec{\rho}\right)=\Delta\delta_1\left(\vec{a}\cdot\vec{\rho}\right)^2+2\Delta\delta_2\left(\vec{a}\cdot(\vec{H}+\vec{\sigma})\right)\left(\vec{a}\cdot\vec{\rho}\right)+\Delta\delta_3\left(\vec{a}\cdot(\vec{H}+\vec{\sigma})\right)^2, \tag{3.26}$$

and

$$\begin{aligned}\Delta\delta_c\left((\vec{H}+\vec{\sigma}),\vec{\rho}\right)=&\Delta\delta_1\left(\vec{a}\cdot\vec{\rho}\right)\left(\vec{b}\cdot\vec{\rho}\right)+\Delta\delta_2\left(\vec{a}\cdot\vec{\rho}\right)\left(\vec{b}\cdot(\vec{H}+\vec{\sigma})\right)+\\&\Delta\delta_2\left(\vec{a}\cdot(\vec{H}+\vec{\sigma})\right)\left(\vec{b}\cdot\vec{\rho}\right)+\Delta\delta_3\left(\vec{a}\cdot(\vec{H}+\vec{\sigma})\right)\left(\vec{b}\cdot(\vec{H}+\vec{\sigma})\right).\end{aligned} \tag{3.27}$$

By substituting Eqs. (3.23) to (3.27) into Eqs. (3.10) and (3.11), and combining Eq. (3.22) with the coefficients in Table 3.1, the polarization aberration functions, $\vec{E}^o$ and $\vec{E}^e$, for plane symmetric optical systems are derived as

$$\vec{E}^o\left(\vec{i},\vec{H},\vec{\rho}\right)=\vec{A}'\left(\vec{i},\vec{H},\vec{\rho}\right)\cdot e^{i\frac{2\pi}{\lambda}\left[\Phi\left(\vec{i},\vec{H},\vec{\rho}\right)+\delta\left(\vec{i},\vec{H},\vec{\rho}\right)+\Delta\delta_b\left(\vec{i},\vec{H},\vec{\rho}\right)\right]}, \tag{3.28}$$

and

$$\vec{E}^e\left(\vec{i},\vec{H},\vec{\rho}\right)=\left[\frac{2\pi}{\lambda}\Delta\delta_c\left(\vec{i},\vec{H},\vec{\rho}\right)\right]\vec{A}'^{\perp}\left(\vec{i},\vec{H},\vec{\rho}\right)\cdot e^{i\frac{2\pi}{\lambda}\left[\Phi\left(\vec{i},\vec{H},\vec{\rho}\right)+\delta\left(\vec{i},\vec{H},\vec{\rho}\right)+\frac{1}{2}\Delta\delta_a\left(\vec{i},\vec{H},\vec{\rho}\right)+\frac{\lambda}{4}\right]}, \tag{3.29}$$

where

$$\vec{A}'\left(\vec{i},\vec{H},\vec{\rho}\right)=\left\{\begin{array}{l}P_0\vec{A}+P_1\left(\vec{\rho}\cdot\vec{\rho}\right)\vec{A}+P_2\left(\vec{H}\cdot\vec{\rho}\right)\vec{A}+P_3\left(\vec{H}\cdot\vec{H}\right)\vec{A}+\ P_4\left(\vec{i}\cdot\vec{\rho}\right)\vec{A}+\\ \quad P_5\left(\vec{i}\cdot\vec{H}\right)\vec{A}+\ \Delta P_0\left(\vec{A}\cdot\vec{i}\right)\vec{i}+\Delta P_1\left(\vec{A}\cdot\vec{\rho}\right)\vec{\rho}+\\ \quad \Delta P_2\left[\left(\vec{A}\cdot\vec{H}\right)\vec{\rho}+\left(\vec{A}\cdot\vec{\rho}\right)\vec{H}\right]+\Delta P_3\left(\vec{A}\cdot\vec{H}\right)\vec{H}+\\ \quad \Delta P_4\left[\left(\vec{A}\cdot\vec{\rho}\right)\vec{i}+\left(\vec{A}\cdot\vec{i}\right)\vec{\rho}\right]+\Delta P_5\left[\left(\vec{A}\cdot\vec{H}\right)\vec{i}+\left(\vec{A}\cdot\vec{i}\right)\vec{H}\right]\end{array}\right\}, \tag{3.30}$$

and $\vec{A}'^{\perp}(\vec{i},\vec{H},\vec{\rho})$ is $\left|\vec{A}'(\vec{i},\vec{H},\vec{\rho})\right|\vec{b}$. $\vec{A}'(\vec{i},\vec{H},\vec{\rho})$ is the field amplitude function at the exit pupil. $\vec{A}$ is the input field amplitude at the entrance pupil of the optical system with q surfaces, and it is a known optical field. The polarization state distribution of $\vec{A}$ over the pupil can be plane symmetric, double plane symmetric or axial symmetric with respect to the OAR of the system. P_0, P_1, P_2, P_3, P_4, and P_5 are the polarization aberration coefficients for piston, defocus, tilt, quadratic piston, field displacement, and linear piston common apodizations. These are scalar aberrations and are independent of the polarization state of the incoming field $\vec{A}$. On the other hand, ΔP_0, ΔP_1, ΔP_2, ΔP_3, ΔP_4, and ΔP_5 are the polarization aberration coefficients for diattenuations. These terms are vector aberrations and are dependent of the polarization state of the incoming field $\vec{A}$ from Eq. (3.30). They would alter the orientation of the incoming field $\vec{A}$. After deriving the formulas of $\vec{E}^o$ and $\vec{E}^e$, the refraction invariants $\overline{A}$ and A need to be redefined so that they can be applied to the plane symmetric systems. All these polarization aberration coefficients are listed in Table 3.2. $\overline{A}$ and A in Table 3.2 are slightly different from $\overline{A}$ and A in Table 3.1 due to the $\cos(I)$ factor for the refraction invariant in a plane symmetric system. In addition, the first order ray slope and ray height are measured relative to the OAR, not relative to the optical axis. The total aberrations of a plane symmetric system can be decomposed into surface contributions, which helps to analyze and optimize the system.

Similar to axial symmetric polarization aberrations, in Eqs. (3.28) and (3.29), $\delta\left(\vec{i},\vec{H},\vec{\rho}\right)$ represents the phase change common to $\vec{E}^o$ and $\vec{E}^e$ fields, while

$\Delta\delta_a\left(\vec{i},\vec{H},\vec{\rho}\right)$ and $\Delta\delta_b\left(\vec{i},\vec{H},\vec{\rho}\right)$ are the retardance functions of $\vec{E}^e$ and $\vec{E}^o$ fields, respectively. $\Delta\delta_c\left(\vec{i},\vec{H},\vec{\rho}\right)$ is also a retardance function. However, the difference is that it does not affect the phase, but the amplitude of the $\vec{E}^e$ field. The amplitude of the $\vec{E}^e$ field is strongly apodized by the retardance function $\Delta\delta_c\left(\vec{i},\vec{H},\vec{\rho}\right)$. These functions at the exit pupil are defined as

$$\delta\left(\vec{i},\vec{H},\vec{\rho}\right)=\delta_0+\delta_1\left(\vec{\rho}\cdot\vec{\rho}\right)+\delta_2\left(\vec{H}\cdot\vec{\rho}\right)+\delta_3\left(\vec{H}\cdot\vec{H}\right)+\delta_4\left(\vec{i}\cdot\vec{\rho}\right)+\delta_5\left(\vec{i}\cdot\vec{H}\right), \tag{3.31}$$

$$\begin{aligned}\Delta\delta_a\left(\vec{i},\vec{H},\vec{\rho}\right)=&\Delta\delta_0+\Delta\delta_1\left(\vec{\rho}\cdot\vec{\rho}\right)+2\Delta\delta_2\left(\vec{H}\cdot\vec{\rho}\right)+\Delta\delta_3\left(\vec{H}\cdot\vec{H}\right)+2\Delta\delta_4\left(\vec{i}\cdot\vec{\rho}\right)\\&+2\Delta\delta_5\left(\vec{i}\cdot\vec{H}\right),\end{aligned} \tag{3.32}$$

$$\begin{aligned}\Delta\delta_b\left(\vec{i},\vec{H},\vec{\rho}\right)=&\Delta\delta_0\left(\vec{a}\cdot\vec{i}\right)^2+\Delta\delta_1\left(\vec{a}\cdot\vec{\rho}\right)^2+2\Delta\delta_2\left(\vec{a}\cdot\vec{H}\right)\left(\vec{a}\cdot\vec{\rho}\right)+\Delta\delta_3\left(\vec{a}\cdot\vec{H}\right)^2\\&+2\Delta\delta_4\left(\vec{a}\cdot\vec{i}\right)\left(\vec{a}\cdot\vec{\rho}\right)+2\Delta\delta_5\left(\vec{a}\cdot\vec{i}\right)\left(\vec{a}\cdot\vec{H}\right),\end{aligned} \tag{3.33}$$

and

$$\begin{aligned}\Delta\delta_c\left(\vec{i},\vec{H},\vec{\rho}\right)=&\Delta\delta_0\left(\vec{a}\cdot\vec{i}\right)\left(\vec{b}\cdot\vec{i}\right)+\Delta\delta_1\left(\vec{a}\cdot\vec{\rho}\right)\left(\vec{b}\cdot\vec{\rho}\right)\\&+\Delta\delta_2\left[\left(\vec{a}\cdot\vec{\rho}\right)\left(\vec{b}\cdot\vec{H}\right)+\left(\vec{a}\cdot\vec{H}\right)\left(\vec{b}\cdot\vec{\rho}\right)\right]+\Delta\delta_3\left(\vec{a}\cdot\vec{H}\right)\left(\vec{b}\cdot\vec{H}\right)\\&+\Delta\delta_4\left[\left(\vec{a}\cdot\vec{i}\right)\left(\vec{b}\cdot\vec{\rho}\right)+\left(\vec{a}\cdot\vec{\rho}\right)\left(\vec{b}\cdot\vec{i}\right)\right]\\&+\Delta\delta_5\left[\left(\vec{a}\cdot\vec{i}\right)\left(\vec{b}\cdot\vec{H}\right)+\left(\vec{a}\cdot\vec{H}\right)\left(\vec{b}\cdot\vec{i}\right)\right].\end{aligned} \tag{3.34}$$

From Eq. (3.31) to Eq. (3.34), $\delta\left(\vec{i},\vec{H},\vec{\rho}\right)$ and $\Delta\delta_a\left(\vec{i},\vec{H},\vec{\rho}\right)$ have nothing to do with the polarization state of the input field $\vec{A}$, while $\Delta\delta_b\left(\vec{i},\vec{H},\vec{\rho}\right)$ and $\Delta\delta_c\left(\vec{i},\vec{H},\vec{\rho}\right)$ are relevant because of the presence of $\vec{a}$. δ_0, δ_1, δ_2, δ_3, δ_4, and δ_5 are the polarization aberration coefficients for constant piston, defocus, tilt, quadratic piston, field displacement, and

linear piston common phase changes, which are related to the first order properties of the optical system. $\Delta\delta_0$, $\Delta\delta_1$, $\Delta\delta_2$, $\Delta\delta_3$, $\Delta\delta_4$, and $\Delta\delta_5$ are the polarization aberration coefficients for retardance. All these polarization aberration coefficients are listed in Table 3.2, too. If the plane symmetric system includes reflective surfaces, the reflection-related coefficients are required, which are the same as those shown at the bottom of Table 3.1 for axial symmetric systems. The aberrations of axial symmetric systems are part of the plane symmetric aberrations, and they are shown as a subgroup. In Figure 3.12, when tilt is zero, or the angle of incidence I is zero, all the polarization aberration functions are back to the polarization aberration functions for axial symmetric systems.

Same as Section 3.2, the polarization aberration functions are based on the assumptions of paraxial approximation and second order approximation. Absorption and dichroism of light are neglected. For paraxial optics, the wavefront aberrations do not exist, but the polarization aberrations do exist. These paraxial assumptions limit the angles of incidence to 30 degrees and the retardance to 30 degrees. The tilt angles of components in a plane symmetric system are also limited to 15 degrees. Further discussion of the limitations on the angle of incidence will be shown in Section 3.4.1.

When the tilts are small enough, the tilts of the object, image and pupil planes can be neglected. In Eq. (3.7), the diattenuation related coefficient Δt is relatively small compared with the amplitude coefficient T, and the refraction invariant A is also small under paraxial approximation. Thus, the direction of the optical field $\vec{E}'$ does not deviate too much from the incident optical field $\vec{E}$. For instance, if n is 1 and n' is 1.5, the

coefficient T is 0.8. However, Δt is only 0.056, and A^2 is 0.32 if i is 0.57. $T\Delta tA^2$ is 0.014, which is almost two orders of magnitude smaller than T. Therefore, this term can be neglected. Similarly, if the surface is an uncoated aluminum, the coefficient R is 0.973. However, Δr is only -0.028 such that $R\Delta rA^2$ is only -0.009 if A^2 is 0.32. This $R\Delta rA^2$ term is two orders of magnitude less than the R term, so the $R\Delta rA^2$ term is negligible. Hence, the vector $\vec{a}$ is approximately parallel to $\vec{E}$, which is $\vec{A}$ in Eq. (3.30) for both refractive and reflection systems. In this chapter, $\vec{a}$ is set as a fixed unit vector of $\vec{A}$ to simplify the calculation.

If input polarization $\vec{E}$ is a uniform linearly polarized optical field with amplitude $\vec{A}$ equal to $\vec{i}$, the optical field amplitude $\vec{A}'$ at the exit pupil would be

$$\vec{A}'\left(\vec{i},\vec{H},\vec{\rho}\right)=\left\{\begin{array}{l}\left(P_0+\Delta P_0\right)\vec{i}+P_1\left(\vec{\rho}\cdot\vec{\rho}\right)\vec{i}+P_2\left(\vec{H}\cdot\vec{\rho}\right)\vec{i}+P_3\left(\vec{H}\cdot\vec{H}\right)\vec{i}+\\ \left(P_4+\Delta P_4\right)\left(\vec{i}\cdot\vec{\rho}\right)\vec{i}+\left(P_5+\Delta P_5\right)\left(\vec{i}\cdot\vec{H}\right)\vec{i}+\Delta P_1\left(\vec{i}\cdot\vec{\rho}\right)\vec{\rho}+\\ \Delta P_2\left(\vec{i}\cdot\vec{H}\right)\vec{\rho}+\Delta P_2\left(\vec{i}\cdot\vec{\rho}\right)\vec{H}+\Delta P_3\left(\vec{i}\cdot\vec{H}\right)\vec{H}+\Delta P_4\vec{\rho}+\Delta P_5\vec{H}\end{array}\right\}. \qquad (3.35)$$

It is a superposition of the $\vec{R}_n$ fields, $\vec{R}_1$ to $\vec{R}_{12}$ in Figure 3.4. Another point worth mentioned is that polar coordinate system is utilized here to describe the aberrations, because most optical systems are constructed by axial symmetric components, such as spherical lenses. If the system involves plane symmetric components, such as cylindrical lenses, it would be more convenient to use Cartesian coordinate system. This theory does apply to systems with plane symmetric components.

Table 3.2 Polarization aberration coefficients for a plane symmetric optical system with q surfaces

$P_0 = T_q\left[1+\sum_{j=1}^{q}\left(t\bar{A}_0^2\right)_j\right]$	constant piston apodization	$\delta_0 = \sum_{j=1}^{q}\left(\delta\bar{A}_0^2\right)_j$	constant piston phase change
$P_1 = T_q\sum_{j=1}^{q}\left(tA^2\right)_j$	defocus apodization	$\delta_1 = \sum_{j=1}^{q}\left(\delta A^2\right)_j$	defocus phase change
$P_2 = 2T_q\sum_{j=1}^{q}\left(tA\bar{A}\right)_j$	tilt apodization	$\delta_2 = 2\sum_{j=1}^{q}\left(\delta A\bar{A}\right)_j$	tilt phase change
$P_3 = T_q\sum_{j=1}^{q}\left(t\bar{A}^2\right)_j$	quadratic piston apodization	$\delta_3 = \sum_{j=1}^{q}\left(\delta\bar{A}^2\right)_j$	quadratic piston phase change
$P_4 = 2T_q\sum_{j=1}^{q}\left(tA\bar{A}_0\right)_j$	field displacement apodization	$\delta_4 = 2\sum_{j=1}^{q}\left(\delta A\bar{A}_0\right)_j$	field displacement phase change
$P_5 = 2T_q\sum_{j=1}^{q}\left(t\bar{A}\bar{A}_0\right)_j$	linear piston apodization	$\delta_5 = 2\sum_{j=1}^{q}\left(\delta\bar{A}\bar{A}_0\right)_j$	linear piston phase change
$\Delta P_0 = T_q\sum_{j=1}^{q}\left(\Delta t\bar{A}_0^2\right)_j$		$\Delta\delta_0 = \sum_{j=1}^{q}\left(\Delta\delta\bar{A}_0^2\right)_j$	
$\Delta P_1 = T_q\sum_{j=1}^{q}\left(\Delta tA^2\right)_j$		$\Delta\delta_1 = \sum_{j=1}^{q}\left(\Delta\delta A^2\right)_j$	
$\Delta P_2 = T_q\sum_{j=1}^{q}\left(\Delta tA\bar{A}\right)_j$		$\Delta\delta_2 = \sum_{j=1}^{q}\left(\Delta\delta A\bar{A}\right)_j$	
$\Delta P_3 = T_q\sum_{j=1}^{q}\left(\Delta t\bar{A}^2\right)_j$		$\Delta\delta_3 = \sum_{j=1}^{q}\left(\Delta\delta\bar{A}^2\right)_j$	
$\Delta P_4 = T_q\sum_{j=1}^{q}\left(\Delta tA\bar{A}_0\right)_j$		$\Delta\delta_4 = \sum_{j=1}^{q}\left(\Delta\delta A\bar{A}_0\right)_j$	
$\Delta P_5 = T_q\sum_{j=1}^{q}\left(\Delta t\bar{A}\bar{A}_0\right)_j$		$\Delta\delta_5 = \sum_{j=1}^{q}\left(\Delta\delta\bar{A}\bar{A}_0\right)_j$	
$A_j = \left(ni\right)_j = \left(nu + ny\cos(I)C\right)_j$		$T_q = \prod_{j=1}^{q}\left(\frac{2n}{n+n'}\right)_j$	$\left(\text{or } \prod_{j=1}^{q}\left(\frac{2\sqrt{nn'}}{n+n'}\right)_j \text{ power transmission effect included}\right)$
$\bar{A}_j = \left(n\bar{i}\right)_j = \left(n\bar{u} + n\bar{y}\cos(I)C\right)_j$		$t_j = \frac{1}{2}\left(\frac{n-n'}{n^2n'}\right)_j$	$\left(\text{or } -\left(\frac{n-n'}{2nn'}\right)_j^2 \text{ power transmission effect included}\right)$
$\left(\bar{A}_0\right)_j = \left(n\sin(I)\right)_j$		$\Delta t_j = \frac{1}{2}\left(\frac{n-n'}{nn'}\right)_j^2$	

3.4 Discussion of Polarization Aberration Functions and Examples

In this section, the assumptions used in deriving the formulas are reviewed in detail. After understanding the limitations imposed by these assumptions, two examples of polarization aberrations in plane symmetric systems will be shown and discussed.

3.4.1 The assumptions and approximations

The paraxial region of polarization aberrations is usually larger than the paraxial region of wavefront aberrations. In the paraxial region, the angle of incidence ϕ at a given curved surface can be expressed as $\phi(\rho) = i\rho$ as shown in Figure 3.14(a). This is the key to expressing the second order approximation of the Fresnel equations as Eq. (3.5) and Eq. (3.6). Meanwhile, this implies that the polarization aberration functions would not be applicable to highly aspherical surfaces, such as the components 104 and 105 of the camera lens system in Figure 3.14(b) [95].

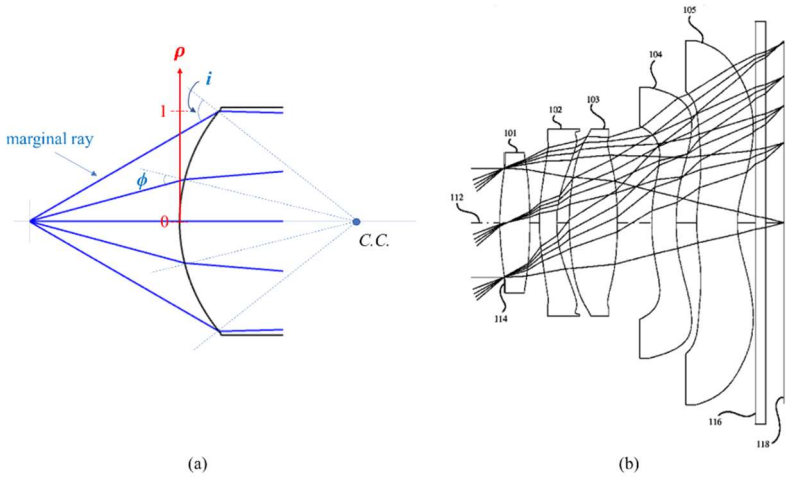

Figure 3.14 The angle of incidence varies with the pupil position

Figure 3.15 shows (a) amplitude and (b) phase of the transmission curves for the quarter-wave MgF_2 coating on BK7 substrate. The Taylor expansion of Fresnel equations with first two terms fits the original equations well in the range of 30° (0.52 rad) angle of incidence. When the angle of incidence increases to 45° (0.79 rad), the $|t_s|$ fitting error is up to 0.6%, which may be acceptable in the simulation for simple optical systems. In terms of phase as shown in Figure 3.15(b), even though there is a small phase difference $\Delta\delta$ between p and s lights from the original Fresnel equations, there is no phase difference under second order approximation.

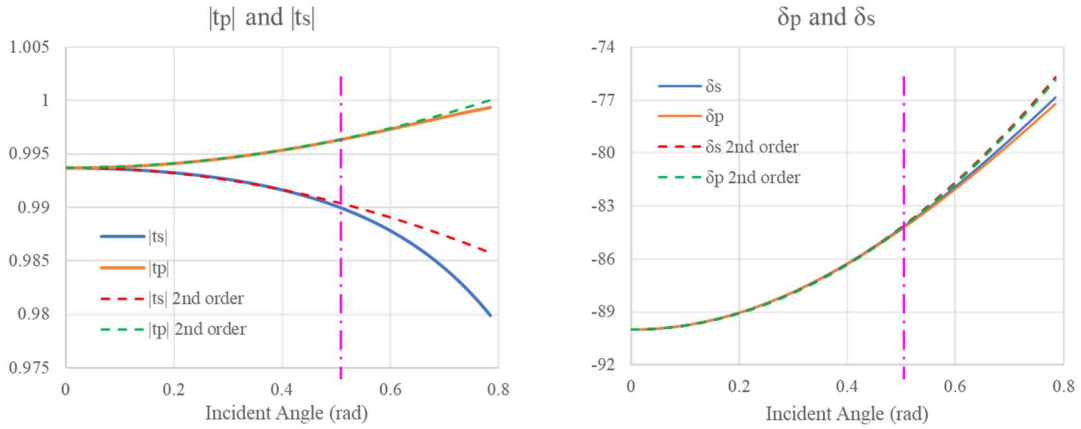

Figure 3.15 The transmission curves of quarter-wave MgF_2 coating on BK7 substrate

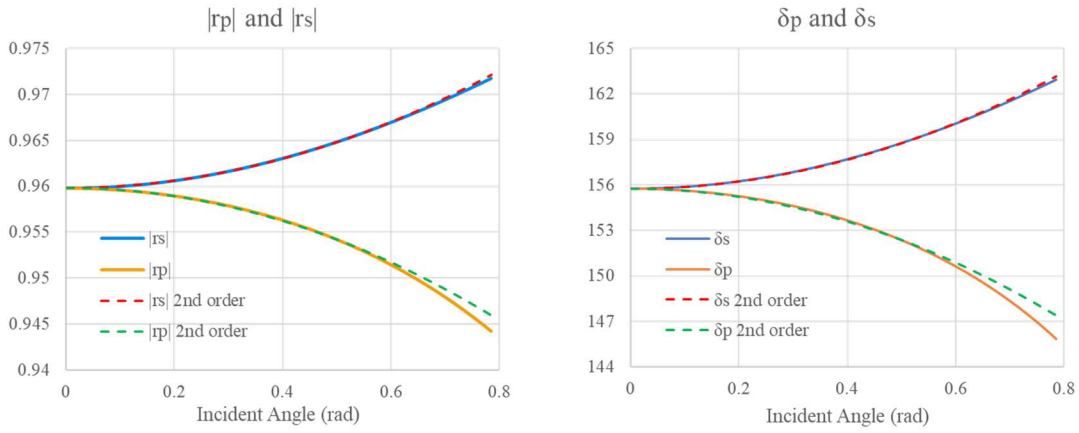

(a) (b)

Figure 3.16 The reflection curves of uncoated aluminum mirror

Figure 3.16 shows (a) amplitude and (b) phase of the reflection curves for a bare aluminum mirror. The Taylor expansion of Fresnel equations with first two terms fits the original equations well within 34° (0.6 rad) angle of incidence. When the angle of incidence is increased to 45° (0.79 rad), the $|r_p|$ fitting error is about 0.2%, which is better than that of MgF_2. Therefore, the mirror systems have a wider range of acceptable angles of incidence.

Eq. (3.8) shows the equation of $\vec{E}_1^o$ before and after the second order approximation. $\cos^2\left[\frac{\pi}{\lambda}\Delta\delta A^2\left(\vec{\rho}\cdot\vec{\rho}\right)\right]$ can be approximated to 1 within a 1% error range only when $\Delta\delta$ is within $\frac{\lambda}{12}$ and i is 0.79. In this chapter, instead of approximating $\sin(I)$ as I, $\sin(I)$ is kept in Eq. (3.22) to count the tilt angle effect of the optical component more accurately and to make the equation more stable. $\sin(I)$ is approximated to I within a 1% error range as I is within 15° (0.26 rad). The acceptable error range will vary depending on

the complexity of the optical system to be simulated. In general, a huge tilt would not be accepted for an imaging optical system. Since the errors are cumulative, the more surfaces in the system, the larger the total accumulated error. In this case, the acceptable error for each single surface in the system is relatively small. Figure 3.17 shows a singlet lens tilted clockwise with respect to the x axis at different angles. The input is a uniform y-polarized light. The amplitudes of the output field with different tilt angles are calculated from the equations in Section 3.3. Compared with the field amplitude results from CODE V polarization ray tracing, the percentage difference is shown in Figure 3.17(b). When the tilt angle I is within 15°, the difference is within 1%.

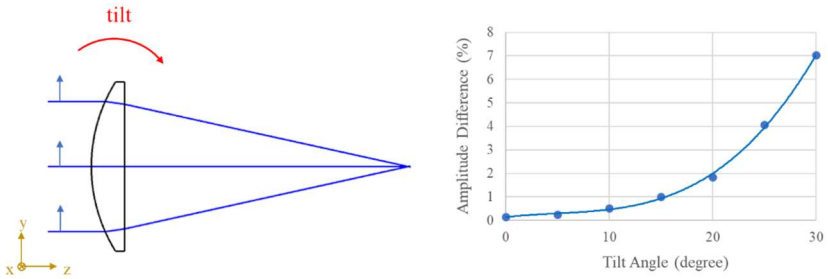

(a) (b)

Figure 3.17 Tilt angle of a singlet v.s. the field amplitude difference

3.4.2 The polarization aberrations of a tilted singlet lens

In this section, the simplest system is studied to understand the polarization aberration functions. The singlet in Figure 3.17 is adopted and analyzed. It is an uncoated BK7 lens with f-number of 2.4, and an additional field is added as 10 mm. The lens is tilted by 15°. Figure 3.18 shows the tilted lens and the field points for simulations. Due to the Scheimpflug principle, the image plane is tilted counterclockwise. $\vec{E}$ is a uniform linearly

polarized optical field with amplitude $\vec{A}$ equal to $\vec{i}$, which is +1 $\vec{y}$. The optical field amplitude $\vec{A}'$ at the exit pupil can be computed from Eq. (3.35).

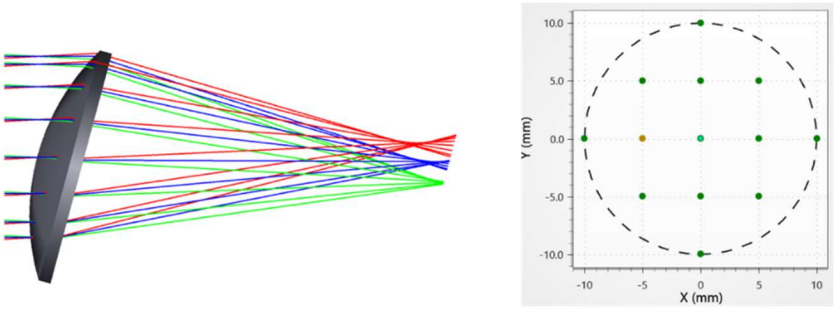

(a) (b)

Figure 3.18 15° tilt lens and the field points

When the field $\vec{H}$ is (0,1), $\vec{A}'$ is decomposed into the related $\vec{R}_n$ fields as shown in Figure 3.19. The numbers on top of each subplot are the magnitudes of the coefficients. All subplots are drawn at the same scale, except for the P_0 plot.

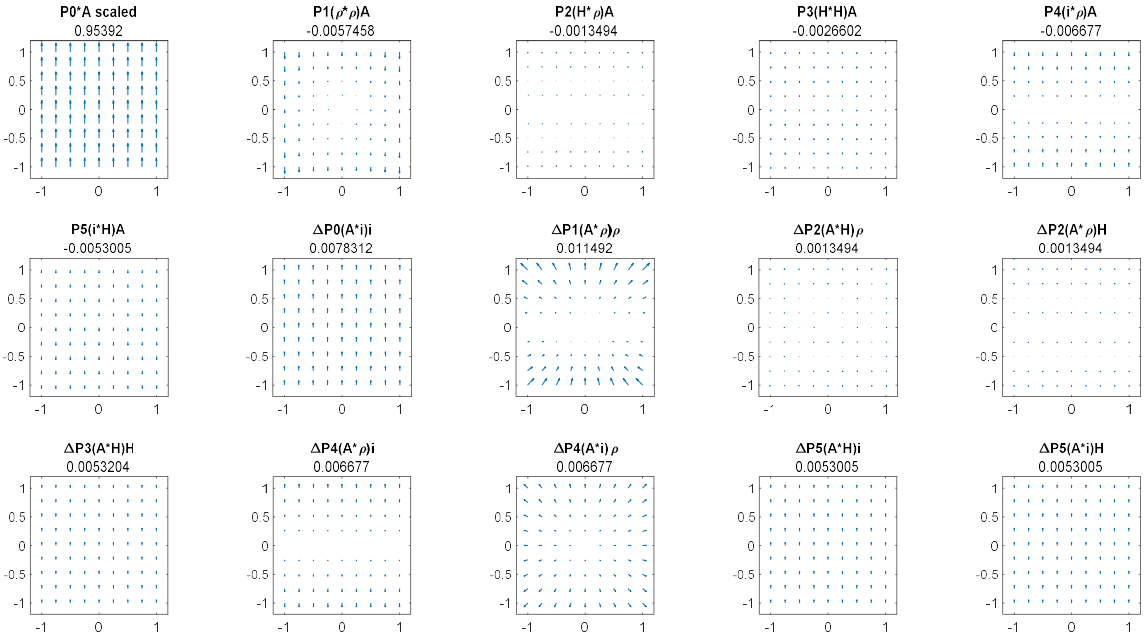

Figure 3.19 Decomposition of the amplitude field of the 15° tilt lens

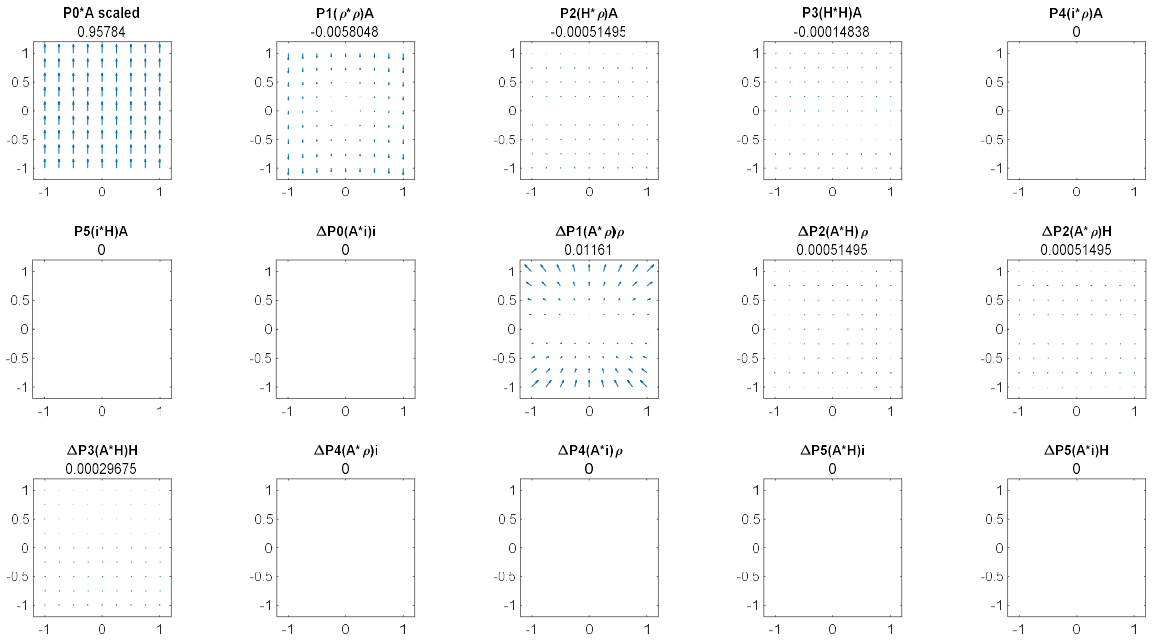

Figure 3.20 Decomposition of the amplitude field of the 0° tilt lens

If the tilt of lens is removed, the system becomes an axial symmetric system. $\vec{A}'$ with $\vec{H} = (0,1)$ is decomposed into the related $\vec{R}_n$ fields as shown in Figure 3.20. Among the scalar apodization terms, the constant piston P_0 dominates, and the defocus P_1 comes second. In the vector diattenuation aberration terms, the defocus ΔP_1 dominates. ΔP_2 and ΔP_3 terms represent tilt and quadratic piston of vector diattenuations, respectively. Comparing

Figure 3.19 and Figure 3.20, the tilt of lens ends up with more polarization aberration terms. In scalar apodizations, field displacement P_4 and linear piston P_5 show up. On the other hand, in vector diattenuations, constant piston ΔP_0, field displacement ΔP_4, and linear piston ΔP_5 are introduced. For this simple system, even though there are more non-zero terms, the dominant terms are still P_0 and ΔP_1. The defocus apodization P_1 and

the defocus diattenuation ΔP_1 hardly change with the tilt of the lens. P_2 and ΔP_2 become larger with the tilt, while P_3 and ΔP_3 become an order of magnitude larger with the tilt.

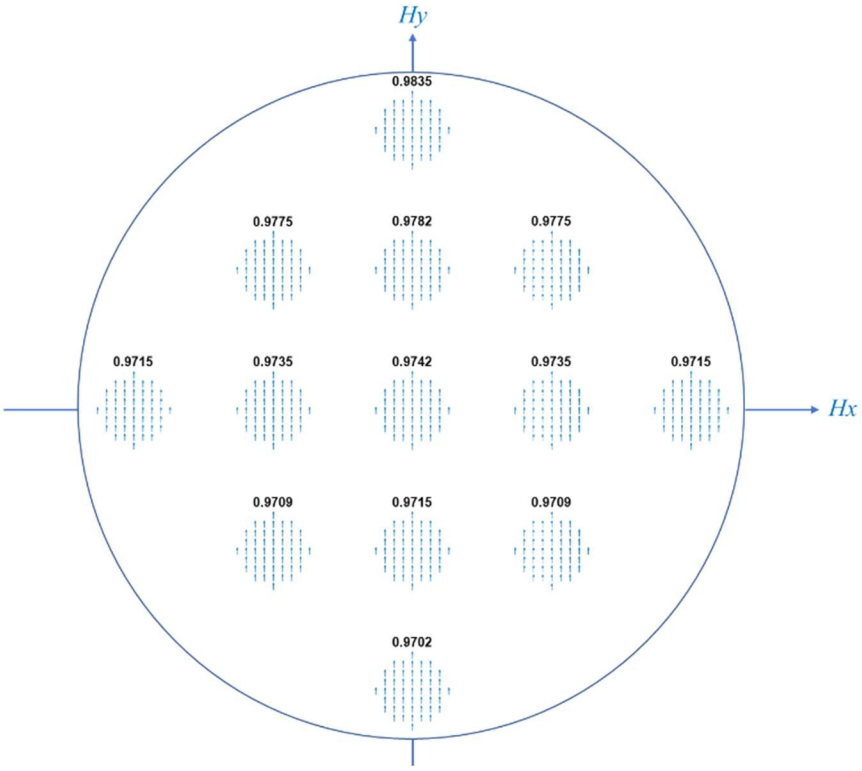

Figure 3.21 Pupil maps of $\vec{A}'$ across the field $\vec{H}$

Figure 3.21 shows the pupil maps of $\vec{A}'$ across the field $\vec{H}$ for the 15° tilt lens. Each number indicates the maximum value of $\vec{A}'$ in the specific pupil map. Compared to the input field $\vec{A}$, the output field $\vec{A}'$ does not change significantly across the field $\vec{H}$ and the pupil $\vec{\rho}$. In order to see the polarization aberrations more easily, $T_q\vec{A}$ is subtracted from $\vec{A}'$. $T_q\vec{A}$ is in the constant piston P_0 term in Figure 3.20, and it is the input field multiplied by the cumulated transmission coefficients of normal incidence.

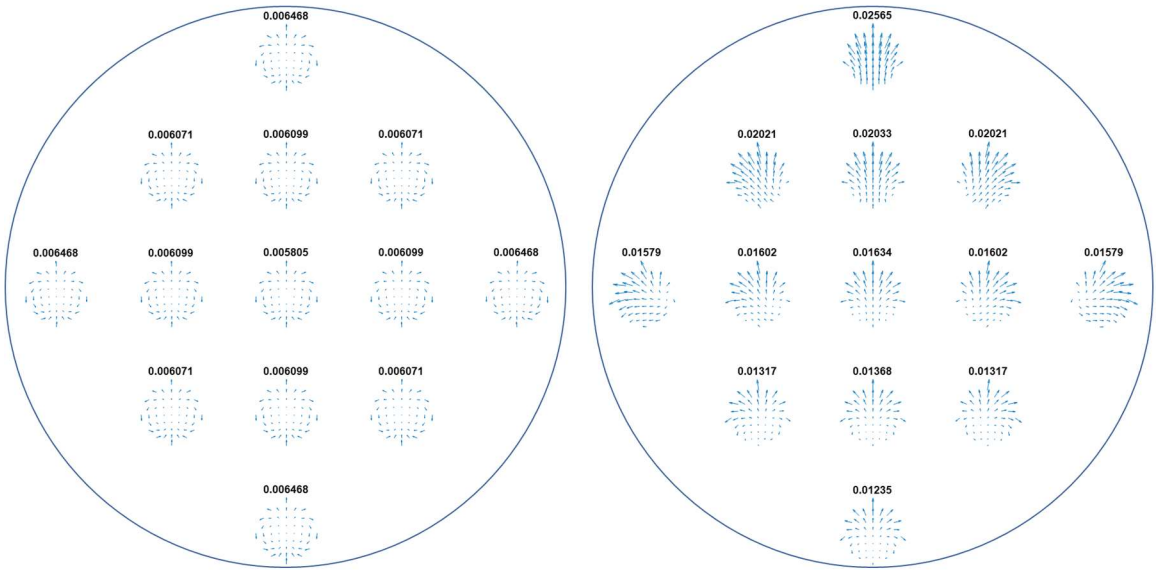

(a) 0° tilt (b) 15° tilt

Figure 3.22 Pupil maps of $(\vec{A}' - T_q\vec{A})$ across the field $\vec{H}$

Figure 3.22 shows the polarization aberrations before and after the tilt of the lens. The dominant term $T_q\vec{A}$ is removed from the maps. In Figure 3.22(a), since the polarization aberration is dominated by the apodization defocus and diattenuation defocus, the aberration patterns look similar throughout the field. The center of aberration field is located at the center of object field. The patterns are plane symmetric about $\vec{i}$ because of the plane symmetry property of the input field $\vec{A}$. In Figure 3.22(b), the aberration patterns are heavily influenced by the tilt because $\vec{\sigma}$ is added into $\vec{H}$. Moreover, since $\vec{\sigma}$ is in $+\vec{y}$ direction, the center of the aberration field would be shifted downward, which is consistent with the schematic plot shown in Figure 3.12. To understand the accuracy of the polarization aberration functions, a comparison is made with the polarization pupil map in CODE V. Figure 3.23 shows the amplitude and orientation differences of the output field

$\vec{A}'$ when the lens is tilted by 15°. The number above the subplot represents the maximum difference in the pupil. For both Figure 3.23(a) and (b), the difference increases with field $\vec{H}$. The amplitude difference is about 1%, while the orientation difference is less than 1.6°. The maximum orientation difference occurs in the sagittal plane. For skew rays, the orientation difference is larger. In CODE V, the polarization data is displayed in the collimated polarization coordinate system, which is the x, y, z coordinates of the surface. The difference of the local coordinate systems could cause the difference of the orientation of the output field.

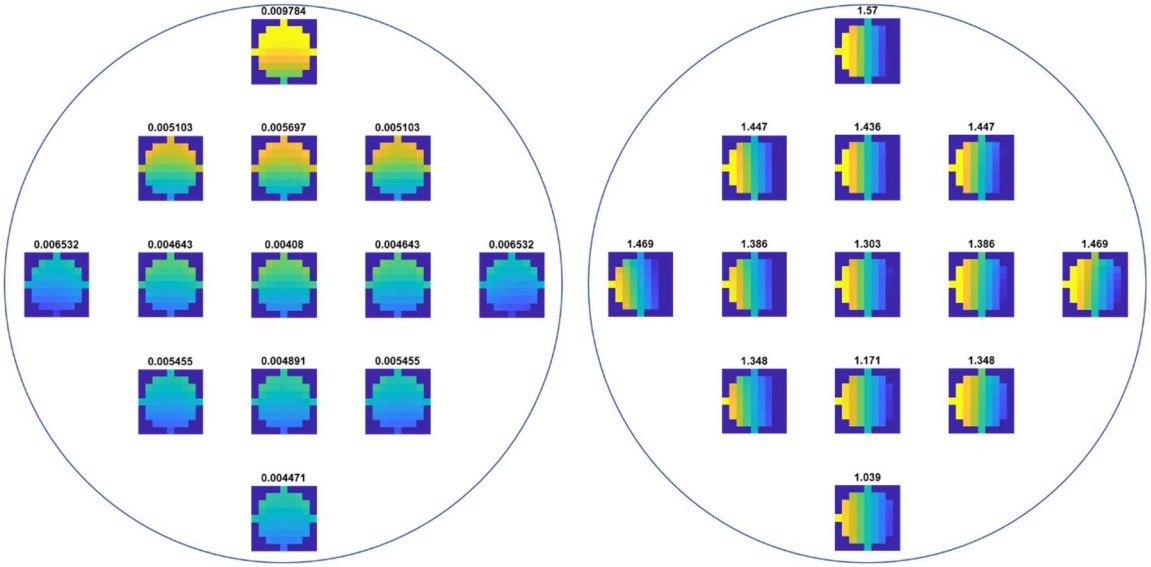

(a) Amplitude difference (b) Orientation difference

Figure 3.23 Comparisons of polarization pupil maps

3.4.3 The polarization aberrations of tilted mirrors

In order to understand the polarization aberrations of a plane symmetric system with retardance, the CODE V example file called ‘three mirror anastigmat’ is adopted. The

original system has three perfect mirrors without any polarization effect. Therefore, a built-in coating 'REFL_al_450nm_700nm' is added to these three mirror surfaces to make them become bare aluminum mirrors. The refractive index of aluminum can be found in the CODE V coating file, and it is inserted into the reflective polarization coefficients in Table 3.1. The mirrors are tilted and decentered, which makes the system plane symmetric about the y-z plane as shown in Figure 3.24. The optical axis ray (OAR) is shown in blue, and it is the reference axis of the polarization aberration functions. The incident angles of the optical axis ray at the mirrors M1, M2 and M3 are -18.6°, 21.9° and -7.7°, respectively. As shown in the figure, the incidence angle spread of M1 is about the same as that of M2, and the incidence angle spread of M3 is relatively small. Thus, the polarization aberrations of M1 and M2 would be larger than M3. Moreover, because there is an intermediate image point after M2, the field is flipped at image plane, and the center of the aberration field will be moved downward, rather than upward. The field points of interest are shown in Figure 3.24(b), with a maximum field height of 2.5 mm.

Same as the previous section, input field $\vec{E}$ is a uniform linearly polarized with amplitude $\vec{A}$ equal to $\vec{i}$, which is +1 $\vec{y}$. When the field $\vec{H}$ is (0,1), $\vec{A}'$ is decomposed into the related $\vec{R}_n$ fields as shown in Figure 3.25. The number on top of each subplot is the value of the coefficient. All subplots are drawn at the same scale, except for the P_0 plot. Among the scalar apodization terms, the constant piston P_0 dominates, and the field displacement P_4 comes second. In the vector diattenuation aberration terms, the defocus ΔP_1 dominates.

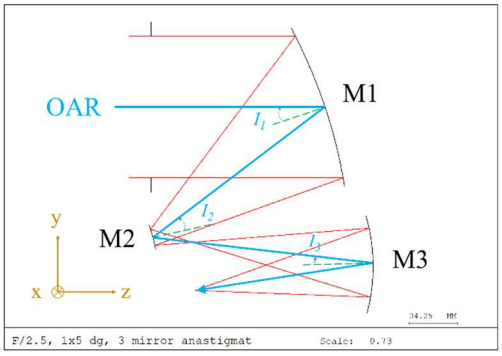

(a) System layout

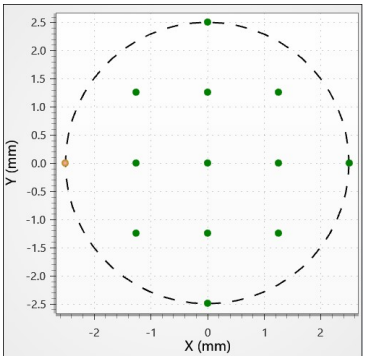

(b) Field points

Surface #	Surface Type	Y Radius	Thickness	Refract Mode	Y Semi-Aperture	X Semi-Aperture	Non-Centered Data	Y Decenter	Alpha Tilt
Object	Sphere	Infinity	Infinity	Refract					
Stop	Sphere	Infinity	139.3584 C	Refract	50.0000	50.0000	Decenter & Return	174.5286 V	0.0000
2	Asphere	-301.4371 V	-135.2648 C	Reflect	78.0096	78.0096	Basic Decenter	51.2571 V	-3.8237 V
3	Asphere	-82.6697 V	149.2891 V	Reflect	15.0248	15.0248	Decenter & Return	2.3784 V	6.4997 V
4	Asphere	-127.8005 V	-131.1611 S	Reflect	68.4166	68.4166	Decenter & Return	29.6383 V	11.7782 V
Image	Sphere	Infinity	9.6924 V	Refract	2.6371	2.6371	Decenter & Return	-13.2168 V	16.4925 V

(c) Lens data

Figure 3.24 Three mirror anastigmat

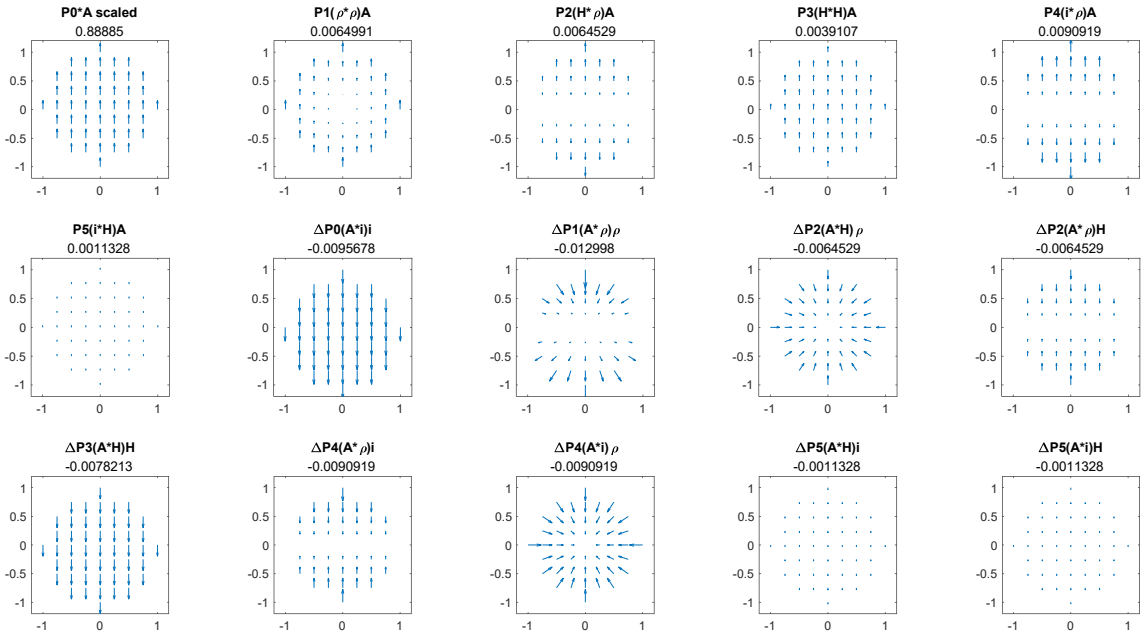

Figure 3.25 Decomposition of the $\vec{E}^o$ amplitude field

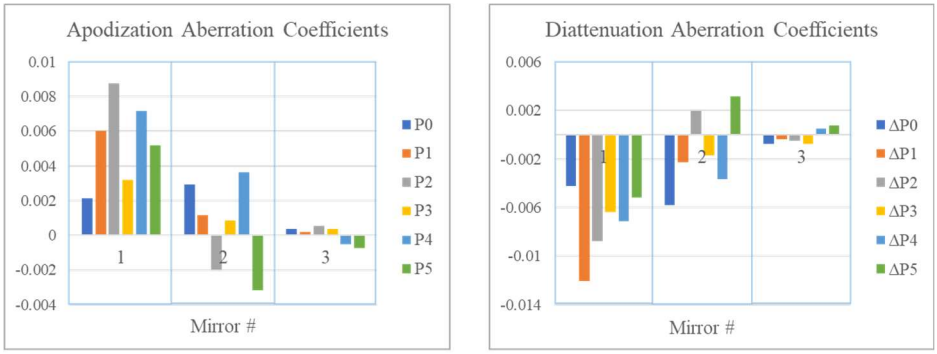

(a) (b)

Figure 3.26 Aberration coefficient diagram: (a) apodization (b) diattenuation

Figure 3.26 shows the apodization and diattenuation aberration coefficients for each mirror. M1 has larger aperture and larger angle of incidence, so the aberrations are larger. M2's aperture is small, but the angle of incidence is still large. Therefore, the polarization aberration contribution of M2 is more than that of M3. Since these mirrors are with retardance, the $\vec{E}^e$ field also exists. Figure 3.27 shows the amplitude distribution of $\vec{E}^o$ and $\vec{E}^e$. $\vec{E}^e$ is roughly one-eighth the magnitude of $\vec{E}^o$. The number on top of each pupil map indicates the maximum amplitude value in the specific pupil map. After subtracting $R_q\vec{A}$ from $\vec{A}'$, the polarization aberrations of the three mirror system is shown in Figure 3.28. The aberration pattern is plane symmetric, and the center of the aberration field is moved downward.

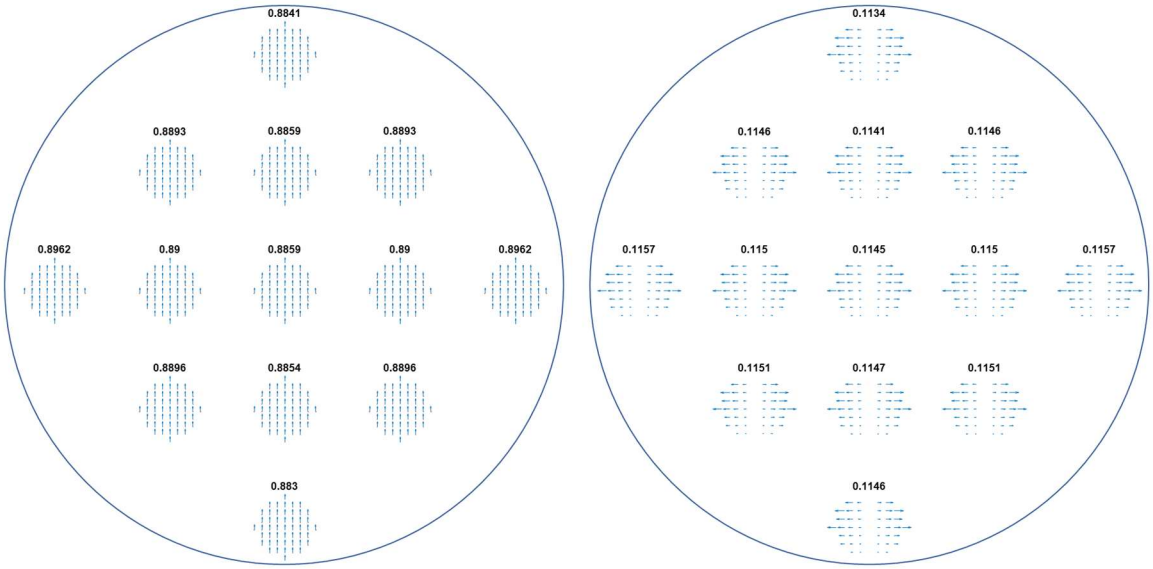

(a) $\vec{E}^o$ amplitude (b) $\vec{E}^e$ amplitude

Figure 3.27 Pupil maps of (a) $\vec{E}^o$and (b) $\vec{E}^e$ amplitudes across the field $\vec{H}$

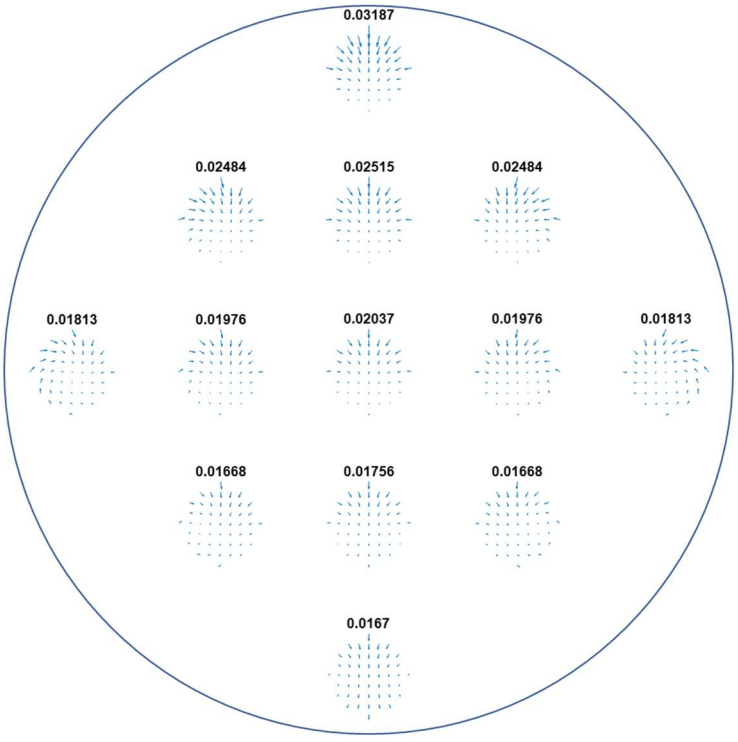

Figure 3.28 Pupil maps of $(\vec{A}' - R_q\vec{A})$ across the field $\vec{H}$

Combining $\vec{E}^o$, $\vec{E}^e$, and their corresponding phases, the polarization pupil map is shown as Figure 3.29. Larger ellipticity in the upper periphery of the pupil is due to the larger angle of incidence. The figure is plotted at field point $\vec{H}$=(0,1).

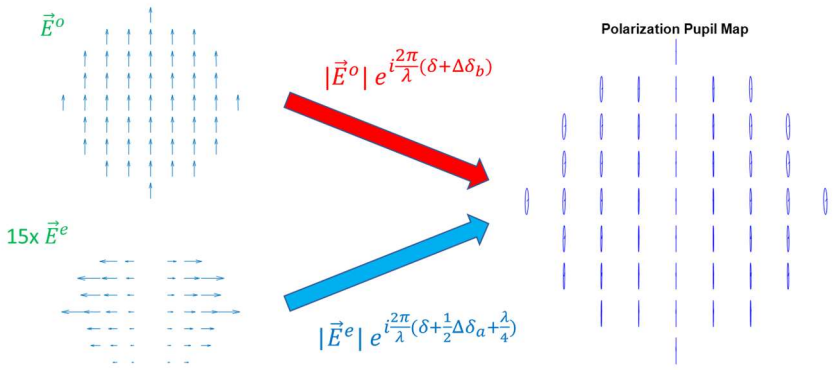

Figure 3.29 Polarization pupil map

Figure 3.30 illustrates the common phase function $\delta\left(\vec{i},\vec{H},\vec{\rho}\right)$ and the retardance aberration functions $\Delta\delta_a\left(\vec{i},\vec{H},\vec{\rho}\right)$, $\Delta\delta_b\left(\vec{i},\vec{H},\vec{\rho}\right)$, $\Delta\delta_c\left(\vec{i},\vec{H},\vec{\rho}\right)$. They are dominated by field displacement phase δ_4 term, defocus phase $\Delta\delta_1$ term, constant astigmatism $\Delta\delta_1$ term, anamorphism $\Delta\delta_1$ term, respectively. Figure 3.31 shows the common phase function and the retardance aberration coefficients for each mirror. Most of aberrations is contributed from M1.

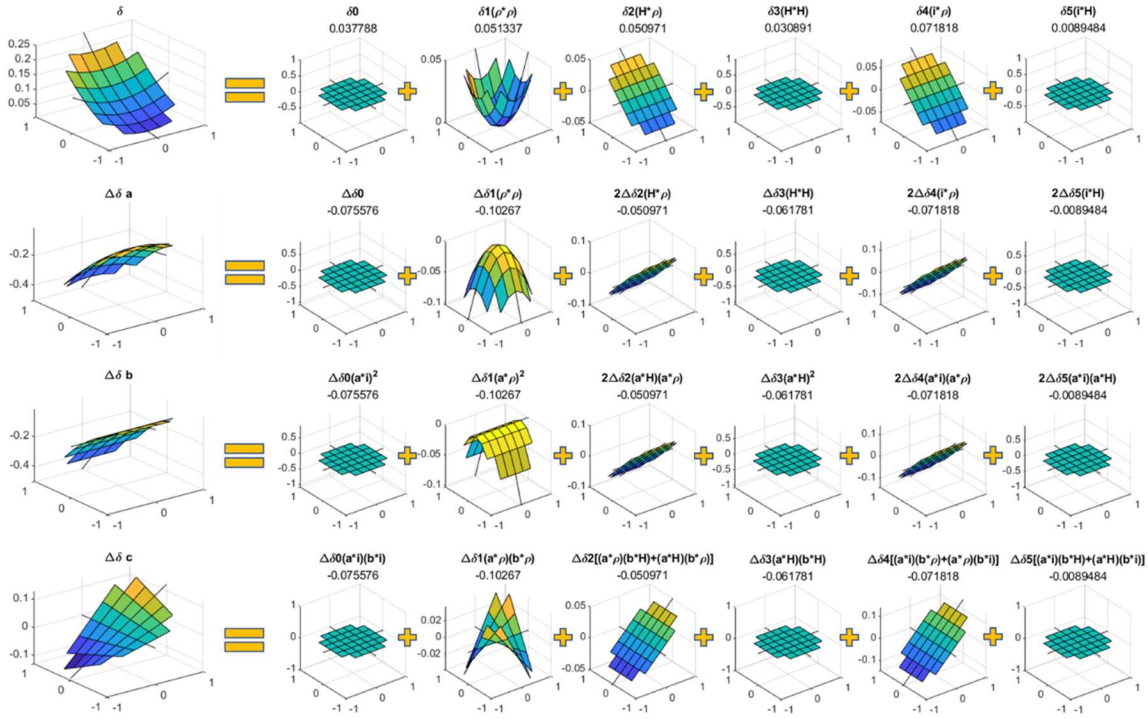

Figure 3.30 Common phase function and the retardance aberration functions

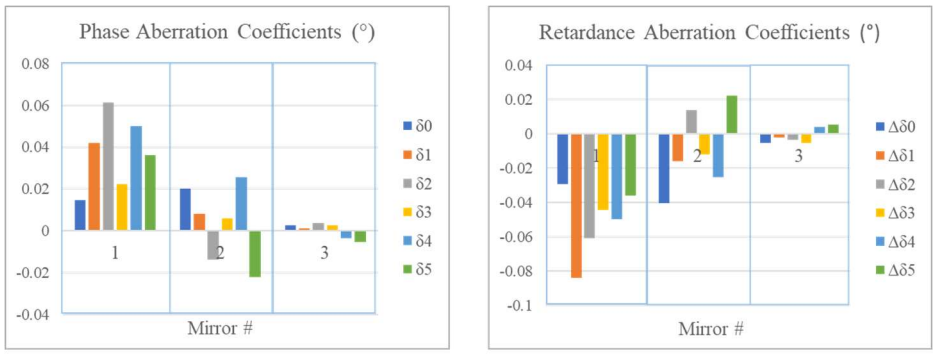

(a) (b)

Figure 3.31 Aberration coefficient diagram: (a) common phase (b) retardance

To understand the accuracy of the polarization aberration functions, a comparison is made with the polarization pupil map in CODE V. Figure 3.32 shows the magnitude and orientation differences of the output field $\vec{E}^o + \vec{E}^e$. Orientation is the tilt angle of the major

axis of the ellipse. Each small number indicates the maximum difference in the pupil. For both Figure 3.32 (a) and (b), the difference at the bottom field is the smallest. Larger the field, higher the difference. The magnitude difference is within 2.5%, while the orientation difference is within 1.3°.

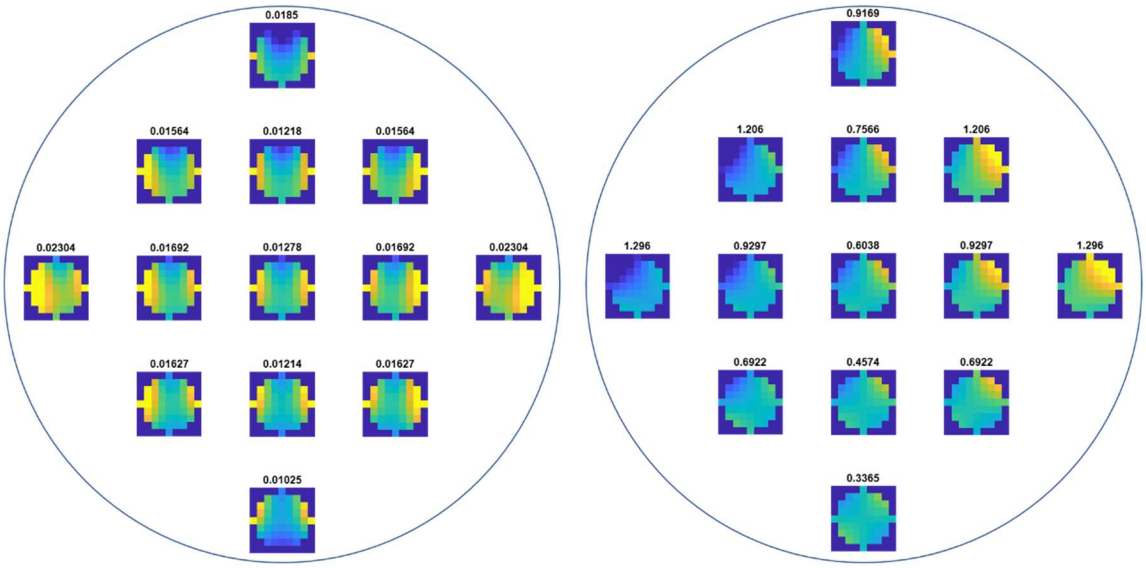

(a) Magnitude difference (b) Orientation difference

Figure 3.32 Comparisons of polarization pupil maps

3.5 Conclusions

In this chapter, the origin of polarization aberrations is discussed, and the polarization aberrations are classified into two major categories: physical and geometrical. After discussing the origins of polarization aberrations, a short review of the prior methods to calculate and analyze the polarization in optical systems is presented. A newly proposed polarization aberration theory by Sasián is reviewed in Section 3.2. Then the polarization aberration theory for plane symmetric optical systems is derived in Section 3.3. By utilizing

the new polarization aberration theory, the polarization aberrations of two examples are demonstrated and analyzed in Section 3.4.

Based on the paraxial and second-order approximation, the polarization aberrations are the sum of the contributions from each surface. It makes this new polarization aberration theory easier to be realized and utilized. Although it is only a second order polarization aberration function, it still has good matching with CODE V real ray tracing. The magnitude difference is less than 2.5%, while the orientation difference is within 1.6°. This theory provides insight of polarization aberration surface by surface and enables a new merit function for polarization aberration optimization in the future.

4. Closing Remarks

This dissertation presented a new adaptive dispersion formula and a set of polarization aberration functions for plane symmetric optical systems. These two studies extend existing aberration theory, provide insight to the correction of chromatic change of focus, and enable a new method to analyze polarization aberrations.

The new adaptive dispersion formula rationalizes the correction of chromatic aberration per spectrum order. A coefficient K in the adaptive dispersion formula permits the convergence and makes the formula adaptive to each type of glass. The adaptive formula provides an average refractive index error of 2.91×10^{-6}, while Buchdahl formula and Sellmeier formula have refractive index errors of 3.63×10^{-6} and 3.82×10^{-6} on average respectively. The adaptive formula coefficients when multiplied by the sag of a lens provide directly the amount of chromatic change of focus as primary, secondary, tertiary, etc. spectra.

In the second half of the dissertation, the polarization aberration functions for axial symmetric optical systems were reviewed and the polarization aberration functions for plane symmetric optical systems were developed. Instead of using Jones matrix or polarization ray tracing, a set of polarization aberration functions was constructed to describe polarization aberrations. The polarization aberrations of an optical system with tilted lens element and of an optical system with plane symmetric reflective optics were demonstrated. The polarization aberration functions up to second order shows good

matching with the polarization ray tracing of CODE V in paraxial region. The magnitude difference is within 2.5%, while the orientation difference is within 1.6°.

As for future work, we can extend the application of the adaptive dispersion formula to the correction for chromatic change of magnification of thin lenses. Moreover, we can extend the application of the adaptive dispersion formula to the correction for general chromatic aberrations of thick lenses. In terms of plane symmetric polarization aberrations, we can enhance the accuracy of the aberration functions by including the higher order terms, for example the 4^{th} order terms. In addition, since the polarization aberrations were provided in the analytical form, we can create corresponding merit functions and minimize the polarization aberrations of an optical system during the optimization.

Appendix A: Index Fitting Comparison

(Errors are in units of 10^{-6})

Number	Glass	Glascode	Adaptive Formula		Buchdahl		Sellmeier		Adaptive Formula	
			six coefficients (q=4)		six coefficients (j=5)		six coefficients (i=3)		four coefficients (q=2)	
			Max error	RMS error	Max error	RMS error	Max error	RMS error	Max error	RMS error
1	F2	620364.360	3.28	1.66	3.48	1.67	3.67	1.78	3.66	1.78
2	F2HT	620364.360	3.28	1.66	3.48	1.67	3.67	1.78	3.66	1.78
3	F5	603380.347	2.43	1.30	2.52	1.31	2.63	1.67	2.41	1.34
4	K10	501564.252	0.82	0.47	2.00	1.20	3.09	1.64	2.68	1.50
5	K7	511604.253	3.28	1.71	3.22	1.71	3.89	2.34	3.29	2.17
6	KZFS12	696363.384	1.63	0.90	2.74	1.83	2.51	1.77	1.90	1.29
7	LAFN7	750350.438	1.20	0.63	1.55	0.66	2.00	1.48	1.27	0.91
8	LF5	581409.322	3.88	2.27	3.86	2.25	3.90	2.71	3.88	2.28
9	LLF1	548458.294	2.10	1.15	5.93	2.88	4.91	2.35	4.24	2.25
10	N-BAF10	670471.375	2.22	1.01	3.25	2.15	3.42	2.15	2.27	1.30
11	N-BAF4	606437.289	3.88	1.80	4.47	2.71	4.44	2.79	4.50	2.93
12	N-BAF51	652450.333	1.42	0.66	2.22	1.27	2.54	1.58	1.60	0.93
13	N-BAF52	609466.305	2.49	1.57	3.41	1.87	3.69	2.55	3.65	2.18
14	N-BAK1	573576.319	3.06	1.40	3.74	2.10	4.02	2.27	3.53	2.10
15	N-BAK2	540597.286	2.65	1.64	3.28	2.20	3.27	2.19	2.68	1.86
16	N-BAK4	569560.305	1.52	0.87	1.42	0.86	3.90	2.68	3.30	1.82
17	N-BALF4	580539.311	2.43	1.46	3.72	1.57	3.90	2.21	3.12	1.53
18	N-BALF5	547536.261	1.01	0.53	1.10	0.65	3.76	2.54	2.77	1.61
19	N-BASF2	664360.315	2.61	1.24	2.78	1.29	3.20	1.99	2.96	1.28
20	N-BASF64	704394.320	1.91	0.84	4.30	1.91	2.62	1.86	2.48	1.86
21	N-BK10	498670.239	2.37	1.43	3.81	2.30	4.27	2.83	3.83	2.37
22	N-BK7	517642.251	1.74	0.91	2.79	1.40	3.64	2.07	3.14	1.81
23	N-BK7HT	517642.251	1.74	0.91	2.79	1.40	3.64	2.07	3.14	1.81
24	N-F2	620364.265	2.48	1.21	3.45	1.99	2.82	1.75	2.47	1.74
25	N-FK5	487704.245	3.28	1.82	3.49	1.84	3.94	2.31	3.67	2.17
26	N-FK51A	487845.368	2.00	0.98	2.96	1.83	2.95	1.93	2.21	1.63
27	N-K5	522595.259	2.98	1.44	3.00	1.41	4.50	2.68	2.80	1.52
28	N-KF9	523515.250	3.24	1.89	3.62	2.32	3.69	2.35	3.27	2.34
29	N-KZFS11	638424.320	3.38	2.28	4.30	2.68	4.48	3.11	4.30	2.89
30	N-KZFS2	558540.255	1.92	1.14	3.23	1.90	4.10	2.75	3.59	2.69
31	N-KZFS4	613445.300	3.21	1.57	3.38	2.08	3.44	2.28	3.19	2.39
32	N-KZFS5	654397.304	3.70	1.79	4.24	2.21	4.28	2.28	4.18	2.33
33	N-KZFS8	720347.320	3.41	1.92	3.89	2.22	4.11	2.52	3.83	2.09
34	N-LAF2	744449.430	3.48	1.59	5.45	2.13	4.45	2.14	4.18	2.08
35	N-LAF21	788475.428	1.54	0.74	3.48	2.04	3.17	1.83	2.03	1.37
36	N-LAF33	786441.436	5.35	3.94	7.59	3.42	4.78	3.37	4.78	3.47
37	N-LAF34	773496.424	3.29	1.86	3.65	2.02	3.98	2.68	3.49	1.96
38	N-LAF35	743494.412	3.78	2.33	4.76	3.11	4.11	2.82	4.12	2.83
39	N-LAF36	800424.443	3.66	2.48	3.67	2.49	4.29	3.09	3.90	2.82
40	N-LAF7	749348.373	3.83	2.08	4.01	2.10	4.07	2.34	4.02	2.22
41	N-LAK10	720506.369	2.45	1.21	4.01	2.67	4.24	2.75	3.80	2.66
42	N-LAK12	678552.410	1.76	1.04	2.90	2.03	4.10	2.41	2.58	1.71
43	N-LAK14	697554.363	2.51	1.19	3.27	1.83	3.89	2.20	2.52	1.34
44	N-LAK21	640601.374	4.60	2.80	6.39	3.09	4.62	2.87	4.51	2.67
45	N-LAK22	651559.377	3.42	1.74	3.66	1.76	4.45	2.43	3.95	1.86

46	N-LAK33A	754523.422	2.66	1.51	3.69	2.40	4.28	2.76	2.93	2.12
47	N-LAK33B	755523.422	1.79	1.22	2.09	1.37	4.33	2.39	2.27	1.65
48	N-LAK34	729545.402	2.47	1.22	2.84	1.56	2.79	1.55	2.66	1.42
49	N-LAK7	652585.384	3.13	1.98	3.44	2.09	4.87	3.18	3.62	2.38
50	N-LAK8	713538.375	4.11	3.00	4.18	3.02	4.41	3.60	4.26	3.58
51	N-LAK9	691547.351	2.18	1.09	2.19	1.08	2.20	1.09	2.27	1.24
52	N-LASF31A	883408.551	4.28	2.56	4.30	2.60	4.40	2.86	4.42	2.77
53	N-LASF40	834373.443	3.38	2.05	5.96	2.59	3.79	2.45	3.67	2.15
54	N-LASF41	835431.485	2.06	1.05	2.21	1.24	3.49	1.98	2.52	1.56
55	N-LASF43	806406.426	3.26	1.60	4.30	2.77	3.81	2.22	3.85	2.35
56	N-LASF44	804465.444	3.77	2.08	4.02	2.07	3.69	2.08	3.79	2.17
57	N-LASF45	801350.363	3.51	1.69	3.75	2.37	3.55	2.10	3.21	1.85
58	N-LASF45HT	801350.363	3.51	1.69	3.75	2.37	3.55	2.10	3.21	1.85
59	N-LASF46A	904313.445	2.06	1.11	2.11	1.11	2.72	1.62	2.06	1.32
60	N-LASF46B	904313.451	2.11	1.03	2.25	1.10	2.68	1.86	2.38	1.35
61	N-LASF9	850322.441	3.46	1.63	3.89	1.97	4.02	2.78	4.03	2.30
62	N-LASF9HT	850322.441	3.46	1.63	3.89	1.97	4.02	2.78	4.03	2.30
63	N-PK51	529770.386	3.38	1.92	3.47	1.98	4.25	2.93	3.60	2.10
64	N-PK52A	497816.370	3.91	2.42	4.86	2.90	4.20	2.91	3.92	2.41
65	N-PSK3	552635.291	4.85	2.75	5.01	3.67	4.90	3.25	4.66	2.93
66	N-PSK53A	618634.357	4.38	2.79	5.34	2.84	4.31	2.60	4.29	2.62
67	N-SF1	717296.303	1.51	0.74	2.51	1.60	2.16	1.43	2.21	1.64
68	N-SF10	728285.305	2.09	1.06	1.97	0.99	4.16	2.69	3.89	2.59
69	N-SF11	785257.322	3.52	2.13	3.94	2.72	3.97	2.87	4.11	2.51
70	N-SF14	762265.312	2.76	1.60	2.90	1.84	2.96	1.85	2.99	1.74
71	N-SF15	699302.292	3.43	1.92	3.51	1.92	4.05	2.68	3.51	2.49
72	N-SF2	648338.272	3.33	1.78	5.02	2.76	3.71	2.41	3.53	1.98
73	N-SF4	755274.315	3.10	1.59	4.05	2.78	3.90	2.55	3.76	2.78
74	N-SF5	673323.286	4.33	2.32	4.45	2.93	4.34	2.93	4.33	2.49
75	N-SF57	847238.353	3.01	1.58	5.53	2.62	3.97	2.45	4.52	3.60
76	N-SF57HT	847238.353	3.01	1.58	5.53	2.62	3.97	2.45	4.52	3.60
77	N-SF57HTultra	847238.353	3.01	1.58	5.53	2.62	3.97	2.45	4.52	3.60
78	N-SF6	805254.337	2.91	1.67	3.16	1.79	3.31	2.13	3.04	2.04
79	N-SF66	923209.400	1.93	1.18	3.01	1.63	4.01	2.60	3.65	1.83
80	N-SF6HT	805254.337	2.91	1.67	3.16	1.79	3.31	2.13	3.04	2.04
81	N-SF6HTultra	805254.337	2.91	1.67	3.16	1.79	3.31	2.13	3.04	2.04
82	N-SF8	689313.290	4.50	1.95	5.08	3.30	4.68	3.00	4.49	2.46
83	N-SK11	564608.308	2.46	1.44	2.86	1.53	3.63	2.15	2.52	1.60
84	N-SK14	603606.344	2.92	1.73	3.09	1.84	4.05	2.67	2.94	1.74
85	N-SK16	620603.358	2.28	1.14	3.44	1.88	3.68	2.03	2.51	1.98
86	N-SK2	607567.355	3.58	1.92	3.80	2.39	3.63	2.35	3.63	2.34
87	N-SK2HT	607567.355	3.58	1.92	3.80	2.39	3.63	2.35	3.63	2.34
88	N-SK4	613586.354	3.58	2.16	3.79	2.34	4.55	3.06	3.49	2.28
89	N-SK5	589613.330	2.71	1.61	2.77	1.71	2.82	1.98	2.75	1.77
90	N-SSK2	622533.353	2.47	1.54	4.95	3.10	4.57	2.80	4.18	2.69
91	N-SSK5	658509.371	3.39	1.78	3.63	1.89	4.90	3.02	4.63	3.14
92	N-SSK8	618498.327	0.75	0.47	1.02	0.53	2.66	1.74	0.79	0.40
93	N-ZK7	508612.249	2.07	0.99	3.33	1.54	3.44	1.98	3.19	1.56
94	P-LAF37	755457.399	3.26	1.70	4.88	3.06	4.11	2.50	3.65	2.34
95	P-LAK35	693532.385	4.62	2.38	4.62	3.22	4.62	3.19	4.02	2.43
96	P-LASF47	806409.454	2.43	1.33	4.13	2.30	4.14	2.82	3.96	2.48
97	P-LASF50	809405.454	3.40	1.98	4.51	2.86	3.54	2.84	3.40	2.51

98	P-LASF51	810409.458	2.29	1.11	2.51	1.76	4.53	3.21	2.46	1.72
99	P-PK53	527662.283	1.49	0.75	1.54	0.74	2.94	1.92	1.60	1.08
100	P-SF67	907214.424	2.16	1.49	3.19	1.84	3.50	2.23	2.74	1.84
101	P-SF68	005210.619	3.99	2.22	4.28	2.30	4.50	2.66	4.08	2.44
102	P-SF69	723292.293	2.07	1.39	3.33	2.05	3.33	2.49	4.08	2.78
103	P-SF8	689313.290	4.31	2.12	4.31	2.12	4.58	2.68	4.36	2.23
104	P-SK57	587596.301	1.66	0.82	2.10	1.11	2.67	1.51	1.68	1.13
105	P-SK58A	589612.297	2.98	1.56	3.06	2.26	3.90	2.52	2.81	1.64
106	P-SK60	610579.308	2.06	1.26	2.98	1.92	3.57	2.38	2.96	2.04
107	SF1	717295.446	1.71	0.83	4.45	2.64	4.78	3.10	3.70	2.63
108	SF10	728284.428	1.92	1.00	1.90	1.00	2.94	1.82	1.85	1.18
109	SF2	648339.386	2.94	1.51	4.31	2.37	4.05	2.37	3.87	2.13
110	SF4	755276.479	2.66	1.53	4.90	2.47	3.52	2.06	3.56	2.09
111	SF5	673322.407	1.72	1.08	2.85	1.52	3.19	2.30	2.87	1.79
112	SF56A	785261.492	3.71	1.92	3.84	2.02	4.49	2.77	4.17	2.71
113	SF57	847238.551	4.51	2.59	4.75	2.60	4.87	2.69	4.86	2.68
114	SF6	805254.518	3.99	2.21	4.15	2.27	4.28	2.43	4.23	2.27
115	SF6HT	805254.518	3.99	2.21	4.15	2.27	4.28	2.43	4.23	2.27
116	SF57HTultra	847238.551	4.51	2.59	4.75	2.60	4.87	2.69	4.86	2.68
117	P-BK7	516641.243	4.78	2.50	4.88	2.74	5.02	3.05	4.63	2.69
118	P-SK57Q1	586595.301	1.61	0.80	1.95	1.04	3.92	2.19	1.71	0.90
119	SF11	785258.474	3.37	1.95	3.40	2.08	3.74	2.49	3.40	2.17
Average			2.91	1.60	3.63	2.06	3.82	2.40	3.38	2.10
Maximum			5.35	3.94	7.59	3.67	5.02	3.60	4.86	3.60

Appendix B: Coefficients of the Adaptive Dispersion Formula

Glass	Glascode	RMS error	Max error	n_0	A_1	A_2	A_3	K
F2	620364.360	1.78×10^{-6}	3.66×10^{-6}	1.6240797991	-0.0175823138	0.0084939540	-0.0039437159	0.4482924521
F2HT	620364.360	1.78×10^{-6}	3.66×10^{-6}	1.6240797991	-0.0175823138	0.0084939540	-0.0039437159	0.4482924521
F5	603380.347	1.34×10^{-6}	2.41×10^{-6}	1.6071803097	-0.0163564579	0.0078466009	-0.0036212272	0.4427577747
K10	501564.252	1.50×10^{-6}	2.68×10^{-6}	1.5034895779	-0.0091235644	0.0039963730	-0.0017361587	0.4078457752
K7	511604.253	2.17×10^{-6}	3.29×10^{-6}	1.5131399068	-0.0086740087	0.0037429354	-0.0016023252	0.4056074727
KZFS12	696363.384	1.29×10^{-6}	1.90×10^{-6}	1.7005486953	-0.0197559775	0.0093812806	-0.0043473655	0.4481076563
LAFN7	750350.438	9.14×10^{-7}	1.27×10^{-6}	1.7545809783	-0.0221108140	0.0106482744	-0.0049607472	0.4508494797
LF5	581409.322	2.28×10^{-6}	3.88×10^{-6}	1.5848200074	-0.0146682637	0.0069250085	-0.0031571546	0.4438275348
LLF1	548458.294	2.25×10^{-6}	4.24×10^{-6}	1.5509865723	-0.0123292334	0.0057038704	-0.0025694851	0.4278574641
N-BAF10	670471.375	1.30×10^{-6}	2.27×10^{-6}	1.6734077339	-0.0146314049	0.0067350023	-0.0030083033	0.4184418426
N-BAF4	606437.289	2.93×10^{-6}	4.50×10^{-6}	1.6089700000	-0.0142513307	0.0066758774	-0.0030899162	0.4489441850
N-BAF51	652450.333	9.32×10^{-7}	1.60×10^{-6}	1.6556884323	-0.0149422042	0.0069230748	-0.0030925600	0.4325816755
N-BAF52	609466.305	2.18×10^{-6}	3.65×10^{-6}	1.6117303475	-0.0134213158	0.0062205045	-0.0028584367	0.4353441662
N-BAK1	573576.319	2.10×10^{-6}	3.53×10^{-6}	1.5748684175	-0.0102142823	0.0045090173	-0.0019318776	0.3974743819
N-BAK2	540597.286	1.86×10^{-6}	2.68×10^{-6}	1.5421182517	-0.0092770487	0.0040325181	-0.0017255081	0.3991595342
N-BAK4	569560.305	1.82×10^{-6}	3.30×10^{-6}	1.5712484846	-0.0104272578	0.0046121424	-0.0020063385	0.3988090023
N-BALF4	580539.311	1.53×10^{-6}	3.12×10^{-6}	1.5821197901	-0.0110506897	0.0049349611	-0.0021552280	0.4052109538
N-BALF5	547536.261	1.61×10^{-6}	2.77×10^{-6}	1.5498197672	-0.0104818527	0.0046568148	-0.0020542052	0.4205205555
N-BASF2	664360.315	1.28×10^{-6}	2.96×10^{-6}	1.6688298093	-0.0190288069	0.0092672742	-0.0043988202	0.4668742354
N-BASF64	704394.320	1.86×10^{-6}	2.48×10^{-6}	1.7082375202	-0.0184101344	0.0087455915	-0.0040350268	0.4456748237
N-BK10	498670.239	2.37×10^{-6}	3.83×10^{-6}	1.4995991678	-0.0076080500	0.0031294407	-0.0013115008	0.4099663546
N-BK7	517642.251	1.81×10^{-6}	3.14×10^{-6}	1.5187231399	-0.0082423581	0.0034670871	-0.0014780390	0.3974299435
N-BK7HT	517642.251	1.81×10^{-6}	3.14×10^{-6}	1.5187231399	-0.0082423581	0.0034670871	-0.0014780390	0.3974299435
N-F2	620364.265	1.74×10^{-6}	2.47×10^{-6}	1.6240782200	-0.0175375790	0.0085327633	-0.0040691987	0.4626006523
N-FK5	487704.245	2.17×10^{-6}	3.67×10^{-6}	1.4891433546	-0.0070749426	0.0029242500	-0.0012380608	0.3878920217
N-FK51A	487845.368	1.63×10^{-6}	2.21×10^{-6}	1.4879384712	-0.0059068330	0.0025012656	-0.0010359913	0.3978994474
N-K5	522595.259	1.52×10^{-6}	2.80×10^{-6}	1.5245807456	-0.0090111084	0.0039395844	-0.0016908912	0.3866981131
N-KF9	523515.250	2.34×10^{-6}	3.27×10^{-6}	1.5258800000	-0.0104309431	0.0046704198	-0.0020642972	0.4244169031
N-KZFS11	638424.320	2.89×10^{-6}	4.30×10^{-6}	1.6413242990	-0.0154572218	0.0070346488	-0.0031457015	0.4230841877
N-KZFS2	558540.255	2.69×10^{-6}	3.59×10^{-6}	1.5608222151	-0.0105831111	0.0045506329	-0.0019952453	0.4022202377
N-KZFS4	613445.300	2.39×10^{-6}	3.19×10^{-6}	1.6166379532	-0.0141662241	0.0064133615	-0.0028566578	0.4241695233
N-KZFS5	654397.304	2.33×10^{-6}	4.18×10^{-6}	1.6580319954	-0.0169592996	0.0079307729	-0.0036180985	0.4386297262
N-KZFS8	720347.320	2.09×10^{-6}	3.83×10^{-6}	1.7253900494	-0.0214061476	0.0103181948	-0.0048140744	0.4541137462
N-LAF2	744449.430	2.08×10^{-6}	4.18×10^{-6}	1.7479141848	-0.0170786547	0.0079119642	-0.0035306274	0.4249444175
N-LAF21	788475.428	1.37×10^{-6}	2.03×10^{-6}	1.7919481935	-0.0170562102	0.0076843951	-0.0033672363	0.4116980367
N-LAF33	786441.436	3.47×10^{-6}	4.78×10^{-6}	1.7900660801	-0.0183571038	0.0084291848	-0.0037395177	0.4218431160
N-LAF34	773496.424	1.96×10^{-6}	3.49×10^{-6}	1.7762100245	-0.0160040393	0.0071242383	-0.0030743615	0.4106525593
N-LAF35	743494.412	2.83×10^{-6}	4.12×10^{-6}	1.7468832604	-0.0154632354	0.0069000200	-0.0029916440	0.4100218811
N-LAF36	800424.443	2.82×10^{-6}	3.90×10^{-6}	1.8040010107	-0.0194328917	0.0090132934	-0.0040182910	0.4233518032
N-LAF7	749348.373	2.22×10^{-6}	4.02×10^{-6}	1.7545912843	-0.0221911537	0.0108482702	-0.0051582917	0.4622501307
N-LAK10	720506.369	2.66×10^{-6}	3.80×10^{-6}	1.7234138048	-0.0146021328	0.0064801613	-0.0028433140	0.4128374690
N-LAK12	678552.410	1.71×10^{-6}	2.58×10^{-6}	1.6808292470	-0.0126183772	0.0055720885	-0.0023795962	0.4066088872
N-LAK14	697554.363	1.34×10^{-6}	2.52×10^{-6}	1.6997984685	-0.0128899178	0.0055939978	-0.0024150832	0.3941892855
N-LAK21	640601.374	2.67×10^{-6}	4.51×10^{-6}	1.6430358364	-0.0109236519	0.0047088586	-0.0020110762	0.3964884655
N-LAK22	651559.377	1.86×10^{-6}	3.95×10^{-6}	1.6539097399	-0.0119713859	0.0052531461	-0.0022351247	0.4042704109
N-LAK33A	754523.422	2.12×10^{-6}	2.93×10^{-6}	1.7573686605	-0.0148093737	0.0065100946	-0.0028006122	0.4019279072
N-LAK33B	755523.422	1.65×10^{-6}	2.27×10^{-6}	1.7584399026	-0.0148281003	0.0065248273	-0.0027987086	0.4003245782
N-LAK34	729545.402	1.42×10^{-6}	2.66×10^{-6}	1.7323497295	-0.0137290651	0.0059757891	-0.0025575582	0.4005969717

N-LAK7	652585.384	2.38×10^{-6}	3.62×10^{-6}	1.6542514454	-0.0114215539	0.0049705738	-0.0021254437	0.3969798108
N-LAK8	713538.375	3.58×10^{-6}	4.26×10^{-6}	1.7161614145	-0.0135852197	0.0059145425	-0.0025517617	0.4059622891
N-LAK9	691547.351	1.24×10^{-6}	2.27×10^{-6}	1.6940115384	-0.0129596539	0.0056502437	-0.0024259547	0.4001959413
N-LASF31A	883408.551	2.77×10^{-6}	4.42×10^{-6}	1.8881497912	-0.0223239746	0.0103835965	-0.0046024807	0.4246510081
N-LASF40	834373.443	2.15×10^{-6}	3.67×10^{-6}	1.8393463295	-0.0230499782	0.0110098574	-0.0050670836	0.4455959336
N-LASF41	835431.485	1.56×10^{-6}	2.52×10^{-6}	1.8396100240	-0.0199259586	0.0091887920	-0.0040816782	0.4151730367
N-LASF43	806406.426	2.35×10^{-6}	3.85×10^{-6}	1.8108138516	-0.0204352429	0.0095477611	-0.0043317186	0.4358174637
N-LASF44	804465.444	2.17×10^{-6}	3.79×10^{-6}	1.8083168468	-0.0177885085	0.0080527492	-0.0035226800	0.4141207665
N-LASF45	801350.363	1.85×10^{-6}	3.21×10^{-6}	1.8064973588	-0.0236284241	0.0114749033	-0.0053604504	0.4553623015
N-LASF45HT	801350.363	1.85×10^{-6}	3.21×10^{-6}	1.8064973588	-0.0236284241	0.0114749033	-0.0053604504	0.4553623015
N-LASF46A	904313.445	1.32×10^{-6}	2.06×10^{-6}	1.9104801688	-0.0297682566	0.0147601775	-0.0070924658	0.4678151691
N-LASF46B	904313.451	1.35×10^{-6}	2.38×10^{-6}	1.9104797602	-0.0297723294	0.0147625982	-0.0070857369	0.4697218911
N-LASF9	850322.441	2.30×10^{-6}	4.03×10^{-6}	1.8565004002	-0.0272843484	0.0134976739	-0.0064046011	0.4635574992
N-LASF9HT	850322.441	2.30×10^{-6}	4.03×10^{-6}	1.8565004002	-0.0272843484	0.0134976739	-0.0064046011	0.4635574992
N-PK51	529770.386	2.10×10^{-6}	3.60×10^{-6}	1.5301899032	-0.0070469975	0.0030663974	-0.0012900414	0.3729718287
N-PK52A	497816.370	2.41×10^{-6}	3.92×10^{-6}	1.4984539223	-0.0062437463	0.0026704784	-0.0011152830	0.3927810524
N-PSK3	552635.291	2.93×10^{-6}	4.66×10^{-6}	1.5543987948	-0.0089117869	0.0037826892	-0.0016127198	0.3916571115
N-PSK53A	618634.357	2.62×10^{-6}	4.29×10^{-6}	1.6203270362	-0.0100073946	0.0043369290	-0.0018381774	0.3958477681
N-SF1	717296.303	1.64×10^{-6}	2.21×10^{-6}	1.7230788269	-0.0250007314	0.0125931085	-0.0061644584	0.4821995426
N-SF10	728285.305	2.59×10^{-6}	3.89×10^{-6}	1.7343038849	-0.0263505052	0.0133516971	-0.0065732515	0.4861876415
N-SF11	785257.322	2.51×10^{-6}	4.11×10^{-6}	1.7919200000	-0.0315657761	0.0163134114	-0.0081839607	0.4944769557
N-SF14	762265.312	1.74×10^{-6}	2.99×10^{-6}	1.7685897572	-0.0296622769	0.0152156956	-0.0075658155	0.4917808625
N-SF15	699302.292	2.49×10^{-6}	3.51×10^{-6}	1.7043827912	-0.0238757709	0.0120198221	-0.0059115440	0.4835039445
N-SF2	648338.272	1.98×10^{-6}	3.53×10^{-6}	1.6522164739	-0.0197434765	0.0097451050	-0.0047122747	0.4738179230
N-SF4	755274.315	2.78×10^{-6}	3.76×10^{-6}	1.7616369437	-0.0284894428	0.0145433323	-0.0071858803	0.4878705757
N-SF5	673323.286	2.49×10^{-6}	4.33×10^{-6}	1.6776343059	-0.0215085407	0.0107121320	-0.0052180846	0.4748545923
N-SF57	847238.353	3.60×10^{-6}	4.52×10^{-6}	1.8550367462	-0.0367928657	0.0192509780	-0.0097598378	0.5014084332
N-SF57HT	847238.353	3.60×10^{-6}	4.52×10^{-6}	1.8550367462	-0.0367928657	0.0192509780	-0.0097598378	0.5014084332
N-SF57HTultra	847238.353	3.60×10^{-6}	4.52×10^{-6}	1.8550367462	-0.0367928657	0.0192509780	-0.0097598378	0.5014084332
N-SF6	805254.337	2.04×10^{-6}	3.04×10^{-6}	1.8126623578	-0.0328088917	0.0169627325	-0.0084838800	0.4947014643
N-SF66	923209.400	1.83×10^{-6}	3.65×10^{-6}	1.9332201486	-0.0456971971	0.0247350682	-0.0130189356	0.5176941936
N-SF6HT	805254.337	2.04×10^{-6}	3.04×10^{-6}	1.8126623578	-0.0328088917	0.0169627325	-0.0084838800	0.4947014643
N-SF6HTultra	805254.337	2.04×10^{-6}	3.04×10^{-6}	1.8126623578	-0.0328088917	0.0169627325	-0.0084838800	0.4947014643
N-SF8	689313.290	2.46×10^{-6}	4.49×10^{-6}	1.6941344935	-0.0227092735	0.0113339902	-0.0055031458	0.4792410058
N-SK11	564608.308	1.60×10^{-6}	2.52×10^{-6}	1.5660520675	-0.0095066046	0.0040949137	-0.0017498076	0.3988303987
N-SK14	603606.344	1.74×10^{-6}	2.94×10^{-6}	1.6054800754	-0.0102048365	0.0044362849	-0.0018956243	0.3826164796
N-SK16	620603.358	1.98×10^{-6}	2.51×10^{-6}	1.6228624360	-0.0105476923	0.0045565682	-0.0019402184	0.3920703755
N-SK2	607567.355	2.34×10^{-6}	3.63×10^{-6}	1.6099400000	-0.0110169758	0.0048474263	-0.0020665778	0.4061529096
N-SK2HT	607567.355	2.34×10^{-6}	3.63×10^{-6}	1.6099400000	-0.0110169758	0.0048474263	-0.0020665778	0.4061529096
N-SK4	613586.354	2.28×10^{-6}	3.49×10^{-6}	1.6152090894	-0.0107268018	0.0046713623	-0.0019892246	0.4079237707
N-SK5	589613.330	1.77×10^{-6}	2.75×10^{-6}	1.5914218317	-0.0098581724	0.0042420575	-0.0018057184	0.3935720756
N-SSK2	622533.353	2.69×10^{-6}	4.18×10^{-6}	1.6250758231	-0.0120033423	0.0053553333	-0.0023291464	0.4126290985
N-SSK5	658509.371	3.14×10^{-6}	4.63×10^{-6}	1.6615195367	-0.0133057042	0.0060148119	-0.0026419345	0.4196164336
N-SSK8	618498.327	3.99×10^{-7}	7.85×10^{-7}	1.6206797598	-0.0127492837	0.0057887464	-0.0025663579	0.4264524196
N-ZK7	508612.249	1.56×10^{-6}	3.19×10^{-6}	1.5104529557	-0.0085050550	0.0036146531	-0.0015493998	0.3924702190
P-LAF37	755457.399	2.34×10^{-6}	3.65×10^{-6}	1.7594363524	-0.0170154717	0.0077258232	-0.0034043649	0.4205756039
P-LAK35	693532.385	2.43×10^{-6}	4.02×10^{-6}	1.6966069692	-0.0133961653	0.0059178072	-0.0025330305	0.3998896170
P-LASF47	806409.454	2.48×10^{-6}	3.96×10^{-6}	1.8107823352	-0.0202929799	0.0094293900	-0.0042274169	0.4276709640
P-LASF50	809405.454	2.51×10^{-6}	3.40×10^{-6}	1.8133478395	-0.0205836749	0.0095863317	-0.0042985416	0.4286654841
P-LASF51	810409.458	1.72×10^{-6}	2.46×10^{-6}	1.8147024567	-0.0203723091	0.0094742139	-0.0042526537	0.4242012288
P-PK53	527662.283	1.08×10^{-6}	1.60×10^{-6}	1.5287999800	-0.0081646983	0.0035075032	-0.0014782476	0.4024669957
P-SF67	907214.424	1.84×10^{-6}	2.74×10^{-6}	1.9167497560	-0.0438093270	0.0234355380	-0.0121713319	0.5128849601

P-SF68	005210.619	2.44×10^{-6}	4.08×10^{-6}	2.0164282808	-0.0495261178	0.0268141690	-0.0140133414	0.5189147100
P-SF69	723292.293	2.78×10^{-6}	4.08×10^{-6}	1.7283340779	-0.0255088982	0.0128853952	-0.0063373237	0.4840822427
P-SF8	689313.290	2.23×10^{-6}	4.36×10^{-6}	1.6941400000	-0.0227468286	0.0113447715	-0.0055057557	0.4763035534
P-SK57	587596.301	1.13×10^{-6}	1.68×10^{-6}	1.5893496888	-0.0100981864	0.0043386314	-0.0018531204	0.4040121040
P-SK58A	589612.297	1.64×10^{-6}	2.81×10^{-6}	1.5914279257	-0.0098714641	0.0042065606	-0.0017878009	0.4047998467
P-SK60	610579.308	2.04×10^{-6}	2.96×10^{-6}	1.6128621970	-0.0108037708	0.0047022991	-0.0020306725	0.3873713228
SF1	717295.446	2.63×10^{-6}	3.70×10^{-6}	1.7231035149	-0.0251075648	0.0125673193	-0.0060116902	0.4684927413
SF10	728284.428	1.18×10^{-6}	1.85×10^{-6}	1.7343009663	-0.0264741281	0.0134132004	-0.0065434517	0.4772122719
SF2	648339.386	2.13×10^{-6}	3.87×10^{-6}	1.6522188635	-0.0197458634	0.0096586395	-0.0045314966	0.4578003217
SF4	755276.479	2.09×10^{-6}	3.56×10^{-6}	1.7616668940	-0.0283017569	0.0143404014	-0.0069289516	0.4729264041
SF5	673322.407	1.79×10^{-6}	2.87×10^{-6}	1.6776403965	-0.0215611103	0.0106447023	-0.0050363143	0.4570775817
SF56A	785261.492	2.71×10^{-6}	4.17×10^{-6}	1.7918016534	-0.0311111204	0.0159366038	-0.0078093522	0.4832333224
SF57	847238.551	2.68×10^{-6}	4.86×10^{-6}	1.8550397739	-0.0367631734	0.0190886727	-0.0094507361	0.4897632624
SF6	805254.518	2.27×10^{-6}	4.23×10^{-6}	1.8126501801	-0.0327353528	0.0168108397	-0.0082324129	0.4817036949
SF6HT	805254.518	2.27×10^{-6}	4.23×10^{-6}	1.8126501801	-0.0327353528	0.0168108397	-0.0082324129	0.4817036949
SF57HTultra	847238.551	2.68×10^{-6}	4.86×10^{-6}	1.8550397739	-0.0367631734	0.0190886727	-0.0094507361	0.4897632624
P-BK7	516641.243	2.69×10^{-6}	4.63×10^{-6}	1.5183229791	-0.0082480646	0.0034688389	-0.0014755126	0.3865069532
P-SK57Q1	586595.301	9.05×10^{-7}	1.71×10^{-6}	1.5883500000	-0.0100982056	0.0043350336	-0.0018536461	0.4077352577
SF11	785258.474	2.17×10^{-6}	3.40×10^{-6}	1.7919001379	-0.0314861864	0.0162653267	-0.0080970464	0.4920624633

References

1. E. Hecht, “Optics,” Addison-Wesley, New York, Chap.7 (2002).

2. J. Sasián, “Introduction to aberrations in optical imaging systems,” Cambridge Univ. Press, Chap. 1 (2013).

3. https://en.wikipedia.org/wiki/Abbe_number

4. R. A. Chipman, W. T. Lam, and G. Young, “Polarized light and optical systems,” CRC Press, Chap. (2018).

5. L. E. Sutton and O. N. Stavroudis, “Fitting refractive index data by least squares,” J. Opt. Soc. Am. **51**(8), 901-905 (1961).

6. P. J. Reardon and R. A. Chipman, “Buchdahl’s glass dispersion coefficients calculated from Schott equation constants,” Appl. Opt. **28**(15), 3520-3523 (1989).

7. G. W. Forbes, “Chromatic coordinates in aberration theory,” J. Opt. Soc. Am. A **1**(4), 344-349 (1984).

8. R. A. Chipman and P. J. Reardon, “Buchdahl’s glass dispersion coefficients calculated in the near infrared,” Appl. Opt. **28**(4), 694-698 (1989).

9. Y. Pi, P. J. Reardon, and D. B. Pollock, “Applying the Buchdahl dispersion model to infrared hybrid refractive-diffractive achromats,” Proc. SPIE **6206**, 62062O (2006).

10. P. N. Robb and R. I. Mercado, “Calculation of refractive indices using Buchdahl’s chromatic coordinate,” Appl. Opt. **22**(8), 1198-1215 (1983).

11. C. L. Li and J. Sasián, “Adaptive dispersion formula for index interpolation and chromatic aberration correction,” Opt. Express **22**(1), 1193-1202 (2014).

12. Schott glass catalogue 2011 (http://www.us.schott.com).

13. K. S. R. Krishna and A. Sharma, “Evaluation of optical glass composition by optimization methods,” Appl. Opt. **34**(25), 5628-5634 (1995).

14. M. Bolser, “Mercado/Robb/Buchdahl coefficients - an update of 243 common glasses,” Proc. SPIE **4832**, 525-533 (2002).

15. J. Sasián, “Introduction to aberrations in optical imaging systems,” Cambridge Univ. Press, Chap. 6 (2013).

16. R. A. Chipman, W. T. Lam, and G. Young, “Polarized light and optical systems,” CRC Press (2018).

17. S. C. McClain, L. W. Hillman, and R. A. Chipman, “Polarization ray tracing in anisotropic optically active media. I. Algorithms,” J. Opt. Soc. Am. A **10**(11), 2371-2382 (1993).

18. W. T. Lam, S. McClain, G. Smith, and R. A. Chipman, “Ray tracing in biaxial materials,” Proc. SPIE **7652**, 76521R (2010).

19. J. Wolfe and R. A. Chipman, “Reducing symmetric polarization aberrations in a lens by annealing,” Opt. Express **12**(15), 3443-3451 (2004).

20. G. Young, W. T. Lam and R. A. Chipman, “A review of skew aberration, the intrinsic polarization aberration in high NA optical systems,” Proc. SPIE **9293**, 92931X (2014).

21. G. Young and R. A. Chipman, “Skew aberration analysis,” Proc. SPIE **8550**, 85500Z (2012).

22. G. Yun, K. Crabtree, and R. A. Chipman, “Skew aberration: a form of polarization aberration,” Opt. Lett. **36**(20), 4062-4064 (2011).

23. J. Ruoff and M. Totzeck, “Orientation Zernike polynomials: a useful way to describe the polarization effects of optical imaging systems,” J. Micro Nanolith. **8**(3), 031404 (2009).

24. D. J. Reiley and R. A. Chipman, “Coating-induced wave-front aberrations: on-axis astigmatism and chromatic aberration in all-reflecting systems,” Appl. Opt. **33**(10), 2002–2012 (1994).

25. M. I. Shribak, S. Inoue, and R. Oldenbourg, “Polarization aberrations caused by differential transmission and phase shift in high numerical aperture lenses: theory, measurement, and retification,” Opt. Eng. **41**(5), 943-954 (2002).

26. X. Xu, W. Huang, and M. Xu, “Orthogonal polynomials describing polarization aberration for rotationally symmetric optical systems,” Opt. Express **23**(21), 27911–27919 (2015).

27. X. Xu, W. Huang, and M. Xu, "Orthonormal polynomials describing polarization aberration for M-fold optical systems," Opt. Express **24**(5), 4906–4912 (2016).

28. N. Yamamoto, J. Kye, and H. J. Levinson, "Polarization aberration analysis using Pauli-Zernike representation," Proc. SPIE **6520**, 65200Y (2007).

29. J. Kye, G. McIntyre, Y. Norihiro, and H. J. Levinson, "Polarization aberration analysis in optical lithography systems," Proc. SPIE **6154**, 61540E (2006).

30. W. T. Lam and R. A. Chipman, "Balancing polarization aberrations in crossed fold mirrors," Appl. Opt. **54**(11), 3236–3245 (2015).

31. R. C. Jones, "A new calculus for the treatment of optical systems I. description and discussion of the calculus," J. Opt. Soc. Am. **31**(7), 488-493 (1941).

32. R. C. Jones, "A new calculus for the treatment of optical systems. VII. properties of the N-matrices," J. Opt. Soc. Am. **38**(8), 671-685 (1948).

33. E. Waluschka, "Polarization ray trace," Opt. Eng. **28**(2), 86-89 (1989).

34. R. A. Chipman, "Polarization ray tracing," Proc. SPIE **766**, 61-68 (1987).

35. R. A. Chipman, "Polarization aberrations," Ph.D. dissertation, The University of Arizona (1987).

36. R. A. Chipman, "Polarization analysis of optical systems," Opt. Eng. **28**(2), 90-99 (1989).

37. J. P. McGuire and R. A. Chipman, “Polarization aberrations. 1. rotationally symmetric optical systems,” Appl. Opt. **33**(22), 5080–5100 (1994).

38. J. P. McGuire and R. A. Chipman, “Polarization aberrations. 2. tilted and decentered optical systems,” Appl. Opt. **33**(22), 5101–5107 (1994).

39. R. A. Chipman, “The mechanics of polarization ray tracing,” Proc. SPIE **1746**, 62-75 (1992).

40. R. A. Chipman, “Mechanics of polarization ray tracing,” Opt. Eng. **34**(6), 1636-1645 (1995).

41. P. Torok, P. Varga, Z. Laczik, and G. R. Booker, “Electromagnetic diffraction of light focused through a planar interface between materials of mismatched refractive indices: an integral representation,” J. Opt. Soc. Am. A **12**(2), 325-332 (1995).

42. P. Torok, P. D. Higdon, and T. Wilson, “Theory for confocal and conventional microscopes imaging small dielectric scatterers,” J. Mod. Opt. **45**(8), 1681-1698 (1998).

43. G. Yun, K. Crabtree, and R. A. Chipman, “Three-dimensional polarization ray-tracing calculus I: definition and diattenuation,” Appl. Opt. **50**(18), 2855-2865 (2011).

44. G. Yun, S. McClain, and R. A. Chipman, “Three-dimensional polarization ray-tracing Calculus II: retardance,” Appl. Opt. **50**(18), 2866-2874 (2011).

45. J. Sasián, “Introduction to aberrations in optical imaging systems,” Cambridge Univ. Press, Chap. 16 (2013).

46. J. Sasián, “Polarization fields for understanding polarization aberrations in optical imaging systems,” Proc. SPIE **8841**, 88410C (2013).

47. J. Sasián, “Polarization fields and wavefronts of two sheets for understanding polarization aberrations in optical imaging systems,” Opt. Eng. **53**(3), 035102 (2014).

48. J. Sasián, “Imagery of the bilateral symmetrical optical system,” Ph.D. dissertation, The University of Arizona (1988).

49. T. Heil, J. Ruoff, J. T. Neumann, M. Totzeck, D. Krähmer, B. Geh, and P. Gräupner, “Orientation zernike polynomials: a systematic description of polarized imaging using high NA lithography lenses,” Proc. SPIE **7140**, 714018 (2008).

50. C. Zhao and J. H. Burge, “Orthonormal vector polynomials in a unit circle, part I: basis set derived from gradients of Zernike polynomials,” Opt. Express **15**(26), 18014-18024 (2007).

51. C. Zhao and J. H. Burge, “Orthonormal vector polynomials in a unit circle, part II : completing the basis set,” Opt. Express **16**(9), 6586-6591 (2008).

52. H. A. Macleod, “Thin-film optical filters,” CRC Press (2010).

53. Sh. A. Furman and A. V. Tikhonravov, “Basics of optics of multilayer systems,” Editions Frontieres, Chap. 1 and 2 (1992).

54. R. A. Chipman, W. T. Lam, and G. Young, "Polarized light and optical systems," CRC Press, 486-496 (2018).

55. J. Sasián, "Modeling light interference figures and isogyres of uniaxial and biaxial birefringent optical elements," Opt. Eng. **60**(5), 055102 (2021).

56. S Yuan, "Aberrations of anamorphic optical systems," Ph.D. dissertation, The University of Arizona (2008).

57. S. Yuan and J. Sasián, "Aberrations of anamorphic optical systems. I: the first-order foundation and method for deriving the anamorphic primary aberration coefficients," Appl. Opt. **48**(13), 2574–2584 (2009).

58. S. Yuan and J. Sasián, "Aberrations of anamorphic optical systems II: the primary aberration theory for cylindrical anamorphic systems," Appl. Opt. **48**(15), 2836–2841 (2009).

59. J. Sasián, "Review of methods for the design of unsymmetrical optical systems," Proc. of SPIE **1396**, 453-466 (1990).

60. J. Sasián, "How to approach the design of a bilateral symmetric optical system," Opt. Eng. **33**(6), 2045-2061 (1994).

61. D. R. Shafer, "Four-mirror unobscured anastigmatic telescopes with all-spherical surfaces," Appl. Opt. **17**(7), 1072-1074 (1978).

62. D. Reshidko and J. Sasián, "Method for the design of nonaxially symmetric optical systems using freeform surfaces," Opt. Eng. **57**(10), 101704 (2018).

63. C. Hou, Q. Xin, and Y. Zang, "Optical zoom system realized by lateral shift of Alvarez freeform lenses," Opt. Eng. **57**(4), 045103 (2018).

64. R. A. Buchroeder, "Tilted component optical systems," Ph.D. dissertation, The University of Arizona (1976).

65. R. V. Shack and K. P. Thompson, "Influence of alignment errors of a telescope system on its aberration field, Proc. SPIE **251**, 146-153 (1980).

66. K. P. Thompson, "Aberration fields in tilted and decentered optical systems," Ph.D. dissertation, The University of Arizona (1980).

67. K. Thompson, "Description of the third-order optical aberrations of near-circular pupil optical systems without symmetry," J. Opt. Soc. Am. A **22**(7), 1389-1401 (2005).

68. K. P. Thompson, "Multinodal fifth-order optical aberrations of optical systems without rotational symmetry: spherical aberration," J. Opt. Soc. Am. A **26**(5), 1090-1100 (2009).

69. K. P. Thompson, "Multinodal fifth-order optical aberrations of optical systems without rotational symmetry: the astigmatic aberrations," J. Opt. Soc. Am. A **28**(5), 821-836 (2011).

70. J. Rolland and K. Thompson, “Freeform optics: Evolution? No, revolution!” SPIE news (2012) (link: spie.org).

71. J. Sasián, “ Design of a Schwarzschild flat-field, anastigmatic, unobstructed, wide-field telescope,” Opt. Eng. **29**(1), 1-6 (1990).

72. L. B. Moore, A. M. Hvisc and J. Sasián, “Aberration fields of a combination of plane symmetric systems,” Opt. Express **16**(20), 15655-15670 (2008).

73. R. Mercado, “Camera lens system with five lens components,” U.S. Patent 9,817,213 (2017).